

UNIVERSITY OF WASHINGTON  
COLLEGE OF ENGINEERING

SOIL ENGINEERING RESEARCH REPORT NO. 17

PORE PRESSURE RISE OF  
SATURATED SANDS DURING  
CYCLIC LOADING

BY

MEHMET A. SHERIF

CHUZO TSUCHIYA

AND

ISAO ISHIBASHI

FEBRUARY 1977

DEPARTMENT OF CIVIL ENGINEERING

UNIVERSITY OF WASHINGTON

SEATTLE, WASHINGTON 98195

*Any opinions, findings, conclusions  
or recommendations expressed in this  
publication are those of the author(s)  
and do not necessarily reflect the views  
of the National Science Foundation.*

## ABSTRACT

Soil liquefaction has become an important consideration in the design of buildings as well as earth structures in seismically active regions, especially in places where the water table is high and soil gradation falls within a critical range. Liquefaction of sands occurs at the extreme stage of the gradual increase in pore pressure during dynamic loading as a result of the volume decreasing tendency in soil skeleton in undrained condition.

Liquefaction studies in the past were focused on the determination of liquefaction potential of a given sand under simple loading conditions and also these studies were restricted to fully saturated soils. It is essential, however, to know the pore pressure rise at any stage of actual earthquake and thereby determining the possible liquefaction time as well as the response of the deposit during earthquakes.

During this research, a new method is established that would predict the pore pressure rise in a sand deposit during dynamic loading. The method is applicable to any type of dynamic loading (from uniform cyclic to random time history of loading such as imposed by actual earthquakes). The authors have found that the incremental rise in pore pressure for a given soil under a given condition during one cycle of loading is affected by three major factors, namely, stress history, cyclic effect, and stress intensity. These factors are defined in terms of pore pressure rise at the end of the preceding cycle,  $U_{N-1}$ , the equivalent number of cycles,  $N_{eq}$ , and the stress ratio,  $\tau_N / \sigma'_{N-1}$ , as shown in the following fundamental equation. This equation predicts the incremental rise in pore pressure,  $\Delta U_N$ , during the  $N^{th}$  cycle and the total pore pressure,  $U_N$ , at the end of the  $N^{th}$  cycle.

$$\Delta U_N = (1 - U_{N-1}) \cdot \frac{C_1 N_{eq}}{N_{eq}^{C_2} - C_3} \cdot \left( \frac{\tau_N}{\sigma_{N-1}'} \right)^S$$

and

$$U_N = U_{N-1} + \Delta U_N$$

where  $C_1$ ,  $C_2$ ,  $C_3$  and  $S$  = material parameters.

The above method is used to determine the liquefaction potential of a sand with different densities under various types of loading, including actual earthquakes. In view of the fact that the above method is based on direct laboratory measurements, the authors believe that it is more dependable and hence easily applicable to various sands as compared to the methods proposed by other researchers (17, 26).

The liquefaction potential of partially saturated sands is also investigated during this study. In view of the fact that most natural geologic deposits consist of soils that are partially saturated, understanding of the liquefaction potential of partially saturated soils is of utmost practical importance. It is shown that partially saturated loose sands do liquefy and their liquefaction potential decreases with the decrease in the initial degree of saturation of the soil.

## TABLE OF CONTENTS

	<u>PAGE</u>
SYMBOLS	v
LIST OF TABLES	ix
LIST OF FIGURES	x
LIST OF PLATES	xiv
ACKNOWLEDGEMENT	xv
CHAPTER 1 - INTRODUCTION	1
CHAPTER 2 - PREVIOUS STUDIES ON SOIL LIQUEFACTION	5
2-1 Field Investigations into the Liquefaction Potential of a Deposit during Earthquakes	5
2-2 Laboratory Studies on the Liquefaction Potential of Saturated Sands	8
2-3 Prediction of Pore Pressure Rise in Saturated Sands during Earthquakes	23
2-4 Studies on Liquefaction of Partially Saturated Sands	28
CHAPTER 3 - SOIL TYPE TESTED AND EXPERIMENTAL PROCEDURES FOLLOWED DURING THIS INVESTIGATION	30
3-1 Testing Equipment	30
3-2 Type of Soil Tested	33
3-3 Test Program	33

TABLE OF CONTENTS (continued)

	<u>PAGE</u>
3-4 Test Procedure	34
 CHAPTER 4 - DISCUSSION AND ANALYSIS OF TEST RESULTS	 38
4-1 Definition of Initial Liquefaction and Complete Liquefaction	38
4-2 Analysis of Pore Pressure Rise Under Uniform Cyclic Loading	39
4-3 Liquefaction Potential of Samples with Different Densities	47
4-4 Prediction of Pore Pressure Rise Under Non-uniform Cyclic Loading	49
4-5 Prediction of Pore Pressure Rise during Actual Earthquake	51
4-6 General Procedures for the Determination of Parameters $S$ , $C_1$ , $C_2$ and $C_3$	55
4-7 Effect of the Degree of Saturation on Liquefaction Potential	56
 CHAPTER 5 - CONCLUSIONS AND RECOMMENDATIONS	 60
5-1 Conclusions	60
5-2 Recommendations	62
 BIBLIOGRAPHY	 64

TABLE OF CONTENTS (continued)

	<u>PAGE</u>
TABLES	71
FIGURES	76
PLATES	141
VITA	144

## SYMBOLS

### SYMBOL

$\bar{B}$	Skempton's pore pressure parameter
$C_S$	Compressibility of soil skeleton under isotropic stresses
$C_1, C_2, C_3$	Material parameters in Eq.4.5
$D_r$	Relative density
$D_0, D_{10}, D_{30},$ $D_{50}, D_{60}, D_{100}$	Soil diameters of which 0, 10, 30, 50, 60 and 100% of soil weights are finer, respectively
$e$	Void ratio
$e_{max}$	Maximum void ratio
$e_{min}$	Minimum void ratio
$G_S$	Specific gravity
$H$	Henry's constant for solubility
$K_w$	Bulk modulus of water
$K_o$	Coefficient of lateral earth pressure at rest
$N$	Number of cycles
$N_L$	Number of cycles to cause liquefaction for virgin sample
$N_R$	Number of cycles to cause liquefaction for previously liquefied sample
$N_{cr}$	Critical number of blows in standard penetration test
$N_{eq}$	Equivalent number of cycles
$(N_{eq})_p$	Equivalent number of cycles in positive region

SYMBOLS (continued)

SYMBOL

$(N_{eq})_n$	Equivalent number of cycles in negative region
$n$	Porosity of the sample
$n_0$	Initial porosity of the sample
$P_a$	Atmospheric pressure
$p'$	Effective mean principal stress ( = $\sigma'_{oct}$ )
$q$	Maximum deviator stress
$R$	Modification factor ( = $1 - U_{N-1}$ )
$S$	Slope of a family of lines in Figs. 4.4, 4.7 and 4.8
$S_0$	Initial degree of saturation in percent
$U_K$	Excess pore pressure due to an increase in mean principal stress
$U_N$	Normalized residual pore pressure at the end of $N^{th}$ cycle
$\Delta U_N$	Normalized pore pressure rise during $N^{th}$ cycle
$(\Delta U_N)_p$	Normalized pore pressure rise during $N^{th}$ cycle due to stress in positive region
$(\Delta U_N)_n$	Normalized pore pressure rise during $N^{th}$ cycle due to stress in negative region
$u$	Pore pressure
$u_b$	Back pressure
$\Delta u$	Increment in pore pressure
$V_0$	Initial total volume of the specimen

SYMBOLS (continued)

SYMBOL

$\Delta V$	Volume change of the specimen
$v_a, v_w$	Volume of air and water in percent
$\gamma$	Cyclic shear strain
$\Delta \epsilon_{vd}$	Total volumetric strain of soil structure
$\Delta \epsilon_{vr}$	Recoverable volumetric strain of soil structure
$\sigma$	Normal stress
$\sigma_h$	Horizontal stress
$\sigma_m$	Mean stress ( average of maximum and minimum principal stress )
$\sigma_v$	Vertical stress
$\sigma_1, \sigma_2, \sigma_3$	Principal stresses
$\sigma'$	Effective normal stress
$\sigma'_c$	Effective confining pressure
$\sigma'_N$	Effective confining pressure at the end of $N^{\text{th}}$ cycle
$\sigma'_v$	Effective vertical stress
$\sigma'_{\text{oct}}$	Effective octahedral stress
$\Delta \sigma_c$	Increment in confining pressure
$\Delta \sigma'_c$	Increment in the effective confining pressure
$\Delta \sigma_d$	Pulsating deviator stress
$\tau_f$	Shear stress at failure

SYMBOLS (continued)

SYMBOL

$\tau_N$	Cyclic shear stress at $N^{\text{th}}$ cycle
$\tau_{hv}$	Shear stress on horizontal and vertical planes
$\tau_{Np}$	Cyclic shear stress at $N^{\text{th}}$ cycle in positive region
$\tau_{Nn}$	Cyclic shear stress at $N^{\text{th}}$ cycle in negative region
$\tau_{\text{oct}}$	Octahedral shear stress
$\Delta\tau_{\text{max}}$	Maximum change in shear stress
$\phi'$	Effective angle of internal friction

## LIST OF TABLES

<u>TABLE</u>		<u>PAGE</u>
1	Physical properties of Ottawa Sand (ASTM C-109 )	71
2	Test Program for Saturated Samples	72
3	Test Program for Partially Saturated Samples	73
4	An Example of $\bar{B}$ Measurement Prior to Testing	74
5	Parameters $C_1$ , $C_2$ and $C_3$ for Different Densities of Ottawa Sand ( ASTM C-109 )	75

## LIST OF FIGURES

<u>FIGURE</u>		<u>PAGE</u>
2.1	Critical Standard Penetration Value, $N_{cr}$ , versus Depth	76
2.2	Zone of Liquefaction	77
2.3	Liquefied Zone and the Damages to Structures	78
2.4	Soils Susceptible to Liquefaction	79
2.5	Equivalent Numbers of Uniform Stress Cycles Based on All Components of Ground Motion	80
2.6	Method of Evaluating Liquefaction Potential	81
2.7	Idealized Field Loading Conditions	82
2.8	Mohr's Diagram Representation of Stresses	83
2.9	Idealized Triaxial Test Conditions	84
2.10	Effect of Void Ratio on Liquefaction Potential	85
2.11	Representation of Liquefaction Potential of Sand	86
2.12	Ratio of Liquefaction Resistance in Triaxial to that in Simple Shear, As Compared by Two Methods	87
2.13	Relationship between $\Delta\tau_{max} / \sigma_{oct}$ and the Number of Cycles to Liquefaction for Various $K_0$ values	88
2.14	Illustration of Stress-Strain Relationship in Loading and Reloading Process	89
2.15	Resistance to Reliquefaction Compared to Resistance to Liquefaction for Ottawa Sand	90
2.16	Effect of the Previous Partial Liquefaction on the Pore Pressure Rise	91
2.17	Effect of Seismic Histories on Liquefaction Characteristics of Sand	92

LIST OF FIGURES (continued)

<u>FIGURE</u>		<u>PAGE</u>
2.18	Effect of Seismic Histories on Liquefaction Potential of Sand	93
2.19	Effect of Frequency on Liquefaction Potential	94
2.20	Cyclic Shear Stress Wave Forms	95
2.21	Relationship between $\Delta u / \tau_{oct}$ and $\tau_{oct} / \sigma_m$	96
2.22	Incremental Volumetric Strain Curves	97
2.23	Yield Loci for Loose Samples	98
2.24	Procedures for Establishing the Process of Pore Pressure Development	99
3.1	Torsional Simple Shear Device ( TSSD )	100
3.2	Sample Shape of the Torsional Simple Shear Device	101
3.3	Cyclic Loading and Recording System	102
3.4	Water Supply and Sample Saturation System	103
3.5	Grain Distribution of Ottawa Sand	104
3.6	Non-uniform Cyclic Loading Patterns	105
4.1	Illustration of Pore Pressure Rise during Uniform Cyclic Loading	106
4.2	Definitions of Initial Liquefaction	107
4.3	Definition of Residual Pore Pressure	108
4.4	Incremental Rise of Pore Pressure in each Cycle ( Loose Sand )	109
4.5	Relationship Between Incremental Rise of Pore Pressure and Number of Cycles ( Loose Sand )	110

LIST OF FIGURES (continued)

<u>FIGURE</u>		<u>PAGE</u>
4.6	Comparison between Predicted and Experimental Pore Pressure Rise during Uniform Cyclic Loading	111
4.7	Incremental Rise of Pore Pressure in Each Cycle ( Medium Dense Sand )	112
4.8	Incremental Rise of Pore Pressure in Each Cycle ( Dense Sand )	113
4.9	Relationship between Incremental Rise of Pore Pressure and Number of Cycles ( Medium Dense Sand )	114
4.10	Relationship between Incremental Rise of Pore Pressure and Number of Cycles ( Dense Sand )	115
4.11	Variation of Parameters $C_1$ , $C_2$ , $C_3$ and $S$ with Density	116
4.12	Variation of $\phi'$ with Density	117
4.13	Comparison between Predicted and Experimental Results of Initial Liquefaction	118
4.14	Comparison of Pore Pressure Rise at Initial Liquefaction Determined by Two Different Definitions	119
4.15	Comparison between Predicted and Experimental Results of Complete Liquefaction	120
4.16	Comparison between Predicted and Measured Pore Pressure Rise Under Non-uniform Cyclic Loading	121
4.17	An Example of Time History of Actual Earthquake	131
4.18	Illustration of Pore Pressure Rise During Half-cycle of Loading	132

## LIST OF FIGURES (continued)

<u>FIGURE</u>		<u>PAGE</u>
4.19	Predicted Pore Pressure Rise during Actual Time History of an Earthquake	134
4.20	Typical Liquefaction Data for a Low $\bar{B}$ and High $\bar{B}$ Value	135
4.21	Pore Pressure Rise at the End of the First Cyclic Loading	136
4.22	Effect of $\bar{B}$ Values on Liquefaction Potential	137
4.23	Relationship between the $\bar{B}$ Values and the Initial Degree of Saturation (back pressure $u_b = 5\text{psi}$ )	138
4.24	Relationship between the $\bar{B}$ Values and the Initial Degree of Saturation (back pressure $u_b = 45\text{psi}$ )	139
4.25	Effect of the Initial Degree of Saturation on Liquefaction Potential	140

## LIST OF PLATES

<u>PLATE</u>		<u>PAGE</u>
I	Torsional Simple Shear Device (TSSD)	141
II	TSSD Base with Sample and Pickups	142
III	MTS Control Panel	143

## ACKNOWLEDGMENT

The authors gratefully acknowledge the financial support of the National Science Foundation, which made this investigation possible.

## CHAPTER 1

### INTRODUCTION

When a loose saturated sand is subjected to cyclic shear stress such as induced by earthquakes, its volume decreases, and if the drainage is prevented, the relaxing soil skeleton transfers some or all of its load to pore water. The load transfer causes a rise in the pore pressure and when the pore pressure becomes equal to the total normal pressure, the sand loses all its shear strength and liquefies. The shear strength  $\tau_f$  is given for sands by the following expression:

$$\tau_f = \sigma' \tan \phi' \quad (1.1)$$

in which  $\sigma'$  is the effective stress and  $\phi'$  is the effective angle of internal friction. Since the effective stress  $\sigma'$  is the total normal pressure  $\sigma$  minus the pore pressure  $u$ , Eq. 1.1 reduces to,

$$\tau_f = (\sigma - u) \tan \phi' \quad (1.2)$$

In Eq. 1.2, as the pore pressure rises the shear strength  $\tau_f$  decreases. In the extreme case where the pore pressure rises to such an extent that the effective normal stress becomes zero, the shear strength also becomes zero and this state is referred to as liquefaction.

The term "liquefaction" was used by Casagrande (2) for the first time to explain the state of loose saturated sands where flow slides occur under monotonic loading. Since then, it has been shown in the laboratory that pore pressure also rises during cyclic loading in medium dense and dense

sands (23, 30) . It has also been observed that pore pressures in the soil specimens continue to rise, resulting in the decrease of effective normal pressures, and increase in large deformations even under constant cyclic stresses. It is known that during static loading the volume of loose samples decreases while the volume of dense samples with void ratios above the critical value increases at high strain levels, resulting in the negative pore pressure rise and stiffening of the samples. On the other hand, during cyclic loading both loose and dense samples show a similar pore pressure rise tendency which indicates that the volume tends to decrease in loose and even in dense sands under undrained condition. This difference in pore pressure rise tendency during static and cyclic loading is due to the cyclic effect.

Castro (3) proposed the term "cyclic mobility" to describe gradual increase in pore pressure rise during cyclic loading as distinct from the term "liquefaction" originally used by Casagrande. It is convenient, however, to generally use the term liquefaction for any kind of granular materials of any density to express the state when the gradual increase in pore pressure during loading results in a large deformation due to the loss of strength.

Liquefaction phenomenon was observed during many large earthquakes, notably during Niigata earthquake and Alaska earthquake in 1964. In Niigata, severe damage to buildings due to settlement and tilting were caused by liquefaction of sand deposits around the Shinano river (18). In the Alaska earthquake, widespread damage resulting from landslides was also found to be intensified by the liquefaction of buried seams of saturated sandy soils(28).

In order to analytically evaluate the liquefaction potential of sand deposits during earthquakes, many researchers ( 5, 11, 33, 42, 47 ), notably Seed and his colleagues (33) started investigations using laboratory cyclic

loading tests. The principle of the cyclic loading tests in the laboratory is to subject representative soil samples to loading conditions similar to those encountered in the field during earthquakes. Since laboratory tests adopted very simplified test conditions such as uniform cyclic loading and completely saturated samples, there still remain lack of informations about:

- (1) effect of the degree of saturation on the liquefaction potential
- (2) pore pressure rise during the actual earthquake

When the liquefaction analysis is extended to general engineering structures such as embankments, dams and backfills, the material in question may or may not be completely saturated and the design procedure using test data for completely saturated sands will lead to a very conservative and expensive design.

It is known that dynamic properties of sands such as shear modulus and damping are highly dependent on the amplitude of effective normal pressure (or confining pressure) and strain level ( 10, 12, 43 ), therefore the appropriate evaluation of these properties during earthquakes requires the complete description of the pore pressure rise at any stage of earthquake loading.

Recently analytical methods have been developed in the laboratory to express the progressive pore pressure increase under randomly loading condition such as those imposed during earthquakes ( 17, 26 ). These analytical methods are based on the stress-deformation relationships exhibited by the soil during laboratory drained cyclic loading and the drained deformation characteristics are transferred into pore pressure rise in undrained condition. The accuracy of pore pressure prediction by these analytical methods depends on the accuracy with which the deformations, especially the volume changes are measured and requires a number of tests to determine those

characteristics with the required degree of accuracy.

There is an urgent need therefore that a simple and dependable pore pressure predicting method be developed and that such a method be also easily applicable to different types of soil through a reasonable number of tests. This research was undertaken to meet the above need and thus focused on the following aspects of sand liquefaction.

- (1) determination of the major factors that govern the incremental rise in pore pressure during dynamic loading.
- (2) establishment of a simple pore pressure predicting method by means of a direct measurement of pore pressure during cyclic loading.
- (3) evaluation of the effect of the degree of sample saturation on the liquefaction potential.

The data shown and the discussions presented in CHAPTER 4 show the extent to which the above objectives have been realized.

## CHAPTER 2

### PREVIOUS STUDIES ON SOIL LIQUEFACTION

#### 2-1 Field Investigations into the Liquefaction Potential of a Deposit during Earthquakes

Based on case histories in Japan, attempts have been made to establish empirical rules for predicting the liquefaction potential of soil deposits during earthquakes.

Koizumi (20) examined the boring data from 20 locations in the Niigata area before and after the Niigata earthquake in an effort to determine the changes in soil density due to the earthquake. He used standard penetration  $N$  values as indication of density changes. Koizumi found the existence of a critical standard penetration value,  $N_{cr}$ , at various depths, at which no change in standard penetration  $N$  value occurred even when the deposit is subjected to an earthquake. Below and above the critical  $N_{cr}$  value, the  $N$  values for the sand deposit would either increase or decrease thus indicating either contraction or expansion.

Koizumi proposed a curve which relates  $N_{cr}$  value to the depth of overburden as shown in Fig. 2.1. The volume contraction in the saturated sandy deposit causes a pore pressure rise which decreases the effective stress in the soil, eventually leading to liquefaction when the effective stress approaches a zero or near zero value. In view of this, Koizumi concluded that the  $N_{cr}$  curve could be regarded as a criterion for soil liquefaction.

Ohsaki (29) compared the actually measured standard penetration  $N$  values of the sites, where a damage to buildings occurred, with the critical

$N_{cr}$  values, and found the results shown in Fig. 2.2 . Between the points a and b in Fig. 2.2, the actually measured standard penetration N values are below the  $N_{cr}$  curve and it is conceivable that the hatched part in Fig. 2.2 may liquefy during earthquake loading. He referred to the points a and b respectively as the upper and lower limits of liquefaction. Based on the upper limit,  $H_u$  , and the lower limit,  $H_l$  , concepts, he surveyed the damaged buildings during the Niigata earthquake in 1964 and found that the soil conditions at the sites where severe building damages occurred fell within a certain range as shown in Fig. 2.3. The implications of the critical range in Fig. 2.3 are such that the severeness of the damages due to liquefaction depends both on the depth of the upper limit,  $H_u$  , and the thickness of the zone between  $H_u$  and  $H_l$  . That is, points  $P_1$  and  $P_2$  in Fig. 2.3 have the same depth  $H_u$  , however, the thickness of the liquefaction zone, indicated by the vertical distance from the point to 45 degree line, are different and only  $P_2$  falls within the critical range. On the otherhand,  $P_2$  and  $P_3$  have the same thickness as the zone of liquefaction, however,  $P_3$  has a greater  $H_u$  indicating greater overburden pressure and that  $P_3$  does not fall within the critical range.

Kishida ( 19 ) examined the characteristics of liquefied sands and concluded that sandy soils, satisfying the following conditions are susceptible to liquefaction if the ground water table is near the ground surface :

- (1) gradation characteristics,  $0.074 \text{ mm} < D_{50} < 2.0 \text{ mm}$   
 $U_c < 10$
- (2) effective overburden pressure less than 2 kg/sq.cm
- (3) relative density less than 75 %

Based on a number of grain size tests on sands that did liquefy during actual earthquakes, envelopes of grain distribution curves such as the ones

shown in Fig. 2.4 were obtained. In Fig. 2.4, the envelope of soils found most likely to liquefy in the laboratory is also superimposed on the field data.

Seed et al ( 35, 37 ) developed a procedure to convert the irregular series of earthquake-induced cyclic stresses to an equivalent series of uniform stress cycles using a weighting technique so that this equivalent series may be compared directly with laboratory test data obtained under uniform cyclic stress conditions. In this method, the equivalent number of uniform stress cycles is evaluated on the basis of 65 % of the highest shear stress observed in the series of irregular stresses. Since this technique was a result of the investigation in a large number of actual earthquake patterns, it is also possible to correlate the equivalent number of cycles to the local magnitude of earthquake magnitudes. Based on the relationship between the equivalent number of cycles and the local earthquake magnitudes as shown in Fig. 2.5, Seed et al proposed an equivalent number of uniform stress cycles for different earthquake magnitudes ( 37 ).

<u>Earthquake Magnitude</u>	<u>Equivalent Uniform Cyclic Stress</u>	<u>Equivalent number of Uniform Stress Cycles</u>
7	$0.65\Delta\tau_{max}$	10
$7\frac{1}{2}$	$0.65\Delta\tau_{max}$	20
8	$0.65\Delta\tau_{max}$	30

Evaluation of liquefaction potential of a deposit at a certain depth can be accomplished by comparing the cyclic stress causing liquefaction at equivalent number of stress cycles in the laboratory and the equivalent uniform cyclic stress determined from dynamic analysis as in Fig. 2.6. It is seen in Fig. 2.6 that when the earthquake stresses exceed the ones that cause liquefaction in the laboratory tests ( shaded zone ) then liquefaction

during a selected earthquake is a possibility. Note that the zone of liquefaction predicted by this method is similar in shape to those obtained by Ohsaki in Fig. 2.2 .

While field investigations provide useful criteria as guidelines for preliminary site evaluation of liquefaction potential, they are not sufficient for determining the time history of pore pressure built-up or response. Time history of pore pressure built-up is required for the dynamic analysis of important engineering structures such as high-rise buildings and nuclear power plants.

## 2-2 Laboratory Studies on the Liquefaction Potential of Saturated Sands

### (1) In-situ Stress Condition during Earthquakes

During earthquakes, a soil element in a deposit is deformed by a system of dynamic stresses as a result of seismic waves passing through the soil medium. It is known that the most significant set of stresses are caused by the propagation of shear waves from the bedrock to the ground surface. For a horizontal soil deposit on a horizontal bedrock formation the stress system during earthquakes can be idealized as shown in Fig. 2.7. Before the earthquake, the soil element is subjected to the principal stresses  $\sigma'_v$  and  $K_0 \sigma'_v$  in which  $K_0$  is the coefficient of earth pressure at rest as is seen in Fig. 2.7 (a). During the earthquake, the element will be deformed by the shear stress  $\tau_{hv}$  as shown in Fig. 2.7 (b) and the resulting stress condition is seen in Fig. 2.7 (c). These stress conditions are illustrated on the Mohr's diagram as shown in Fig. 2.8. It is noted in Fig. 2.8 that the earthquake imposed shear stress  $\tau_{hv}$

causes a rotation in principal planes ( $\frac{\alpha}{2}$  degrees in Fig. 2.8 ).

Finn (7) summarized the static and dynamic conditions that prevail within the soil deposit during an earthquake as follows :

- " (a) the initial principal effective stress system is  $\sigma'_v$  vertically, and  $K_0 \sigma'_v$  horizontally (  $K_0 \approx 0.4$  )
- (b) shear stresses are generated on the horizontal and vertical plane
- (c) deformations under cyclic loading occur in plane strain with no drainage of water
- (d) as a consequence of (b) the principal stresses rotate under cyclic loading during an earthquake. "

## (2) Laboratory Cyclic Loading Tests

There are four types of laboratory tests that are currently used in sand liquefaction studies.

These are :

- (a) cyclic triaxial test
- (b) cyclic simple shear test
- (c) cyclic torsional shear test
- (d) shake table test

Although these laboratory tests have been developed to simulate the field stress conditions of a soil element during an earthquake, most of these tests have advantages and disadvantages resulting from the boundary conditions, the geometry of the sample and the type of stresses applied on the sample. In the following paragraphs, the advantages and disadvantages of each of the above test are briefly discussed.

(A) Cyclic triaxial tests

The cyclic triaxial test was originally developed by Seed and Lee (33) to study the factors affecting the liquefaction of saturated sands under cyclic loading conditions. In this test a saturated cylindrical sample is consolidated under an effective ambient pressure  $\sigma'_c$ . All drainage is prevented and the sample is then subjected to cyclic axial stress changes,  $\pm\Delta\sigma_d/2$ . The stress conditions developed during this loading procedure are shown in Fig. 2.9. It is seen in Fig. 2.9 that the shear stress reaches the maximum value of  $\Delta\sigma_d/2$  on  $45^\circ$  plane through the sample when the effective ambient stress remains  $\sigma'_c$ .

There are four main theoretical objections to the suitability of the triaxial test for investigating the liquefaction problem :

- (a) the ratio between initial vertical and horizontal principal stresses is unity:  $K_0 = 1$  instead of actual field  $K_0$  values.
- (b) deformations do not occur in plane strain.
- (c) the principal stresses do not rotate during testing as in the field.
- (d) cylindrical sample shape can not be maintained during cyclic stress application especially when the deformation becomes large.

The effect of these limitations of the triaxial type tests are likely to cause test specimens to liquefy at stress levels higher than those which would be required under the corresponding field conditions ( 30, 34 ).

(B) Cyclic simple shear tests

The cyclic simple shear test - Roscoe type (31) was developed to overcome the theoretical objections to the triaxial tests ( 6, 30, 34 ). In this test, a soil sample of rectangular cross-section is confined in a

shear box with rigid sides. It is then consolidated one-dimensionally under a vertical stress of  $\sigma'_v$ . During testing drainage is prevented and a cyclic shear stress is applied to the top and bottom of the sample. During shear stress application, two sides of the shear box rotate in such a way as to produce the uniform shear strain condition throughout the sample. Thus the test appears to simulate closely the conditions in the field when horizontal deposit is shaken by shear waves propagating upwards. The test results obtained by Seed and Peacock (34) and Peacock and Seed (30), however, showed that the shear stresses required to cause liquefaction were quite low compared to the estimated field data. They explained this discrepancy resulted from the non-uniform stress and strain distribution inside the sample due to the boundary conditions such as wall frictions, leading to premature liquefaction and thus to the underestimation of the shear stresses to cause liquefaction.

(C) Cyclic torsion tests

The triaxial torsion shear apparatus was developed by Ishihara and Li (14) in which cyclic torsional stress is applied to both ends of the cylindrical sample that is similar to the sample in cyclic triaxial tests. Since the vertical and horizontal stresses are controllable independently, the arbitrary combinations of the vertical and horizontal stresses, that is, the arbitrary  $K_0$  condition can be produced. The main shortcoming of this device was the apparent non-uniform strain distribution inside the sample varying from the maximum value at the outside of the specimen to zero strain along the vertical axis through the center of the specimen. This was, however, improved by adopting the hollow cylindrical shape for the specimen (16). The ring-shaped torsional shear device developed by

Yoshimi et al (47) eliminates the nonuniformity in strain distribution by adopting an unique sample shape having the constant ratio of the sample height to the radius of the specimen. This device, however, has the same difficulty in side boundaries as was seen in simple shear type tests since the ring-shaped torsional shear device adopts a special container to prevent the lateral deformations.

Recently Ishibashi and Sherif (11) developed an unique device called "Torsional Simple Shear Device (TSSD)" which possesses both advantages found in the triaxial torsion shear device and the ring-shaped torsional shear device. That is, in this device, the triaxial type cell and the sample shape having the constant ratio of the sample height to the radius are used to permit the uniform strain distribution inside the sample ( 11, 13, 22 ) and also the test can be conducted under arbitrary  $K_0$  condition. The plane strain condition during cyclic shear loading can be achieved by adopting the technique so called "closed system", in which the entry of the water into cell is totally prohibited during tests.

#### (D) Shake table tests

The first laboratory investigation of liquefaction under vibratory loading conditions employed various size of shake tables ( 27, 45, 46 ). These tests generally consisted of placing saturated sand in a box or tank on a shake table and measuring the horizontal table acceleration at which liquefaction occurred. These values were related directly to field measured accelerations. In shake table tests, it was found that the size and geometry of the container have a significant effect on the test results and should be selected so as to satisfy free field soil behavior, i.e., to eliminate non-representative boundary restraints (21). For this purpose,

fairly large samples, 7'-6" long by 3'-6" wide and 4 inches thick (38); 6' long by 1'-6" wide and 7 inches thick (7,8), have been used for the liquefaction study using shake tables. It is likely that meaningful data will result from shake table tests if the uniform placement of the sample in the container and the measurements inside the sample are appropriately performed.

### (3) Factors Influencing Liquefaction of Saturated Sands

Based on cyclic loading tests performed in laboratories, there are four major factors that influence the resistance to liquefaction of a saturated sand, these are:

- (a) void ratio or relative density of the sand
- (b) intensity of cyclic shear stress
- (c) duration of cyclic load or number of cycles of load application
- (d) the initial effective confining pressure

Factors (b) and (d) can be combined. That is, the ratio of the cyclic shear stress to the initial effective confining pressure is considered as an independent variable.

In the following paragraphs a discussion of the factors influencing the liquefaction of sands will be given. These include, void ratio, stress ratio, the number of cycles and the stress or strain history.

#### (A) Void ratio or relative density

Laboratory tests have verified that the lower the relative density (or the higher the void ratio of a soil), the more easily a sample will liquefy. The relative density  $D_r$  is defined as :

$$D_r = \frac{e_{\max} - e}{e_{\max} - e_{\min}}$$

where  $e$  = void ratio

$e_{\max}, e_{\min}$  = maximum and minimum void ratios

Relative density expresses the denseness of a sand and it is widely used as a basis for comparing the liquefaction potential of different sands of approximately the same mean grain size.

Fig. 2.10 shows a typical result indicating the effect of relative density on the liquefaction potential of a sand. These results were obtained by using cyclic simple shear tests (4). Similar results were obtained by using cyclic simple shear tests (6,30) and triaxial type tests (23).

(B) The stress ratio and the number of cycles

The ratio of cyclic shear stress to the initial effective confining stress has proven to be a useful expression for presenting the combined effect of both static and cyclic stresses on liquefaction potential. Fig. 2.11 shows typical test results obtained by using cyclic simple shear test device. It is seen in Fig. 2.11 that the number of cycles to cause liquefaction increases with the decrease in the initial effective stress ratio. The same tendency were obtained in the triaxial tests (23), torsional tests (11, 14, 47) and in shake table tests (7,38). Among these tests, two different stress ratios are used, which are  $\Delta\sigma_d/2\sigma'_c$  for triaxial type tests and  $\tau_{hv}/\sigma'_v$  for simple shear and torsional type tests. The former ratio indicates the ratio of the cyclic shear stress on 45° plane to the effective ambient stress  $\sigma'_c$  and the latter indicates

the ratio of the applied shear stress  $\tau_{hv}$  to the effective vertical stress  $\sigma'_v$ . Finn et al (6) proposed to use the mean effective principal stress  $(\sigma'_v + K_0 \sigma'_v)/2$  as the effective confining pressure in simple shear type tests. Since the mean effective principal stress indicates the normal stress on  $45^\circ$  plane, it is now possible to compare the results obtained by different type of test devices on the same basis. Fig.2.12 shows the comparison of two stress ratios at a given number of cycles to cause liquefaction determined by the cyclic simple shear tests and the cyclic triaxial tests. It is seen in Fig. 2.12 that the ratio of two stress ratios at any given number of cycles to cause liquefaction becomes unity when using the mean effective principal stress. And thus, Finn et al concluded that the ratio of cyclic shear stress to the effective mean principal stress is an independent variable for expressing the liquefaction potential irrespective of the type of test devices used.

(C) Initial principal effective stress ratio  $K_0$

As discussed in section 2-2(1), the actual stresses that act on a soil element during an earthquake are the vertical effective stress  $\sigma'_v$ , the horizontal effective shear stresses  $K_0 \sigma'_v$  and the shear stresses in plane strain condition.

The effect of the initial effective stress ratio  $K_0$  on the liquefaction potential was examined successfully by using torsional simple shear tests (11, 15). In this type of test, an arbitrary combination of the vertical and the horizontal stresses and thus an arbitrary  $K_0$  condition can be produced by adopting the same diameter of vertical loading shaft as the specimen diameter. A technique called the "closed-system experiment", where the total volume of the water inside the chamber is kept constant

throughout the experiment, assumes the plane strain condition.

Ishihara, et al (15) compared the test results of pore pressure rise and liquefaction in the isotropically consolidated soil ( ICT-test,  $K_0 = 1$ , triaxial test ) and the anisotropically consolidated laterally confined soil ( ACOT-test,  $K_0$  variable, simple shear test ). From these studies, they concluded that the pore pressure at liquefaction in the ACOT-test consists of the contributions from cyclic loading and from a gradual increase in lateral pressure while in ICT-test, only the cyclic nature of stress change is responsible for the development of pore pressure. Based on the above evidence, Ishihara et al derived the following interrelationships between ACOT-test and ICT-test regarding the pore pressure rise and liquefaction.

$$\frac{\tau_{vh}}{\sigma'_v} = \left( 1 - \frac{U_k}{\sigma'_v} \right) \left( \frac{\Delta\sigma_d}{2\sigma'_v} \right) \quad (2.1)$$

where  $\frac{\tau_{vh}}{\sigma'_v}$  = initial stress ratio in ACOT-test to cause liquefaction at  $N_L$  cycle

$\frac{\Delta\sigma_d}{2\sigma'_v}$  = initial stress ratio in ICT-test to cause liquefaction at  $N_L$  cycle

$U_k$  = pore pressure rise in ACOT-test due to an increase in mean principal stress and a decrease in deviator stress

Eq. 2.1 can be expressed in the following manner by introducing the

effective octahedral stress  $\sigma'_{\text{oct}}$  and the maximum change in the shear stress during cyclic loading,  $\Delta\tau_{\text{max}}$  :

For ICT-test ( triaxial type )

$$\begin{aligned}\sigma'_{\text{oct}} &= \sigma'_v \\ \Delta\tau_{\text{max}} &= \frac{\Delta\sigma_d}{2}\end{aligned}$$

For ACOT-test ( simple shear type )

$$\begin{aligned}\sigma'_{\text{oct}} &= \frac{1 + 2K_0}{3} \cdot \sigma'_v \\ \Delta\tau_{\text{max}} &= \tau_{vh}\end{aligned}$$

Therefore Eq. 2.1 becomes

$$\left( \frac{\Delta\tau_{\text{max}}}{\sigma'_{\text{oct}}} \right)_{\text{ACOT}} = \frac{3}{1 + 2K_0} \left( 1 - \frac{U_k}{\sigma'_v} \right) \left( \frac{\Delta\tau_{\text{max}}}{\sigma'_{\text{oct}}} \right)_{\text{ICT}} \quad (2.2)$$

Experimental results showed that  $(1 - U_k / \sigma'_v)$  measurements for various  $K_0$  values were nearly equal to  $\frac{1 + 2K_0}{3}$  irrespective of the variation in the void ratio of the sample. Thus, Eq. 2.2 leads to the following relationship :

$$\left( \frac{\Delta\tau_{\text{max}}}{\sigma'_{\text{oct}}} \right)_{\text{ACOT}} = \left( \frac{\Delta\tau_{\text{max}}}{\sigma'_{\text{oct}}} \right)_{\text{ICT}} \quad (2.3)$$

Eq. 2.3 indicates that the variable  $\Delta\tau_{\max} / \sigma'_{\text{oct}}$  is unique for determining the liquefaction potential of sand under isotropically and anisotropically consolidated conditions. This conclusion is significant since it proves that the test results of the ICT-test can be easily converted to the ACOT-test condition with arbitrary  $K_0$  value, which simulates most closely the field behavior of a soil element during an earthquake.

Ishibashi and Sherif (11) conducted both ICT-test and ACOT-test in the Torsional Simple Shear Device developed at the University of Washington and examined the effects of the initial  $K_0$  values on the liquefaction potential. The test results obtained by them confirmed the uniqueness of the  $\Delta\tau_{\max} / \sigma'_{\text{oct}}$  ratio in determining the liquefaction potential of a sand for different  $K_0$  conditions as shown in Fig. 2.13.

#### (D) Stress or strain history

It has been assumed that the resistance to liquefaction of a sand under cyclic loading is a function of its current void ratio, effective confining stress and intensity of cyclic stress. The previous stress or strain history of a sand has not yet been considered. It is apparent, however, that the previous stress or strain history affects the subsequent deformation characteristics of a sand. Fig. 2.14 illustrates a typical example of the stress strain relationship during the loading and reloading process. It is seen that during the reloading process the plastic strain is apparently smaller compared to the plastic strain that follows the virgin stress-strain curve. This indicates the effect of stress or strain history on the subsequent pore pressure rise in undrained condition.

Finn et al ( 5) examined the effects of previous liquefaction and quasistatically induced shear strains on the resistance of a sand to

liquefaction potential. The significant findings derived from their study of Ottawa sand are summarized below:

- (a) Previous liquefaction leads to a considerable decrease in the resistance of the sample to reliquefaction. Fig. 2.15 shows the comparison of the number of cycles to cause liquefaction at a given stress condition, which is expressed as  $N_L$  for a virgin sample ( with no strain history ) and  $N_R$  for a previously liquefied sample with strain history respectively. It is clear from Fig. 2.15 that  $N_R$  is considerably smaller than the  $N_L$  of the virgin sample at a given void ratio.
- (b) Partial liquefaction, on the other hand, in which the strains are quite small, leads to a considerable increase in the resistance of a sand to a subsequent reliquefaction. Fig. 2.16 shows the effect of partial liquefaction on pore pressure rise during the subsequent liquefaction test. In Fig. 2.16, a sample is subjected to cyclic loading until the pore pressure reached  $1.0 \text{ kg/cm}^2$  and then the pore pressure is released and cyclic loading is again applied on the same sample. It is seen in Fig. 2.16 that the pore pressure rise during the subsequent loading is smaller than that of the virgin sample although a slight difference in void ratio of both samples exists due to the soil consolidated or reduction of pore pressure at the beginning of the subsequent loading.
- (c) Strains caused by static stresses have a similar effect on the resistance to reliquefaction in cyclic loading tests. That is, a statically pre-strained sample shows higher resistance to liquefaction compared to a virgin sample during cyclic loading.

Finn et al explained these changes in the resistance to liquefaction as the results of new structures that are created in the original sample due to the strain history. A strain history when the strain is below the threshold value results in a better interlocking of particles in the original structure. The type of new structure created by shear strains above the threshold value may be a uniform structural arrangement which is particularly weak in resisting cyclic shear loads. It is also pointed out that the shear strains may develop a non-uniform structure leading to non-uniform deformations.

This non-uniformity of the sample clearly explains the reduction in the resistance to liquefaction of the previously liquefied sample because in the simple shear test a severe stress concentration will result along the side walls, especially when the cyclic strain is large such as during liquefaction.

Seed et al (38) conducted a large scale liquefaction test using a shaking table to eliminate the boundary effects associated with tests on small-scale samples.

The samples were subjected to a series of small shocks designed to represent the effects of a series of small magnitude (about 5) earthquakes. The pore pressure built-up during each small shock was allowed to dissipate and the sample was reconsolidate under the initial effective overburden pressure. Finally after 5 or 6 small shocks, the sample was subjected to a large shock to determine the stress conditions required to cause liquefaction. Fig. 2.17 shows a typical result obtained from the above large scale test. It is seen in Fig. 2.17 that small seismic histories result in increase in the resistance of the sample to subsequent liquefaction. On the basis of these results, Seed et al reached the same

conclusion as Finn et al while the cyclic strains are small. They also pointed out the importance of the method of sample preparation. Samples that are subjected to vibration during sample preparation show higher resistance to liquefaction compared to the samples that are not vibrated. Fig. 2.18 shows the relationships between the applied stress ratio and the number of cycles required to cause liquefaction for samples with no previous vibration history and for samples subjected to low levels of vibration during sample preparation process. It is seen in Fig. 2.18 that the number of cycles required to cause liquefaction of the samples with vibration history always higher than those of the samples that have not been subjected to initial vibration.

(E) Frequency and wave form of cyclic loading

Although the frequency components of seismic waves are spread over a wide range, the predominant frequency of shear waves propagated from the bedrock falls within a rather narrow range of 1 to 10 Hz depending on the site characteristics (25).

Laboratory tests using the triaxial type tests(30) and torsional type tests (47) proved that the effect of the frequency of uniform cyclic loading is insignificant over a range of 1/6 Hz to 12 Hz. The test results obtained by Yoshimi et al (47) using torsional type tests are shown in Fig. 2.19. It is clear in Fig. 2.19 that the effect of frequency on the liquefaction potential is negligible. It is interesting to note that these results coincide with the fact that dynamic properties of sands such as shear modulus and damping are also frequency independent (10, 48).

Typical wave forms used in the laboratory cyclic loading tests are shown in Fig. 2.20. The effect of the difference in the wave forms on the

pore pressure rise or liquefaction has not been analyzed quantitatively yet. It is considered, however, that the effect will be small since the liquefaction data obtained by different groups using different wave forms show a reasonable agreement when compared under the same stress conditions.

#### (4) Summary

Four laboratory cyclic loading tests have been developed in an effort to simulate the field loading conditions subjected to a soil element during earthquake as shown in Figs. 2.7 and 2.8. Among these tests, cyclic torsional test will better duplicate the field stress or strain conditions by eliminating those limitations as boundary effects in cyclic simple shear test or large sample deformation in cyclic triaxial test. Shake table test will also provide means for advancing the state of knowledge of liquefaction, using large samples to minimize boundary effects.

The major factors that affect the occurrence of liquefaction of a soil are void ratio (or relative density), stress ratio  $\tau/\sigma'_c$  (or  $\Delta\tau_{\max}/\sigma'_{\text{oct}}$ ), number of stress cycles and stress or strain history. The higher is the void ratio (or the lower is the relative density), the more easily a sample liquefies as shown in Fig. 2.10. As for the magnitude of stress ratio and the number of stress cycles, all studies showed of course that the higher are these forcing functions, the easier it is to cause liquefaction. Two research groups (5, 38) proved that the strain history prior to cyclic loading leads to a reduction in liquefaction potential as long as the strain amplitude is small enough not to cause liquefaction. The previously liquefied samples, however, showed higher liquefaction potential compared to the original samples. These changes in the resistance to liquefaction was explained as the results of new structures that are created in the original samples (5).

## 2-3 Prediction of Pore Pressure Rise in Saturated Sands during Earthquakes

Since liquefaction occurs at the extreme stage of the gradual increase in pore pressure during dynamic loading, the prediction of pore pressure becomes an essential problem in liquefaction study.

The methods to predict pore pressure rise during randomly excited loading such as during earthquakes were developed quite recently (17,26).

The prediction techniques of pore pressure rise including liquefaction potential can be categorized into two groups, namely, the empirical approach and the analytical approach as described in the following paragraphs.

The empirical approach includes the direct analysis of the pore pressure rise during cyclic loading and reaches to the prediction of the pore pressure rise and the evaluation of liquefaction potential under irregular time history of shear stress application. Analytical approach combines the following characteristics of a sand during cyclic loading and arrives at the prediction of the pore pressure rise under irregular time history of shear stress application.

- (a) stress-dilatancy relationship including the effect of strain or stress history in drained condition
- (b) volume change - pore pressure rise relationship in undrained condition
- (c) combination of (a) and (b) leads to the stress - pore pressure rise relationship in undrained condition

### (1) Empirical Approach

Shibata et al (42) analyzed the pore pressure increment obtained from uniform cyclic triaxial tests. They found that there exists a linear

relationship between the pore pressure increment divided by the octahedral shear stress,  $\Delta u / \tau_{\text{oct}}$ , and the octahedral shear stress divided by the mean principal stress,  $\tau_{\text{oct}} / \sigma_m$ , as shown in Fig. 2.21 .

On the basis of these results, they derived the following equation to express the increment in pore pressure during each loading cycle.

$$\frac{\Delta u}{\tau_{\text{oct}}} = a \left\{ \left( \frac{\tau_{\text{oct}}}{\sigma_m} \right) - \left( \frac{\tau_{\text{oct}}}{\sigma_m} \right)_c \right\} \quad (2.4)$$

where  $\Delta u$  = the increment in pore pressure during each loading cycle

$\tau_{\text{oct}}$  = the octahedral shear stress

$\sigma_m$  = mean principal stress

$a$ , and  $\left( \frac{\tau_{\text{oct}}}{\sigma_m} \right)_c$  = coefficients

Eq. 2.4 was applied to predict the pore pressure rise during irregular cyclic loading including the actual time history of the Niigata earthquake. Shibata et al stated, however, that there still remains uncertainties in the physical meanings of the coefficients, included in Eq. 2.4 .

Shibata also points out that there was no consideration of the effects of stress history on the pore pressure rise. Stress history is very important especially when relating the results obtained from uniform cyclic loading to the irregular cyclic loading conditions.

## (2) Analytical Approach

Analytical approach relates volume change characteristics of the sample in undrained condition to pore pressure rise due to the compressibility of the water in undrained condition. This relationship is generally expressed as follows :

$$\frac{n \cdot \Delta u}{K_w} = f \left( \frac{\Delta V}{V_o} \right) \quad (2.5)$$

where

- $n$  = porosity of the sample
- $\Delta u$  = increase in the residual pore pressure at the end of each stress cycle
- $K_w$  = bulk modulus of water
- $\Delta V/V_o$  = volumetric strain of the sample at the end of each stress cycle

Based on the above, Martin et al (26) derived the following equation expressing the relationship between pore pressure rise in the undrained condition and volume change in the drained condition.

$$\frac{n \cdot \Delta u}{K_w} = \Delta \epsilon_{vd} - \Delta \epsilon_{vr} \quad (2.6)$$

and

$$\Delta \epsilon_{vr} = \Delta u / \bar{E}_r$$

where

- $\Delta \epsilon_{vd}$  = total volumetric strain of sand structure
- $\Delta \epsilon_{vr}$  = recoverable volumetric strain of sand structure

$\bar{E}_r$  = tangent modulus of the one-dimensional unloading curve at a point corresponding to the initial vertical effective stress

Solving Eq. 2.6 for  $\Delta u$ ,

$$\Delta u = \frac{\Delta \epsilon_{vd}}{\frac{1}{\bar{E}_r} + \frac{n}{K_w}} \quad (2.7)$$

In order to obtain the total volumetric strain  $\Delta \epsilon_{vd}$  per cycle including the effect of the strain history, Martin et al (26) conducted a series of uniform cyclic triaxial tests and obtained the results shown in Fig. 2.22. It is noticeable in Fig. 2.22 that the effect of the strain history on the incremental volumetric strain per cycle is expressed by the total volumetric strain existing prior to the corresponding cycle. For computational purposes, they fitted the family of curves in Fig. 2.22 by the following expression.

$$\Delta \epsilon_{vd} = D_1 ( \gamma - D_2 \epsilon_{vd} ) + \frac{D_3 ( \epsilon_{vd} )^2}{\gamma + D_4 \epsilon_{vd}} \quad (2.8)$$

where

$\epsilon_{vd}$  = total strain existing prior to the cycle

$\gamma$  = cyclic shear strain amplitude

$D_1, D_2, D_3$  and  $D_4$  = material constants

Combining Eqs. 2.7 and 2.8 reveals that the incremental pore pressure rise per cycle is affected by the residual pore pressure existing prior to the cycle, which itself is affected by the strain history.

Ishihara et al (15, 17) performed both drained and undrained cyclic tests to establish the deformation model of sand including the stress-dilatancy and stress-strain relationship. By observing the subsequent yield points during re-loading process, they came to the following conclusions.

- (a) Yield loci in  $p'$ - $q$  plane can be uniquely determined irrespective of the stress history to which the sample has previously been subjected. The yield loci are interpreted as the curve at which yielding begins whenever stresses are altered across it. And when stresses are changed in the lower side of the currently effective locus, the associated deformation is elastic.

Fig. 2.23 shows the yield loci in the compression region.

- (b) The yield loci in the compression or extension region is independent of the stress history in the opposite region.

The above mentioned results are well represented by the illustration of the stress paths during undrained cyclic loading, which is shown in Fig. 2.24. In Fig. 2.24, the stress path from point 1 to 2 traces along a virgin curve of stress-strain relationship. The reloading and loading cycle from point 2 to 3 and point 3 to 4 is postulated to produce no plastic strain and hence no residual pressure rise because points 2, 3 and 4 stay below the current yield locus as seen in Fig. 2.24(b). From point 4 the stress path traces the original virgin curve again and creates a new yield locus while producing plastic deformation and hence generating the residual pore pressure. Unloading from point 5 to 6 involves only

elastic strains and no additional residual pore pressure is generated. At point 6, where the shear stress changes direction, the sample will again undergo plastic deformation by tracing along the virgin curve.

The stress-dilatancy and the stress-strain relationships are then expressed in a computable manners by approximating the yield loci and stress paths on  $p'$ - $q$  plane into a family of straight lines and circular arcs with the center located on  $q = 0$  line .

The validity of this computational scheme was proved by comparing the computed results with field observations of liquefaction occurred during earthquakes in Japan (17).

The authors disagree with Ishihara et al's assertion about yield loci in which no stress cycle below the pre-peak stress amplitude contributes to volume change of the sample. Experimental fact shows that volume change increases gradually in drained condition during uniform cyclic loading. The implication of the above fact is that volume change takes place even if the cyclic shear stress does not exceed the pre-peak value of shear stress and this phenomenon may be explained as "cyclic effect". Therefore, Ishihara et al's assumption may lead to the underestimation of pore pressure rise by neglecting the possible pore pressure increase during cyclic stresses below the current peak value.

#### 2-4 Studies on Liquefaction of Partially Saturated Sands

In an undrained state, when soil dilates under shear stresses, a load transfer from the soil skeleton to the pore fluid (pore-water with air bubbles) also takes place in the partially saturated sands. The magnitude of the pore pressure rise associated with such a load transfer is influenced

by the relative compressibility of the pore fluid and the soil skeleton. Since the compressibility of water is negligible, the compressibility of the pore fluid is considered to be equal to that of the air in the soil pores. Consequently, the magnitude of the load transferred to the pore fluid resulting from a volume change will be quite low in partially saturated soils as compared with saturated ones. This fact was observed during the liquefaction study in the laboratory. For saturated sands, compressibility of water  $1/K_w = 2.5 \times 10^{-8}$  1/psf, whereas compressibility of soil skeleton in one-dimensional,  $1/\bar{E}_r$ , is generally of the order of  $10^{-6}$  1/psf (26). Considering the relative orders of magnitude of the compressibility, the water may be assumed to be effectively incompressible. For non-saturated samples, Martin et al (26) reported that the compressibility of pore fluid,  $1/K_w$ , rapidly increases for small reduction in the degree of saturation  $S_o$ . For example,  $1/K_w$  becomes of the same order as  $1/\bar{E}_r$  for values of  $S_o \approx 99\%$ , and thus, from Eq. 2.7 in Section 2-3(2) it may be seen that increase in the residual pore pressure per cycle,  $\Delta u$ , would be reduced considerably. For quantitative understanding of the effects of degree of saturation on pore pressure rise or liquefaction potential, no further research has yet been made up to date.

## CHAPTER 3

### SOIL TYPE TESTED AND EXPERIMENTAL PROCEDURES FOLLOWED DURING THIS INVESTIGATION

#### 3-1 Testing Equipment

##### (1) Torsional Simple Shear Device ( TSSD )

All tests were conducted in the torsional simple shear device which is shown in Fig. 3.1 and Plate I. The details of the device are presented in Refs. 11, 12, 40 and 41.

The torsional simple shear device accommodates a "donutlike" soil sample with 4 inches outside diameter, 2 inches inside diameter. The sample is 1 inch outside and 1/2 inch inside height as shown in Fig. 3.2. The soil can simultaneously be subjected to a vertical stress  $\sigma_v$ , horizontal stress  $\sigma_h$ , respectively, and a cyclic shear stress  $\tau_{vh}$  applied on top of the sample as shown in Fig. 3.2. When the shear stress  $\tau_{vh}$  is applied, the line AB (see Fig. 3.2(c)) moves to A'B', thus introducing a shear strain  $\gamma$  defined as:

$$\gamma_A = \frac{S_1}{h_1} = \frac{r_1\theta}{h_1}, \quad \gamma_B = \frac{S_2}{h_2} = \frac{r_2\theta}{h_2} \quad (3.1)$$

From the above, it is noted that when the ratio of  $\frac{r_1}{r_2}$  is made equal to  $\frac{h_1}{h_2}$ , this insures that the shear strains throughout the sample will be uniform; that is,  $\gamma_A = \gamma_B$ . The above relationship when compared with Fig. 3.2, means that this device establishes uniform shear strains and

hence uniform shear stresses throughout the sample.

## (2) Cyclic Loading System

The entire Torsional Simple Shear Device is bolted on a rigid table which is connected to an MTS ( Material Testing System ) actuator shown in Fig. 3.3. The MTS (Model 903.73) is a single channel electrohydraulic, closed loop testing system and it has a  $\pm 10,000$  pound dynamic load and  $\pm 3.0$  inch stroke capability with discrete functions of variable wave forms, amplitudes and frequencies. The system also has the capability to apply any loading patterns including actual earthquake loading. The vertical up and down movement of the MTS actuator A is transferred to a back and forth horizontal motion applied by the loading rod B as shown in Fig. 3.3. This horizontal motion of rod B is translated into rotational movement on the soil sample.

## (3) Water Supply and Saturation System

In Fig. 3.4 is shown the water supply and sample saturation system. One drainage line is provided from the top and another from the bottom of the specimen. These lines are used to circulate the water through the soil during the saturation process. To obtain a substantial saturation of the specimen, the de-aired water in Tank A is circulated through the bottom specimen. This is accomplished by applying a slightly higher pressure on Tank A than on Tank B which is connected to the soil from the top. In no case should the pressure in Tank A exceed the confining chamber pressure around the soil specimen.

## (4) Pickups and the Recording System

The torque pickup transducer is built into the loading shaft just above the specimen (see Fig. 3.1 and also Plate II). In this way, the true torque applied directly on the sample can be measured without including frictional effects on the wall of the loading shaft. The torque pickup itself includes four strain gauges oriented at  $45^\circ$  from the horizontal placed on a hollow stainless steel cylinder which is a part of the loading shaft.

Two beryllium copper plates  $3/8$  inches wide, 3 inches high and 0.011 inches in thickness that are placed  $180^\circ$  apart on opposite sides of the specimen. These plates are used for measuring the shear deformations experienced by the soil sample. Two strain gauges are placed vertically on both sides of each plate. The bottom ends of the plates are rigidly fixed to the base of the chamber, and the top ends are supported between two small rods which are fixed to the top plate of the soil specimen (see Fig. 3.1 and also Plate II). In this manner, the relative movement between the bottom and the top of the soil sample is detected and recorded.

Two bonded strain gauge type pressure transducer (Standard Controls, Inc., Model 800) is used to measure the pore water pressure in the drainage line from the top of the specimen.

The following signals can be amplified and then recorded by a six-channel analog, Brush Model 260 Recorder.

- (a) torque applied to the sample
- (b) sample torsional deformation
- (c) pore water pressure in the sample
- (d) vertical movement of the MTS actuator
- (e) vertical displacement of the sample (measured by a Linear Variable Displacement Transducer attached to

the loading shaft)

### 3-2 Type of Soil Tested

The Ottawa sand, ASTM designation C-109, was used for all the liquefaction tests. This is a relatively uniform, natural silica sand. The grain size distribution is shown in Fig. 3.5. The distribution falls within the region of the most liquefiable soils as seen in Fig. 2.4. The physical properties of this sand are shown in Table 1.

### 3-3 Test Program

#### (1) Tests on Fully Saturated Samples

Tests were conducted on the above Ottawa Sand at three different densities, namely, loose, medium dense and dense conditions. For each density, both uniform and non-uniform cyclic shear loadings were applied while measuring pore pressure change in the sample. The static confining pressures (vertical and horizontal) were kept constant throughout the test. Three types of non-uniform cyclic stress patterns were applied on the soil during this investigation. These were:

- (a) discretely varying shear stress (Type A)
- (b) exponentially varying shear stress (Type B)
- (c) single shock type shear stress (Type C)

Typical time histories of these loading patterns are shown in Fig.3.6.

Table 2 shows the summary of test programs for saturated samples.

#### (2) Tests on Partially Saturated Samples

Tests were conducted on loose samples under uniform cyclic loading only.

The initial pore pressure parameter  $\bar{B}$  as indications of the sample saturation was controlled from about 0.25 to 0.80. The results were to be compared with those of saturated samples under uniform cyclic loading described in the preceding section(1). Table 3 shows the summary of test program for partially saturated samples.

During the tests on saturated and partially saturated samples, the initial principal stress ratios  $K_0$  was kept unity (vertical and horizontal confining stresses being equal) and sinusoidal cyclic shear stress pattern was used.

### 3-4 Test Procedure

#### (1) Sample Preparation

The dry sample is weighed and submerged in water overnight. The entrapped air in the sample is removed by circulating the submerged sample with de-aired water which entered from the bottom of the sample through a small tube.

The inside and the outside membranes were fixed to the base of the shear device and confined vertically by specimen molds. Before placing the soil between the inner and outer molds, the sample area is filled with de-aired water and also, the upper porous stone is kept submerged in the water. Vacuum and compressed de-aired water are then applied one after another through the lines leading to the bottom and top of the specimen to remove any entrapped air in the porous stones and saturation lines. Thereafter, the previously de-aired specimen is slowly and evenly poured between the specimen molds with a spoon. The top plate with the porous stone is placed on the specimen and then the membranes are clamped to it.

After applying vacuum into the specimen through the line leading to the top of the specimen, the outside specimen mold is removed while the inner mold collapses by removing the rod which sustained the inner mold. The torque pickup and the deformation measurement plates are set up on the specimen (see Plate II).

## (2) Sample Saturation

A qualitative understanding of the degree of saturation of the sample was obtained by measuring the pore pressure parameter  $\bar{B}$  which is defined as ( 1, 44 ),

$$\bar{B} = \frac{\Delta u}{\Delta \sigma_c} \quad (3.2)$$

where,  $\Delta u$  is the pore pressure increment generated by subjecting the soil specimen to an increment of isotropic stress,  $\Delta \sigma_c$ , in an undrained condition.

The control of the  $\bar{B}$  value of the specimen prior to the test was accomplished by:

- (a) controlling the amount of de-aired water circulated through the specimen (percolation method)
- (b) controlling the back water pressure applied to the specimen (back pressure method)

At first, the de-aired water was circulated from the bottom to the top of the specimen by applying 5 psi at the bottom and 0 psi at the top of the specimen while applying the initial 10 psi horizontal and vertical confining

pressures. Both the horizontal and vertical confining stresses  $\sigma_h$  and  $\sigma_v$  were then increased to 20 psi after closing the valves that connect the samples to the de-aired water supply system. Under this condition, pore water rise was measured and the  $\bar{B}$  value was calculated. If the  $\bar{B}$  value was found to be lower than the desired value, the same procedure was repeated by increasing all pressure components by 10 psi. Table 4 shows the  $\bar{B}$  values obtained during one complete saturation cycle. Throughout this procedure, it was found that the parcolation method is not as effective as the back pressure method in generating a higher  $\bar{B}$  value condition.

### (3) Control of the Sample Density

Three different sample densities, namely, loose, medium dense and dense samples were obtained using the following procedures:

#### (a) Loose samples

Loose samples were obtained by just gently pouring the soil into the mold as described in the previous section and without any compaction. The samples obtained by this method had void ratios ranging from 0.690 to 0.709 (with the mean value of 0.700).

#### (b) Medium dense samples

Before clamping the membranes, the specimen in the mold was placed on the vibrating table and vibrated at high frequency for 5 seconds. During this vibration counterweight of 400 g was placed on top of the specimen to protect them from the bouncing of the cap and from undergoing uneven settlements. After the vibration, the same procedure was followed as in loose sample

preparation.

The samples obtained by this method had void ratios ranging from 0.629 to 0.657 (with the mean value of 0.644).

(c) Dense samples

After placing the sample between the inside and outside molds, a kneading type compaction was applied using a cone shaped edge with 45 degree slope. The cone was pressed 60 times on the surface of the specimen with equal force. After the compaction, the sample surface was smoothed, the top cap was placed on and the sample was placed over the vibrating table for 20 seconds. The sample obtained by this method had void ratio ranging from 0.574 to 0.614 ( with mean value of 0.595 ).

(4) Cyclic Loading

The desired wave form, frequency and number of cycles to be run were set directly into the MTS 903.73 control panel ( shown in Plate III). The amplitude of torsional stress during uniform cyclic loading was controlled by adjusting the stroke of MTS actuator. The desired values of torsional stress were obtained by setting the stroke to a pre determined position based on experience.

Non-uniform cyclic loading was applied by use the Data Trak Model 411.01 (see Plate III). The desired wave forms were etched on the metalized surface of the chart and the chart was taped to the rotating drum. The detector , follows the etched line on the rotating drum and transmits the signal to control the movement of the MTS actuator.

## CHAPTER 4

### DISCUSSION AND ANALYSIS OF TEST RESULTS

#### 4-1 Definition of Initial Liquefaction and Complete Liquefaction

It is known that the residual pore pressure in loose saturated sands increases at different rates during the liquefaction process under constant cyclic shear stress application. Fig.4.1 shows a typical example of the liquefaction process for a saturated loose sand. In Fig. 4.1, it is convenient to divide the liquefaction process into four stages on the basis of different rates of increase in the residual pore pressure. The characteristics of each of these stages can be summarized as (40) :

Stage 1....During this stage a rapid increase in pore-water pressure is observed (Initial stage).

Stage 2....During this stage an almost constant rate of increase in pore-water pressure is noted (Secondary stage).

Stage 3....The rate of pore-water pressure buildup gradually accelerates (Initial liquefaction stage).

Stage 4....During this stage the rate of pore-water pressure increase becomes zero (Final liquefaction stage).

The initial rapid increase in residual pore-water pressure is due to the rapid and substantial rearrangement of soil particles to accommodate the instantaneous change in stress conditions due to shear stress application. During the second stage, the volume change (which is responsible for the pore pressure build-up continues because of the increase in the stress ratio,  $\tau / \sigma'_c$  (shear stress / effective confining pressure). When the stress ratio,  $\tau / \sigma'_c$ , reaches a certain value, the shear deformation

increases rapidly; as a consequence, the residual pore pressure values accelerate. Peacock and Seed (30) proposed to designate the onset of partial liquefaction as the initial liquefaction, which is defined as "when the soil exhibits no resistance to deformation over a strain range less than that considered to constitute failure." Based on the above concept, the initial liquefaction is reached when the strain amplitude increases immediately.

Initial liquefaction is also defined in another two different ways. One involves the stress ratio concept; the other relates to the first turn-over point on the effective stress path (12, 42). Fig. 4.2(a) graphically illustrates the above-mentioned first definition, indicating that the soil enters the liquefaction stage when the ratio of  $\tau / \sigma'_c$  reaches the failure envelope for the first time. The second definition of initial liquefaction is shown in Fig. 4.2(b). In this figure the point "A" (where the effective stress path reverses direction for the first time) corresponds to initial liquefaction.

The complete liquefaction is reached when the pore pressure becomes equal to the confining pressure.

#### 4-2 Analysis of Pore Pressure Rise Under Uniform Cyclic Loading

In this section, the gradual increase in pore pressure during the uniform cyclic loading is analyzed for loose, medium dense and dense Ottawa sands respectively.

##### (1) Pore Pressure Rise in Loose Sand

The residual pore pressure at the end of each cycle was analyzed in order to find factors that affect the magnitude of the residual pore pres-

sure build-up during cyclic loading.

The residual pore pressure is defined as the one remaining when the cyclic shear stress becomes zero at the end of each cycle. The increment in the residual pore pressure is obtained from the difference in the values between  $(N - 1)^{\text{th}}$  cycle and  $N^{\text{th}}$  cycle as shown in Fig. 4.3, which gives the following relationship :

$$\Delta u_N = u_N - u_{N-1} \quad (4.1)$$

where  $\Delta u_N$  = increment in residual pore pressure during the  $N^{\text{th}}$  cycle  
 $u_N$  = residual pore pressure at the end of  $N^{\text{th}}$  cycle  
 $u_{N-1}$  = residual pore pressure at the end of  $(N-1)^{\text{th}}$  cycle

In order to evaluate pore pressure rise under different confining pressures, it is convenient to normalize the pore pressure by dividing it with the confining pressure such as :

$$U = u / \sigma_c \quad (4.2)$$

where  $U$  = normalized pore pressure rise  
 $u$  = actual pore pressure rise  
 $\sigma_c$  = initial confining pressure

By using the normalized pore pressure, Eq. 4.1 is expressed in the following manner:

$$\Delta U_N = U_N - U_{N-1} \quad (4.3)$$

Fig.4.4 shows the relationship between the incremental increase in the residual pore pressure per cycle (  $\Delta U_N / 1 - U_{N-1}$  ) and the effective stress ratio (  $\tau_N / \sigma'_{N-1}$  ) at the beginning of the corresponding cycle.

It is seen in Fig. 4.4 that the incremental rise in the modified pore pressure,  $\Delta U_N / 1 - U_{N-1}$  (per cycle) increases with the increase of the effective stress ratio  $\tau_N / \sigma'_{N-1}$ . Since the lines in Fig. 4.4 show almost the same slope ( $S=2.4$ ) on a log-log scale, they can therefore be expressed by the following relationship:

$$\Delta U_N / R = f(N) \cdot (\tau_N / \sigma'_{N-1})^S$$

therefore,

$$\Delta U_N = R \cdot f(N) \cdot (\tau_N / \sigma'_{N-1})^S \quad (4.4)$$

where

$R = 1 - U_{N-1}$  = modification factor

$f(N)$  = function of the number of cycles at which the pore pressure rise is considered

$\tau_N$  = cyclic shear stress at  $N^{\text{th}}$  cycle

$\sigma'_{N-1}$  = effective confining pressure at the beginning of  $N^{\text{th}}$  cycle ( equal to the effective confining pressure at the end of  $(N-1)^{\text{th}}$  cycle )

$S$  = slope of the lines in Fig. 4.4 which is equal to 2.4

The above modification factor  $R (= 1 - U_{N-1})$  is proposed on the basis that :

- (a) The increment in residual pore pressure ( $\Delta U_N$ ) becomes smaller when the residual pore pressure at the end of the preceeding cycle ( $U_{N-1}$ ) is high even if the effective stress ratios are equal.
- (b) The increment in the residual pore-water pressure becomes zero when the normalized residual water pressure ( $U_N$ ) becomes unity ( this is equivalent to the complete liquefaction condition ).

The implication of the modification factor is significant because it provides the boundary values regarding the effect of stress history on the pore pressure rise during cyclic loading. The values of the modification factor  $R$  can also be examined based on the following boundary conditions.

- (a) Before the first cycle of loading, the stress time history effect must be zero and therefore,  $R=1$  .
- (b) As long as the stress time history effect on the pore-water pressure rise is considered, the effect must be maximum when the residual pore pressure reaches the ultimate value where the complete liquefaction takes place and hence,  $R=0$  when such a stage is reached.

The complete description of the stress history effects on the pore pressure rise requires an additional factor such as a function dependent on the number of stress cycles. This is so because the magnitude of the pore pressure rise during cyclic loading is also affected by the number of cycles as seen in Fig. 4.4 even after modifying the data by the introduction of the modificatin factor  $R$  . In order to clarify the effect of the number of cycles on pore pressure rise, the data is plotted as shown in Fig. 4.5. Fig. 4.5 shows experimentally determined data points revealing

a relationship between the factor  $f(N)$  and the number of cycles  $N$ . A mathematical curve which has the following is fitted through data points.

$$f(N) = \frac{C_1 \cdot N}{N^{C_2} - C_3} \quad (4.5)$$

where  $N$  = number of cycles

$C_1, C_2, C_3$  = material parameters

when the material parameters  $C_1, C_2$  and  $C_3$  in Eq. 4.5 are taken as 6.13, 1.77 and 0.46 respectively, the curve shown in solid line is generated indicating good correlation between the experimental data and the results obtained from Eq. 4.5.

By combining Eqs. 4.4 and 4.5, the following equation for a saturated loose sand is defined.

$$\begin{aligned} \Delta U_N &= (1 - U_{N-1}) \cdot \left( \frac{C_1 \cdot N}{N^{C_2} - C_3} \right) \cdot \left( \frac{\tau_N}{\sigma'_{N-1}} \right)^S \\ &= (1 - U_{N-1}) \cdot \left( \frac{6.13 \cdot N}{N^{1.77} - 0.46} \right) \cdot \left( \frac{\tau_N}{\sigma'_{N-1}} \right)^{2.4} \end{aligned} \quad (4.6)$$

Where  $\Delta U_N$  = the increment in pore pressure at  $N^{\text{th}}$  cycle

$U_{N-1}$  = the residual pore pressure at  $(N-1)^{\text{th}}$  cycle

$\tau_N$  = the shear stress at  $N^{\text{th}}$  cycle

$\sigma'_{N-1}$  = the effective confining pressure at the end of  $(N-1)^{\text{th}}$  cycle

From Eq. 4.6, it is seen that the incremental pore pressure rise during dynamic loading is a function of stress intensity and stress history, which are represented by  $(\tau_N / \sigma'_{N-1})^S$  and  $R \cdot f(N)$  in Eq. 4.6 respectively. Furthermore, Fig. 4.6 shows a very good correlation between the theoretical pore pressure values calculated from Eq. 4.6 and the experimental data points.

The apparent slight discrepancy between the experimental data and the theoretical line ( constant cyclic shear stresses are assumed ) at a latter stage of loading is attributed to the fact that at this stage pore pressure increases excessively and hence applied cyclic shear stresses slightly decrease due to the rapid softening of the specimen during the laboratory tests.

## (2) Pore Pressure Rise in Dense and Medium Dense Sands

The previously developed theoretical concept to predict pore pressure rise in loose sand can be applied for medium dense and dense sands. Pore pressure rise in medium dense and dense sands was determined experimentally following the same procedure as used in the investigation of loose sands.

Figs. 4.7 and 4.8 show the relationship between the modified pore pressure rise and the stress ratio for medium dense and dense sands respectively. It is seen from Figs. 4.7 and 4.8, that the pore pressure rise in medium dense and dense sands is similar to the one in loose sands. The slopes of the lines in Fig. 4.7 and 4.8 are unique for each soil density which implies that the slope of the lines in each figure is density dependent. The three parameters  $C_1$ ,  $C_2$  and  $C_3$  in Eq. 4.5 for medium dense and dense sands can also be determined from Figs. 4.9 and 4.10 respectively.

It is therefore concluded that Eq. 4.6 in its general form will also

predict the incremental pore pressure rise values in medium dense and dense saturated sands under uniform cyclic loading. The parameters  $C_1$ ,  $C_2$ ,  $C_3$  and the slope of the lines for the three different density conditions tested during this study are summarized in Table 5.

### (3) Effect of Density on Pore Pressure Rise

In analyzing the pore pressure rise in the previous section, it was found that the samples with different densities have different  $C_1$ ,  $C_2$ ,  $C_3$  and  $S$  values in Eq. 4.6.

Fig. 4.11 show the variations of the above four parameters  $C_1$ ,  $C_2$ ,  $C_3$  and  $S$  with respect to soil density. In the following paragraphs the implications of each of the above four parameters are discussed :

#### (a) Parameters $C_1$ and $C_3$ ;

These values determine the magnitude of pore pressure rise at the initial stage of loading such as from 1 to 10 cycles where the pore pressure rise is normally high.

Loose samples show higher values of  $C_1$  and  $C_3$  than dense samples. The value of  $C_3$  becomes almost zero for the dense sample, which implies that the incremental rise in pore pressure decreases linearly with the increase in the number of cycles.

#### (b) Parameter $C_2$ ;

This value determines the slope of a line ( see Fig.4.5,4.9 and 4.10 ) which becomes almost straight line after several cycles of loading. The higher is the density, the lower the parameter  $C_2$  becomes; that is, the incremental rise in pore pressure in dense soils becomes less as compared with the loose soils.

## (c) Slope S;

The slope S indicates the sensitivity of pore pressure rise to the change in applied stresses. The S value for loose samples is slightly higher than for dense samples, which implies that the pore pressure in loose samples are more sensitive to stress changes than the dense samples.

## (4) Summary

The analysis of measured pore pressure rise of saturated sands during uniform cyclic loading showed that the incremental rise in pore pressure  $\Delta U_N$  can be expressed as a function of stress intensity  $(\tau_N / \sigma'_{N-1})^S$  and stress history  $(R \cdot f(N))$  ( see Eqs. 4.4, 4.5, 4.6 ).

The predicted pore pressure rise based on Eq. 4.6 agreed well with the measured pore pressure rise as seen in Fig. 4.6. Furthermore, it is proved that Eq. 4.6 is also applicable for dense samples in predicting the pore pressure rise during cyclic loading simply by finding the values of the four parameters S,  $C_1$ ,  $C_2$  and  $C_3$  corresponding to the soil density. The variation of these four parameters with soil density ( expressed in terms of void ratio or relative density ) is shown in Fig. 4.11.

#### 4-3 Liquefaction Potentials of Samples with Different Densities

The liquefaction potentials in terms of the initial effective stress ratio  $\tau_N / \sigma'_C$  and the number of cycles to cause liquefaction  $N_L$  were predicted for samples with different densities by using Eq. 4.6 and parameters shown in Table 5 and Fig. 4.11. The predicted initial liquefaction points were obtained by finding the number of cycles at which the maximum effective stress ratio in the static shear test is reached during cyclic loading ( see the discussion of the stress ratio concept in section 4-1 ). The maximum effective stress ratio is usually expressed in terms of the angle of internal friction such as :

$$\left( \frac{\tau}{\sigma'} \right)_{\max} = \tan \phi' \quad (4.7)$$

where  $\phi'$  = the angle of internal friction

$\left( \frac{\tau}{\sigma'} \right)_{\max}$  = the maximum effective stress ratio

The variation of the angle of internal friction  $\phi'$  with density was obtained for the Ottawa sand ( ASTM C109 ) by Ishibashi (12) using a direct shear device as shown in Fig. 4.12. The angle of internal friction corresponding to each of the three densities employed during this study is determined from Fig. 4.12 as follows :

For loose sand,  $\phi' = 30^\circ$  ,  $\left( \frac{\tau}{\sigma'} \right)_{\max} = 0.58$

For medium dense sand,  $\phi' = 34.5^\circ$  ,  $\left( \frac{\tau}{\sigma'} \right)_{\max} = 0.69$

For dense sand,  $\phi' = 38^\circ$  ,  $\left( \frac{\tau}{\sigma'} \right)_{\max} = 0.78$

The complete liquefaction point is determined from the number of cycles when the predicted pore pressure rise reaches the initial effective confining pressure for the first time.

Fig. 4.13 shows the comparison of the predicted and experimental initial liquefaction potentials defined by the effective stress turn over concept ( see the definition of initial liquefaction in section 4-1 ). It is seen in Fig. 4.13 that the predicted and the measured data show good agreement.

The normalized pore pressures at the initial liquefaction points both of fully and partially saturated samples are examined by using two different definitions, namely, the first turnover point and the maximum effective stress ratio concepts ( see section 4-1 ). By plotting the normalized pore pressure values at the initial liquefaction points, a graph such as the one shown in Fig. 4.14 is obtained. The data points in Fig. 4.14 show that the above two criteria defining initial liquefaction yield similar results. It is also interesting to note from Fig. 4.14 that residual pore pressure,  $U_N$  ( at the point of initial liquefaction ) increases slightly with the number of cycles necessary to induce initial liquefaction.

The predicted and the measured complete liquefaction potentials are also shown in Fig. 4.15. The slight discrepancy between the predicted and the measured complete liquefaction points comes from the fact that during experiments the cyclic shear stress can not always be kept constant but decreases slightly with the increase of number of cycles due to the rapid softening of the material especially at the liquefaction stage, while the predicted curves are based on the constant cyclic shear stress during the test (see Fig. 4.6).

## 4-4 Prediction of Pore Pressure Rise Under Non-uniform Cyclic Loading

## (1) Equivalent Number of Cycles at Different Shear Stress

In the previous section, the effect of number of cycles on the incremental rise in pore pressure was obtained by the use of the following expression ( see Eq. 4.5 ) :

$$f(N) = \frac{C_1 \cdot N}{N^{C_2} - C_3} \quad (4.8)$$

where  $f(N)$  = the effect of number of cycles

$N$  = number of cycles

$C_1, C_2, C_3$  = material parameters

It should be noted that the number of cycles  $N$  in Eq. 4.8 is evaluated equally for each cycle of loading. This is reasonable only for the uniform cyclic loading where all the cyclic stresses are equal throughout the loading. For non-uniform cyclic loading, however, a certain equivalent number of cycles should be introduced to evaluate all the number of cycles of different stress amplitudes prior to the cycle at which the pore pressure is to be predicted. This is done by replacing the term  $N$  in Eq. 4.8 into the equivalent number of cycles  $N_{eq}$ , which is defined as :

$$N_{eq} = \sum_{i=1}^N \left( \frac{\tau_i}{\tau_N} \right)^\beta \quad (4.9)$$

where  $\tau_i$  = cyclic shear stress at  $i^{\text{th}}$  cycle ( $i \leq N$ )  
 $\tau_N$  = cyclic shear stress at  $N^{\text{th}}$  cycle  
 $\beta$  = parameter

Since the parameter  $\beta$  in Eq. 4.9 indicates the sensitivity to stress change, therefore the same values can be used for the parameter  $\beta$  as those slopes  $S$  ( see section 4-2 and note that the slopes  $S$  indicate the effect of stress intensity  $\tau_N / \sigma'_{N-1}$  on the incremental rise in pore pressure ). By simply replacing  $N$  by  $N_{\text{eq}}$  in Eq. 4.6 , the final equation for predicting the pore pressure rise under non-uniform cyclic loading is expressed as follows :

$$\Delta U_N = (1 - U_{N-1}) \cdot \frac{C_1 \cdot N_{\text{eq}}}{N_{\text{eq}}^{C_2} - C_3} \cdot \left( \frac{\tau_N}{\sigma'_{N-1}} \right)^S$$

and

$$U_N = U_{N-1} + \Delta U_N$$

(4.10)

where

$$N_{\text{eq}} = \sum_{i=1}^N \left( \frac{\tau_i}{\tau_N} \right)^S$$

## (2) Comparison of Measured and Predicted Pore Pressure Rise

Figs. 4.16(a) to (f) show the comparison of the experimentally measured and the predicted pore pressure rise for loose samples under three types of non-uniform cyclic loading.

It is seen in Figs 4.16(a) to (f) that the predicted pore pressure values are in good agreement with the experimental data for all of the

types of non-uniform cyclic loading. Note that the parameter  $C_1$  is very sensitive to a slight change in void ratio, leading to a significant difference in pore pressure rise at the initial stages of loading.

For medium dense or dense samples, however, a slight change in void ratio does not affect the value of  $C_1$  as much as was the case with loose samples.

Figs. 4.16(g) to (j) show the comparison of measured pore pressure rise with the predicted values for medium dense and dense samples. Comparisons were made only for one non-uniform loading, Type A, in Fig. 3.6. It is seen in Figs. 4.16(g) to (j) that a good agreement exists between the predicted and the measured pore pressure values for both medium dense and dense samples. It can therefore be concluded that Eq. 4.10 provides a valid base for the prediction of pore pressure rise under non-uniform cyclic loading.

#### 4-5 Prediction of Pore Pressure Rise during Actual Earthquake

In the previous section, the derived equations 4.6 and 4.10 were shown to be applicable for predicting the pore pressure rise in soils under both uniform and non-uniform cyclic loadings. Before applying the derived equations to the prediction of pore pressure rise during earthquake loadings, it is necessary to consider the fact that during an earthquake loading, the shear stress amplitudes vary erratically from one cycle to another. Fig. 4.17 shows an example of the time history of shear stress in a deposit during an earthquake (37). In Fig. 4.17, it may be appropriate to express the randomness of earthquake loading by the following characteristics.

- (a) abrupt change in the amplitude of shear stress during the time history

- (b) antisymmetry in the peak values of shear stress during one cycle
- (c) more than one peak exit during half cycle  
(above or below the zero shear stress line)
- (d) frequency changes randomly from one cycle to another

It can be realized that the prediction of pore pressure rise is to be made for every half cycle because of the antisymmetry in the peak values during one cycle. Supposing that a half of the total residual pore pressure rise per cycle results at the end of the half cycle under uniform cyclic loading as shown in Fig. 4.18(a), pore pressure rise at  $N^{\text{th}}$  cycle can be expressed as :

$$\Delta U_N = \frac{1}{2} \left\{ (\Delta U_N)_p + (\Delta U_N)_n \right\} \quad (4.11)$$

where  $\Delta U_N$  = pore pressure rise during  $N^{\text{th}}$  cycle

$(\Delta U_N)_p$  = pore pressure rise in positive region under cyclic shear stress  $\tau_{Np}$  during  $N^{\text{th}}$  cycle

$(\Delta U_N)_n$  = pore pressure rise in negative region under cyclic shear stress  $\tau_{Nn}$  during  $N^{\text{th}}$  cycle

Eq. 4.11 also applies for the case where the amplitudes of shear stress in the positive and negative regions of the cycle are not equal, which condition is illustrated in Fig. 4.18(b). It is seen in Fig.4.18(b) that the pore pressure rise due to  $\tau_{Np}$  in positive region is expressed

by the line AB while the pore pressure rise due to  $\tau_{Nn}$  in negative region is expressed by the line BC.

The values of  $(\Delta U_N)_p$  and  $(\Delta U_N)_n$  in Eq. 4.11 are computed by the same equation as used for the prediction of pore pressure rise during non-uniform cyclic loading ( i.e. Eq. 4.10 ). The only difference lies in the computation of the equivalent number of cycles  $N_{eq}$ . Since shear stresses are now considered independently in positive and negative region, the equivalent number of cycles should also be evaluated independently in each region. That is, at  $N^{th}$  cycle, shear stress amplitudes from 1st cycle to  $N^{th}$  cycle in positive region give the equivalent number of cycles in positive region,  $(N_{eq})_p$ , and the same is true for negative region. Hence,  $(\Delta U_N)_p$  or  $(\Delta U_N)_n$  can be expressed by the following equation:

In compression region,

$$(\Delta U_N)_p = (1 - U_{N-1}) \cdot \frac{c_1 (N_{eq})_p}{(N_{eq})_p^{c_2} - c_3} \cdot \left( \frac{\tau_{Np}}{\sigma_{N-1}} \right)^S$$

and

$$(N_{eq})_p = \sum_{i=1}^N \left( \frac{\tau_{ip}}{\tau_{Np}} \right)^S \quad (4.12)$$

where  $\tau_{ip}, \tau_{Np}$  = the amplitude of shear stress in positive region at  $i^{th}$  or  $N^{th}$  cycle

$(N_{eq})_p$  = equivalent number of cycles in positive region at  $N^{th}$  cycle

The same equation is applied in the negative region. It is clear in Eq. 4.11 and 4.12 that if shear stresses in positive and negative

regions are equal, that is  $(\Delta U_N)_p$  equals to  $(\Delta U_N)_n$ , then the same value of  $\Delta U_N$  is obtained as in the case of uniform cyclic loading.

Previous studies ( 30, 47 ) proved that the difference in the frequency of cyclic shear stress had not a significant effect on the pore pressure rise and the liquefaction potential of sands.

The smaller peaks other than the maximum value that exist during the half cycle of time history in shear stress may not affect significantly the pore pressure rise that is determined solely by the maximum shear stress in the half cycle. No further investigations on this problem have been done up to date.

It is concluded that in spite of the randomness of the time history in shear stress during earthquakes, Eq. 4.12 will provide the appropriate basis for the prediction of pore pressure rise during earthquakes. The time history is evaluated in Eq. 4.12 simply by the peak stress during half cycle and the number of cycles, in which one cycle consists of two peak stresses in opposite direction and three crossings at the zero stress line.

Fig. 4.19 shows the results of the computations of pore pressure rise based on Eq. 4.12 during the actual earthquake time history shown in Fig. 4.17. The computations were made for three different densities, the void ratios of which are 0.700, 0.644 and 0.594 respectively. It is assumed that the deposit consists of Ottawa sand (ASTM designation C-109) and the water level is located at the surface of the ground. According to the computed results in Fig. 4.19, when the deposit is loose or medium dense, it liquefies at 5 or 10 seconds respectively, however for dense case ( $e = 0.594$ ) the deposit does not liquefy throughout the earthquake. It is also interesting to note in Fig. 4.19 that only few large peak shear stresses contrib-

ute to pore pressure rise significantly. Although there is no field data to compare with the computed results of pore pressure rise, it should be pointed out that the appropriate determination of the field soil density is crucial for the determination of liquefaction potential of soils.

#### 4-6 General Procedures for the Determination of Parameters

$S$ ,  $C_1$ ,  $C_2$  and  $C_3$

In order to determine the material parameters  $C_1$ ,  $C_2$ ,  $C_3$  and  $S$  in the proposed method, the following tests and analysis are required for a given condition of sand.

- (1) At least 3 or 4 uniform cyclic loading tests are performed with varying the initial stress ratio  $\tau/\sigma_c$  so that the liquefactions occur at different number of cycles within 1 to 300 cycles.
- (2) The incremental rises in the residual pore pressure at the end of appropriate number of cycles, i.e., 1, 2, 3, 5, 7, 10, 20, 30<sup>th</sup> cycles, etc., and cyclic shear stress at the corresponding cycle are to be calculated.

The total residual pore pressure increment at the end of these cycles are also obtained from Eq. 4.3.

- (3) Plot  $\Delta U_N / R$  vs.  $\tau_N / \sigma'_{N-1}$  and obtain such figure as shown in Fig. 4.4, and determine the slope,  $S$ , from the data points at small number of cycles assuming the  $S$  value is nearly constant at any number of cycles.
- (4) Plot  $\Delta U_N / R \cdot (\tau_N / \sigma'_{N-1})^S$  vs.  $N$  as shown in Fig. 4.5 and determine the three parameters  $C_1$ ,  $C_2$  and  $C_3$  by the fitting

technique.

- (5) The same procedure can be followed to determine parameters,  $S$ ,  $C_1$ ,  $C_2$  and  $C_3$  for soils with any density if required.

#### 4-7 Effect of the Degree of Saturation on Liquefaction Potential

The samples with different degree of saturation was investigated to evaluate the effect of the degree of saturation as manifest in the magnitude of the pore pressure parameter  $\bar{B}$  on the liquefaction potential.

Typical actual liquefaction test data for a fully saturated sample and for a sample with low  $\bar{B}$  value are shown in Fig. 4.20. It is seen from this figure that the low  $\bar{B}$  value soil sample also exhibits liquefaction potential, and the residual pore pressure rise tendency in this sample is similar to that of the saturated sample except during the early stages of loading.

Fig. 4.21 shows the measured residual pore pressure buildup for different  $\bar{B}$  value samples at the end of the first cyclic loading. It is seen from this figure that the residual pore pressure (at the end of the first cycle) increases with the increase in  $\bar{B}$  value.

The difference in pore pressure rise for different  $\bar{B}$  value samples is explained by the difference in the compressibility of pore fluid especially in the initial stage of loading. That is, at the initial stage, the compressibility of pore fluid in low  $\bar{B}$  value samples remains low and therefore the load transfer from soil skeleton to pore fluid remains small and hence the lower pore pressure rise. With the progressive volume change during loading, the compressibility of pore fluid increases and the portion of the load transferred to pore fluid increases. Finally when the

compressibility of pore fluid becomes much greater than that of soil skeleton like water, almost all of the load is transferred to pore fluid and the soil enters complete liquefaction stage.

As a result of the difference in pore pressure rise during the early stage of loading, the liquefaction potential is also affected by the initial value of  $\bar{B}$ .

Fig. 4.22 shows a relationship between the applied stresses and the number of cycles to liquefaction as a function of the pore pressure parameter,  $\bar{B}$ . From this figure it is noted that the low  $\bar{B}$  value soils possess low liquefaction potential. Although a qualitative understanding of the degree of saturation of the sample is obtained from the magnitude of  $\bar{B}$  prior to testing, the determination of the absolute degree of saturation will be of more practical value to the engineer, and hence an attempt is made to establish a quantitative relationship between the absolute degree of soil saturation and its corresponding  $\bar{B}$  value.

The fundamental relationship between the pore pressure rise and the volume change of the air in the pores is derived from Boyle's law for the compressibility of the air and from Henry's law for its solubility (9, 49).

$$\Delta u = \frac{(P_a + u_b) \cdot \Delta}{V_a + H \cdot V_w - \Delta} \quad (4.13)$$

where

$\Delta u$  = increment in pore pressure

$P_a$  = atmospheric pressure

$u_b$  = back pressure

$V_a, V_w$  = initial volume of the air and water in the specimen divided by the initial total volume

H = Henry's constant for solubility which is equal to  
0.02 for 20° C

$\Delta$  = volumetric strain

Assuming that the volumetric strain of the specimen under isotropic stress conditions is proportional to the increment in the effective confining stress (that is  $\Delta = C_s \cdot \Delta\sigma'_c$ ), Eq. 4.13 can be rearranged to read as follows:

$$\Delta u = \frac{(P_a + u_b) \cdot \Delta\sigma'_c}{S'/C_s - \Delta\sigma'_c} \quad (4.14)$$

where  $S' = n_0 (1 - S_0 + HS_0)$

$n_0$  = initial porosity

$S_0$  = initial degree of saturation

$C_s$  = the compressibility of the soil skeleton

In order to establish a direct relationship between the initial degree of saturation,  $S_0$ , and the pore pressure parameter,  $\bar{B}$ , it is convenient to express the pore pressure increment in terms of the total confining pressure increment,  $\Delta\sigma_c$ . This can be done by simply replacing the  $\Delta\sigma'_c$  by  $(\Delta\sigma_c - \Delta u)$  in Eq. 4.14 and solving for  $\bar{B}$ , which leads to the following relationship:

$$\bar{B} = \frac{\Delta u}{\Delta\sigma_c} = \frac{1}{2} \cdot \left[ - \left( \frac{S'}{C_s \Delta\sigma_c} + \frac{P_a + u_b}{\Delta\sigma_c} - 1 \right) + \sqrt{\left( \frac{S'}{C_s \Delta\sigma_c} + \frac{P_a + u_b}{\Delta\sigma_c} - 1 \right)^2 + \frac{4(P_a + u_b)}{\Delta\sigma_c}} \right] \quad (4.15)$$

The compressibility of the soil skeleton  $C_s$  in Eq. 4.15 is found to be 0.0012 1/psi. The above value is obtained through an iteration process using the measured  $\bar{B}$  values of 0.92 (average of four measurements) at 45 psi back pressure, which implies that the soil is almost fully saturated. The value of  $C_s = 0.0012$  1/psi compares very well with the previously published data by Scott (32) for a loose sand.

Fig. 4.23 and 4.24 show the results of computation based on Eq. 4.15, which determine the relationship between the  $\bar{B}$  values and the initial degree of saturation when the back pressure is 5 psi and 45 psi respectively.

Using the established relationship between the  $\bar{B}$  values and the initial degree of soil saturation, a plot relating the number of cycles necessary to cause liquefaction for soils with different degrees of saturation is shown in Fig. 4.25. From this figure it is seen that the liquefaction potential for a given soil increases as the degree of saturation of the soil increases.

## CHAPTER 5

### CONCLUSIONS AND RECOMMENDATIONS

#### 5-1 Conclusions

The following conclusions were obtained from the pore pressure investigations in saturated sands during dynamic loading.

(1) Based on the analysis of measured pore pressure rise during cyclic loading tests using Torsional Simple Shear Device, an unique method to predict pore pressure rise was established. In this method, the incremental rise in pore pressure rise during uniform cyclic loading is predicted by the equation in its basic form as shown below:

$$\Delta U_N = R \cdot f(N) \cdot \left( \frac{\tau_N}{\sigma_{N-1}} \right)^S \quad (4.4)$$

where

$$R = 1 - U_{N-1}$$
$$f(N) = \frac{C_1 \cdot N}{N^{C_2} - C_3} \quad (4.5)$$

$N$  = number of cycles

$S$ ,  $C_1$ ,  $C_2$  and  $C_3$  are constants shown in Fig. 4.11  
for a Ottawa sand

The above equation is shown to be applicable for predicting the pore pressure rise in saturated sands under any type of loading patterns (i.e. actual earthquake loading) provided the following modifications are made.

- (a) when the cyclic shear stress amplitudes are randomly variable but symmetrical with respect to the zero stress axis, the pore pressure rise can be calculated by replacing  $N$  in Eq. 4.5 by the equivalent number of cycles  $N_{eq}$ , which is defined as:

$$N_{eq} = \frac{N}{\sum_{i=1}^N} \left( \frac{\tau_i}{\tau_N} \right)^S \quad (4.9)$$

The predicted and measured pore pressure values are compared in Fig. 4.6 and showed a good agreement.

- (b) When the cyclic shear stress amplitudes are antisymmetrical with respect to zero stress axis like actual earthquake loading, Eq. 4.4 are also applicable to the determination of the pore pressure rise due to the shear stresses in positive or negative side of the neutral axis independently. And the incremental rise in pore pressure during  $N^{th}$  cycle is obtained from the following equation.

$$\Delta U_N = \frac{1}{2} \left\{ (\Delta U_N)_p + (\Delta U_N)_n \right\} \quad (4.11)$$

Predicted pore pressure rise during an actual earthquake is shown in Fig. 4.19.

- (2) Both initial and complete liquefaction points during dynamic loading can be determined from the computation of the pore pressure rise during cyclic loading. A good agreement exists between the computed and

experimentally determined liquefaction points as shown in Fig. 4.13 and 4.15.

(3) The proposed pore pressure prediction equation derived during this research will be applicable for other type of sand by following the procedure that is shown in section 4-6.

(4) The effective stress ratio criterion ( see Fig. 4.2(a) ) and the effective stress path turnover point criterion ( see Fig. 4.2(b) ), defining the initial soil liquefaction, correlate very well and essentially yield the same results as shown in Fig. 4.14.

Based on the results of pore pressure rise in partially saturated sands during dynamic loading, the following conclusions can be reached regarding partially saturated soils.

(5) Partially saturated loose sands do liquefy and that the pore pressure buildup pattern is similar to that generated during tests conducted on fully saturated loose sands.

(6) Based on the data shown in Figs. 4.22 and 4.25 , it is concluded that the liquefaction potential for soils decreases with decreasing  $\bar{B}$  values or with decreasing degrees of soil saturation.

## 5-2 Recommendations

(1) The proposed method for predicting the pore pressure rise during dynamic loading is based on the analysis of one kind of material ( Ottawa sand ASTM designation C-109 ). It is recommended that wide variety of sands having different physical properties be tested and analyzed using

the same procedure as was followed during this research.

(2) Research should be undertaken to determine whether the pore pressure rise can be estimated by the method proposed in this study when the initial  $K_0$  value is other than unity. When the initial  $K_0$  value is unity, the initial stress ratio  $\tau_N / \sigma'_{N-1}$  in the proposed method (see Eq. 4.6) is equivalent to  $\Delta\tau_{\max} / \sigma'_{\text{oct}}$  which was proved to be unique in determining the initial liquefaction of the samples with various  $K_0$  values. It has not been proved experimentally, however, that the ratio  $\Delta\tau_{\max} / \sigma'_{\text{oct}}$  is also unique in determining the incremental rise in pore pressure of the samples having different  $K_0$  values.

(3) In the case of partially saturated sands, it is possible to derive a theoretical relationship between the pore pressure rise and the volume change of the specimen (see Eq. 4.13), however, experimental investigations are required to determine the boundary conditions such as the threshold volume changes when the  $\bar{B}$  values become zero or unity corresponding to a certain degree of saturation. This could be accomplished by measuring the actual volume change of the specimen as well as the pore pressure.

## BIBLIOGRAPHY

1. Bishop, A. W., and Eldin, G. (1950), " Undrained Triaxial Tests on Saturated Sands and Their Significance in the General Theory of Shear strength," Geotechnique, Vol. II.
2. Casagrande, A. (1936), " Characteristics of Cohesionless Soils Affecting the Stability of Slopes and Earth Fills," Jornal of Boston Society of Civil Engineers, January.
3. Castro, G. (1975), " Liquefaction and Cyclic Mobility of Saturated Sands," Journal of the Geotechnical Engineering Division, ASCE, Vol. 101, No. GT6.
4. De Alba, P., Chan, C. K. and Seed, H. B. (1975), " Determination of Soil Liquefaction Characteristics by Large-Scale Laboratory Tests," Earthquake Engineering Research Center , University of California, Berkeley, Report No. EERC 75-14.
5. Finn, W. D. L., Bransby, P. L. and Pickering, D. J. (1970), " Effect of Strain History on Liquefaction of Sand," Journal of the Soil Mechanics and Foundations Division, ASCE, Vol. 96, No. SM6.
6. Finn, W. D. L., Pickering D. J. and Bransby, P. L. (1971), " Sand Liquefaction in Triaxial and Simple Shear Tests," Journal of the Soil Mechanics and Foundations Division, ASCE, Vol. 97, No. SM4.
7. Finn, W. D. L. (1972), " Soil Dynamics-Liquefaction of Sands," Proceedings of the International Conference on Microzonation for Safer Construction Research and Application, Seattle, Washington, Vol. I.
8. Finn, W. D. L., Emery, J. J. and Gupta, Y. P. (1971), " Liquefaction of Large Samples of Saturated Sand on a Shaking Table," Proceedings, 1st Canadian Conf. on Earthquake Eng., Vancouver, University of

## British Columbia.

9. Gibbs, H. J., Hilf, W. J., Holtz, W. G. and Walker, F.C. (1960), " Shear strength of Cohesive Soils," Research Conf. on Shear Strength of Cohesive Soils, ASCE, Colorado.
10. Hardin, B. O. and Drnevich, V. P. (1972) , " Shear Modulus and Damping in Soils : Measurement and Parameter Effect," Journal of the Soil Mechanics and Foundations Division , ASCE, Vol. 98, No. SM6.
11. Ishibashi, I. and Sherif, M. A. (1974), " Soil Liquefaction by Torsional Simple Shear Device," Journal of the Geotechnical Engineering Division, ASCE, Vol. 100, No. GT8.
12. Ishibashi, I. (1974), " Torsional Simple Shear Device, Liquefaction and Dynamic Properties of Sands," dissertation submitted in partial fulfillment of the requirements for the degree of Doctor of Philosophy, University of Washington, Seattle, Washington.
13. Ishibashi, I. and Sherif, M. A. (1976), " Closure for Soil Liquefaction by Torsional Simple Shear Device," Journal of the Geotechnical Engineering Div., ASCE, Vol. 100, No. GT8.
14. Ishihara, K. and Li, S. (1972), " Liquefaction of Saturated Sand in Triaxial Torsion Shear Test," Soils and Foundations , Japanese Society of Soil Mechanics and Foundation Engineering, Vol. 12, No. 2.
15. Ishihara, K., Tatsuoka, F. and Yasuda, S. (1975), " Undraind Deformation and Liquefaction of Sand Under Cyclic Stresses," Soils and Foundations, Japan Society of Soil Mechanics and Foundation Engineering, Vol. 15, No. 1.
16. Ishihara, K. and Yasuda, S. (1975), " Sand Liquefaction in Hollow

- Cylinder Torsion Under Irregular Excitation," Soils and Foundations, Japan Society of Soil Mechanics and Foundation Engineering, Vol. 15, No.1.
17. Ishihara, K., Lysmer, J., Yasuda, S. and Hirao, H. (1976), " Prediction of Liquefaction in Sand Deposits During Earthquakes," Soils and Foundations , Japan Society of Soil Mechanics and Foundation Engineering, Vol. 16, No. 1.
  18. Kawasumi, H. (1968), " General Report on the Niigata Earthquake of 1964," Editorial Committee of " General Report on the Niigata Earthquake of 1964, " March, 1968.
  19. Kishida, H. (1969), " Characteristics of Liquefied Sands during Mino-Owari, Tonankai and Fukui Earthquakes, " Soils and Foundations, Japan Society of Soil Mechanics and Foundation Engineering, Vol. 9, No. 1.
  20. Koizumi, Y. (1966), " Changes in Density of Sand Subsoil Caused by Niigata Earthquake," Soils and Foundations, Japanese Society of Soil Mechanics and Foundation Engineering, Vol. 6, No. 2.
  21. Kovaks, W. D., Seed, H. B. and Chan, C. K. (1971)," Dynamic Moduli and Damping Ratios for a Soft Clay," Journal of Soil Mechanics and Foundations Division, ASCE, Vol. 97, No. SM1.
  22. Ladd, R. S. and Silver, M. L. (1975), " Discussion on Soil Liquefaction by Torsional Simple Shear Device," Journal of Geotechnical Engineering Division, ASCE, Vol. 101, No. GT8.
  23. Lee, K. L. and Seed, H. B. (1967)," Cyclic Stress Conditions Causing Liquefaction of Sand," Journal of the Soil Mechanics and Foundations Division, ASCE, Vol. 93, No. SM1.
  24. Lee, K. L. and Fitton, J. A. (1968), " Factors affecting the Cyclic

Loading Strength of Soil," Special Technical Pub. No. 450,  
Symposium on Vibration Effects of Earthquakes on Soils and  
Foundations, ASTM.

25. Lysmer, J., Seed, H. B. and Schnabel, P. B. (1970), "Influence of Base Rock Characteristics on Ground Response," Earthquake Engineering Research Center, University of California, Berkeley, Report No. EERC 70-7.
26. Martin, G. R., Finn, W. D. L. and Seed, H. B. (1975), "Fundamentals of Liquefaction Under Cyclic Loading," Journal of the Geotechnical Engineering Division, ASCE, Vol. 101, No. GT5.
27. Maslov, N. N. (1958), "Problem of High Earth Dam Density in Conditions of Seismic Activity," Proceedings of 6th International Congress on Large Dams, Vol. III-R, 115.
28. National Academy of Sciences (1973), "The Great Alaska Earthquake of 1964 - Engineering," Committee on the Alaska Earthquake of the Division of Earthquake Sciences, National Research Council.
29. Osaki, Y. (1966), "Niigata Earthquakes, 1964 Building Damage and Soil Condition," Soils and Foundations, Japan Society of Soil Mechanics and Foundation Engineering, Vol. 6, No. 2.
30. Peacock, W. H. and Seed, H. B. (1968), "Sand Liquefaction Under Cyclic Loading Simple Shear Conditions," Journal of the Soil Mechanics and Foundations Division, ASCE, Vol. 94, No. SM3.
31. Roscoe, K. H. (1953), "An apparatus for the Application of Simple Shear to Soil Samples," Proceedings, 3rd International Conference on Soil Mechanics and Foundation Engineering, Vol. 1.
32. Scott, R. F. (1963), Principles of Soil Mechanics, Addison-Wesley Publishing Company, Inc., 1963.

33. Seed, H. B. and Lee, K. L. (1966), " Liquefaction of Saturated Sands During Cyclic Loading, " Journal of the Soil Mechanics and Foundations Division, ASCE, Vol. 92, No. SM6.
34. Seed, H. B. and Peacock W. H. (1971), " Test Procedures for Measuring Soil Liquefaction Characteristics," Journal of the Soil Mechanics and Foundations Division, ASCE, Vol. 97, No. SM8.
35. Seed, H. B. and Idriss, I. M. (1971), " Simplified Procedure for Evaluating Soil Liquefaction Potential, Journal of the Soil Mechanics and Foundations Division, ASCE, Vol. 97, No. SM9.
36. Seed, H. B. and Idriss, I. M. (1967), " Analysis of Soil Liquefaction: Niigata Earthquake," Journal of the Soil Mechanics and Foundation Division, ASCE, Vol. 93, No. SM3.
37. Seed, H. B. , Idriss, I. M. , Makdisi, F. and Banerjee, N. (1975), " Representation of Irregular Stress Time History by Equivalent Uniform Stress Series in Liquefaction Analyses," Earthquake Engineering Research Center, University of California, Berkeley, Report No. 75-29.
38. Seed, H. B. , Mori, K. and Chan, C. K. (1975), " Influence of Seismic History on Liquefaction Characteristics of Sands," Earthquake Engineering Research Center, University of California, Berkeley, Report No. 75-25.
39. Shannon and Wilson, Inc. and Agbabian-Jacobsen Associates (1972), " Soil Behavior Under Earthquake Loading Conditions," Report to Union Carbide Corporation, Nuclear Division, Oak Ridge National Laboratory, Oak Ridge, Tennessee.
40. Sherif, M. A. , Ishibashi, I. and Tsuchiya, C. (1977), " Liquefaction of Partially Saturated Soils," Proceedings, Sixth World

Conference on Earthquake Engineering, New Delhi, India.

41. Sherif, M. A. , Ishibashi, I. and Tsuchiya, C. (1977), " Pore Pressure Rise Mechanism and Soil Liquefaction," Paper submitted to Journal of the Geotechnical Engineering Division, ASCE.
42. Shibata, T. , Yukitomo, H. and Miyoshi, M. (1972), " Liquefaction Process of Sand During Cyclic Loading," Soils and Foundations , Japanese Society of Soil Mechanics and Foundation Engineering, Vol. 12, No.1.
43. Shilver, M. L.(1971), " Deformation Characteristics of Sands Under Cyclic Loading," Journal of the Soil Mechanics and Foundation Div. , ASCE, Vol. 97, No. SM8.
44. Skempton, A. W. (1954), " The Pore Pressure Coefficients A and B," Geotechnique, Vol. IV
45. Tanimoto, K. (1967), " Liquefaction of Sand Layer Subjected to Shock and Vibratory Loads," Proceedings, 3rd Asian Regional Conference on Soil Mechanics and Foundation Engineering, Haifa, Vol. 1.
46. Yoshimi, Y. (1967)," An Experimental Study of Liquefaction of Saturated Sands," Soils and Foundations, Japan Society of Soil Mechanics and Foundation Engineering, Vol. 7, No. 2.
47. Yoshimi, Y. and Oh-hara, H. (1975)," Influence of Degree of Shear Stress Reversal on the Liquefaction Potential of Saturated Sands," Soils and Foundations, Japan Society of Soil Mechanics and Foundation Engineering, Vol. 15, No. 3.
48. Walsh, J. B. (1966), " Seismic Wave Attenuation in Rock Due to Friction," Journal of Geophysical Research, Vol. 71, No. 10.
49. Wu, Ming-Jium (1968), " Short Term Failure Criterion For Seattle Clays," thesis submitted in partial fulfillment of the

requirements for the degree of Master of Science, University of  
Washington, Seattle, Washington.

TABLE 1  
PHYSICAL PROPERTIES OF OTTAWA SAND

Ottawa sand (ASTM C-109)	
Grain size	$D_{100} = 0.60 \text{ mm}$ , $D_{60} = 0.42 \text{ mm}$ , $D_{50} = 0.40 \text{ mm}$ $D_{10} = 0.2 \text{ mm}$ , $D_0 = 0.15 \text{ mm}$
Uniformity coefficient	2.1
Specific Gravity	2.67
Maximum void ratio, $e_{\max}$	0.76*
Minimum void ratio, $e_{\min}$	0.50

\*  $e_{\max} = 0.82$  was reported by Finn et al (1971) for the same sand.

TABLE 2  
TEST PROGRAM FOR SATURATED SAMPLES

	Uniform cyclic loading	Non-uniform cyclic loading
Sample type	Ottawa sand (ASTM C-109)	
$\bar{e}$	Varied between 0.89 and 0.94	
Back pressure	45 psi for all tests	
Wave shape	Sine wave for all tests	
Densities	Three different density levels, loose ( $\bar{e} = 0.700$ ), medium dense ( $\bar{e} = 0.644$ ) and dense ( $\bar{e} = 0.595$ )	
Frequency	2 cps	
Wave patterns	Constant cyclic shear stress amplitude	Non-uniform patterns, Type (A),(B) and (C) for loose samples, Type (A) for medium dense and dense samples.
Initial effective vertical and horizontal stresses	10, 20, 30 psi	20 psi

TABLE 3. TEST PROGRAM FOR PARTIALLY  
SATURATED SAMPLES

Pore pressure parameter, $\bar{B}$	0.25	0.45	0.6	0.8	> 0.9
Back Pressure, $U_b$ , psi	5, 15	5, 15	15, 25	25	25, 45
Initial Effective Ver- tical stress, $\sigma_v$ , psi	10, 20, 30				
Initial Effective Hori- zontal stress, $\sigma_h$ , psi	10, 20, 30				
Frequency, $H_z$	2				
Wave Shape	Sinusoidal				

TABLE 4  
AN EXAMPLE OF  $\bar{B}$  MEASUREMENT PRIOR TO TESTING

Trial No.	$\sigma_v$ psi	$\sigma_h$ psi	Water pressure in specimen		Pore water pressure psi	$\Delta\sigma$ psi	$\Delta u$ psi	$\bar{B}$
			at top psi	at bottom psi				
1	10	10	0	5				
	10	10	closed	5	5			
	20	20	closed	closed	9.5	10	4.5	0.45
2	20	20	10	15				
	20	20	closed	15	15			
	30	30	closed	closed	22.2	10	7.2	0.72
3	30	30	20	25				
	30	30	closed	25	25			
	40	40	closed	closed	33.4	10	8.4	0.84
4	40	40	30	35				
	40	40	closed	35	35			
	50	50	closed	closed	43.9	10	8.9	0.89
5	50	50	40	45				
	50	50	closed	45	45			
	60	60	closed	closed	54.3	10	9.3	0.93

TABLE 5  
 PARAMETERS  $C_1$ ,  $C_2$ ,  $C_3$  and S FOR  
 DIFFERENT DENSITIES OF OTTAWA SAND

Densities	Parameters			
	$C_1$	$C_2$	$C_3$	S
Loose ( $\bar{e} = 0.700$ )	6.13	1.77	0.46	2.40
Medium dense ( $\bar{e} = 0.644$ )	2.40	1.82	0.30	2.17
Dense ( $\bar{e} = 0.595$ )	2.09	2.03	0.09	2.00

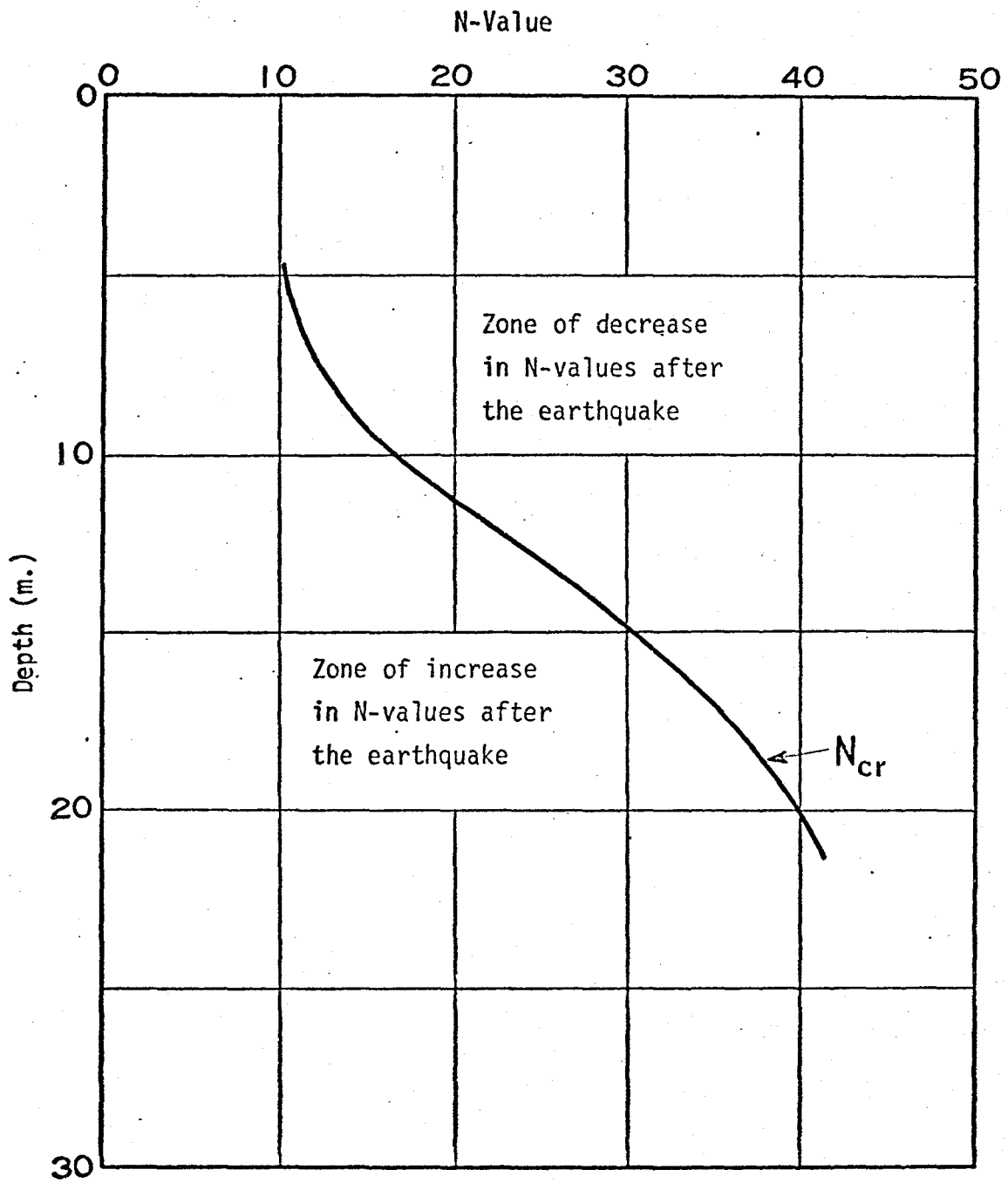


Fig. 2.1 Critical Standard Penetration Value,  $N_{cr}$ , versus Depth ( After Koizumi, 1966 )

N-Value

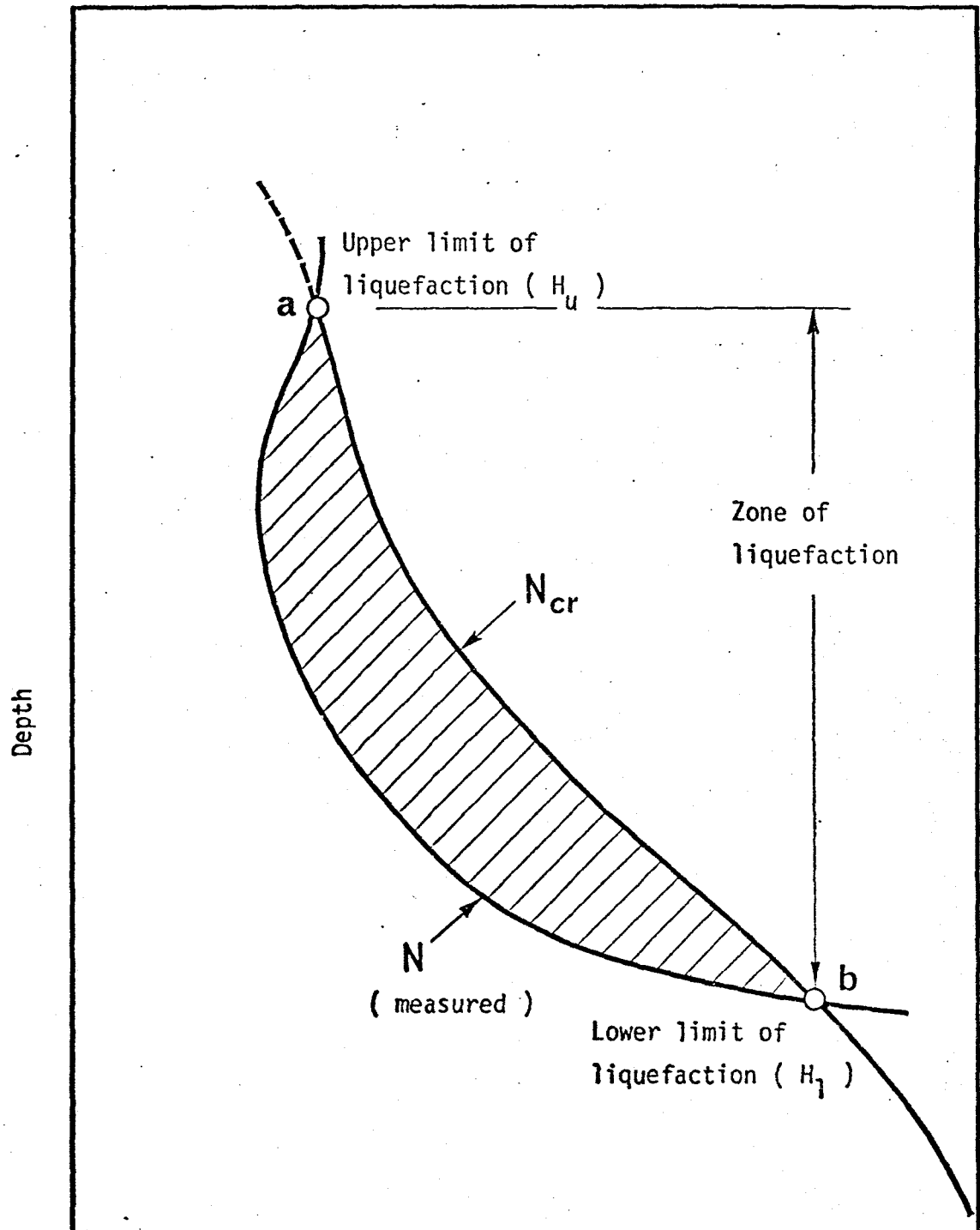


Fig. 2.2 Zone of Liquefaction  
( After Osaki, 1968 )

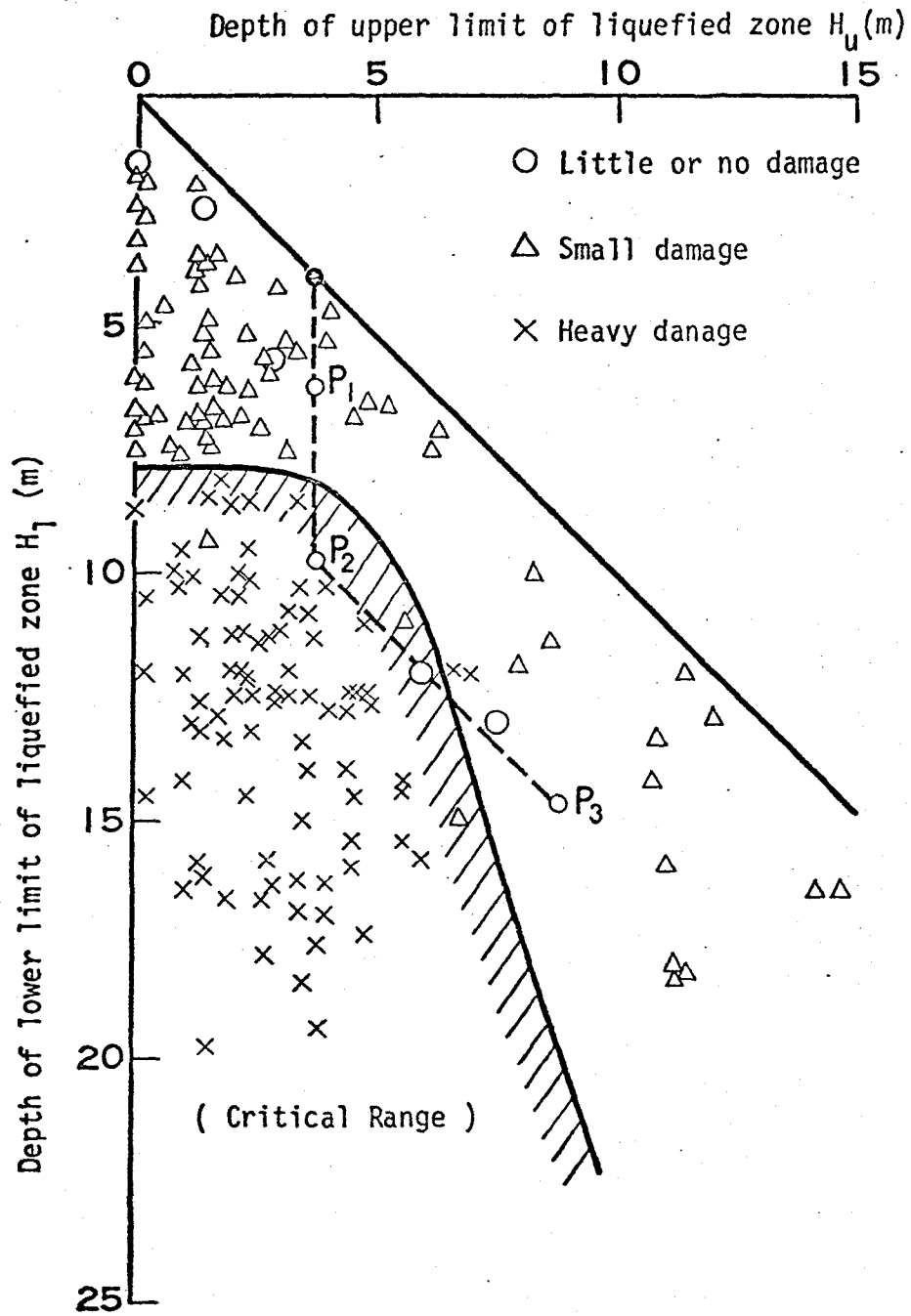


Fig. 2.3 Liquefied Zone and the Damages to Structures ( After Osaki, 1968 )

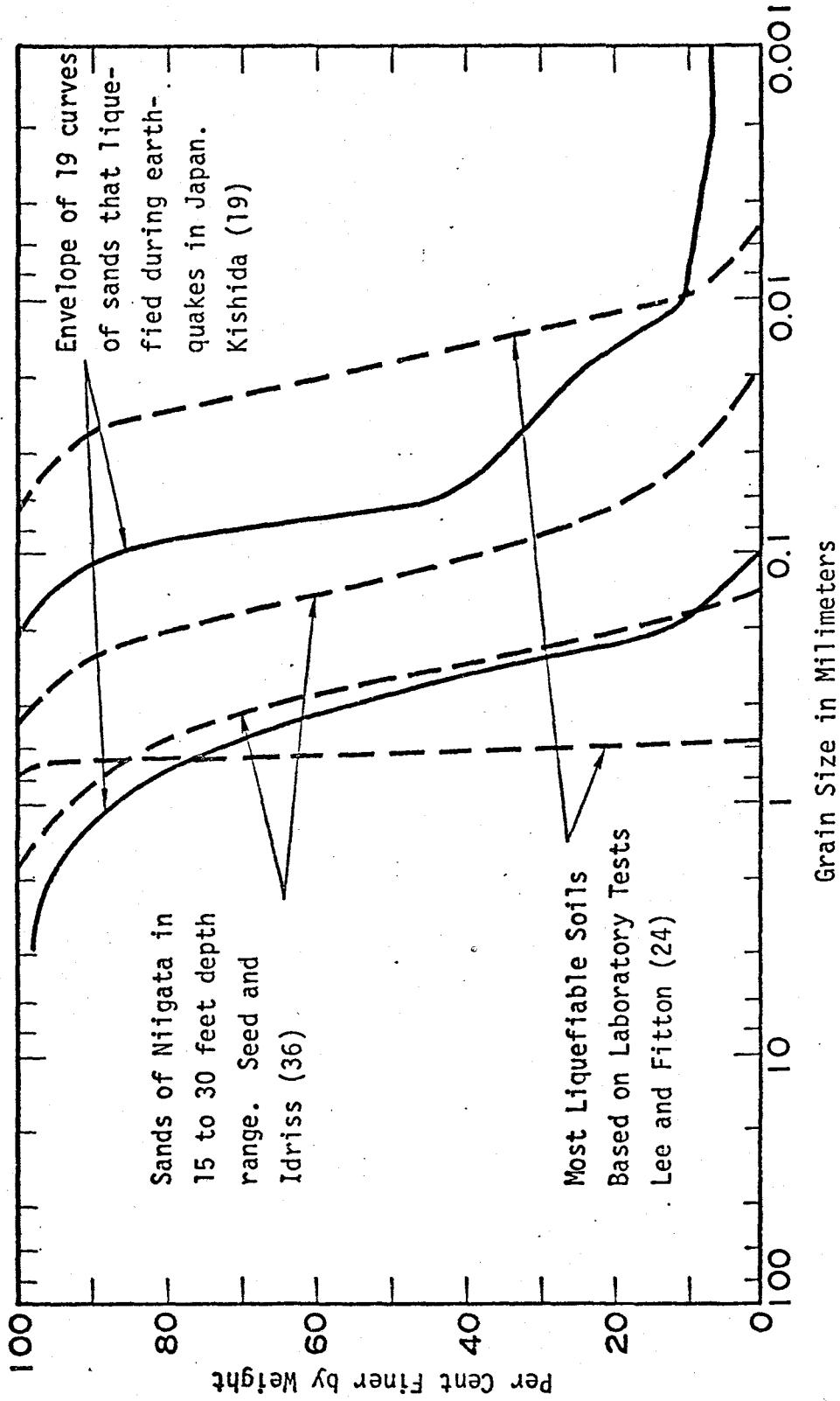


Fig. 2.4 Soils Susceptible to Liquefaction

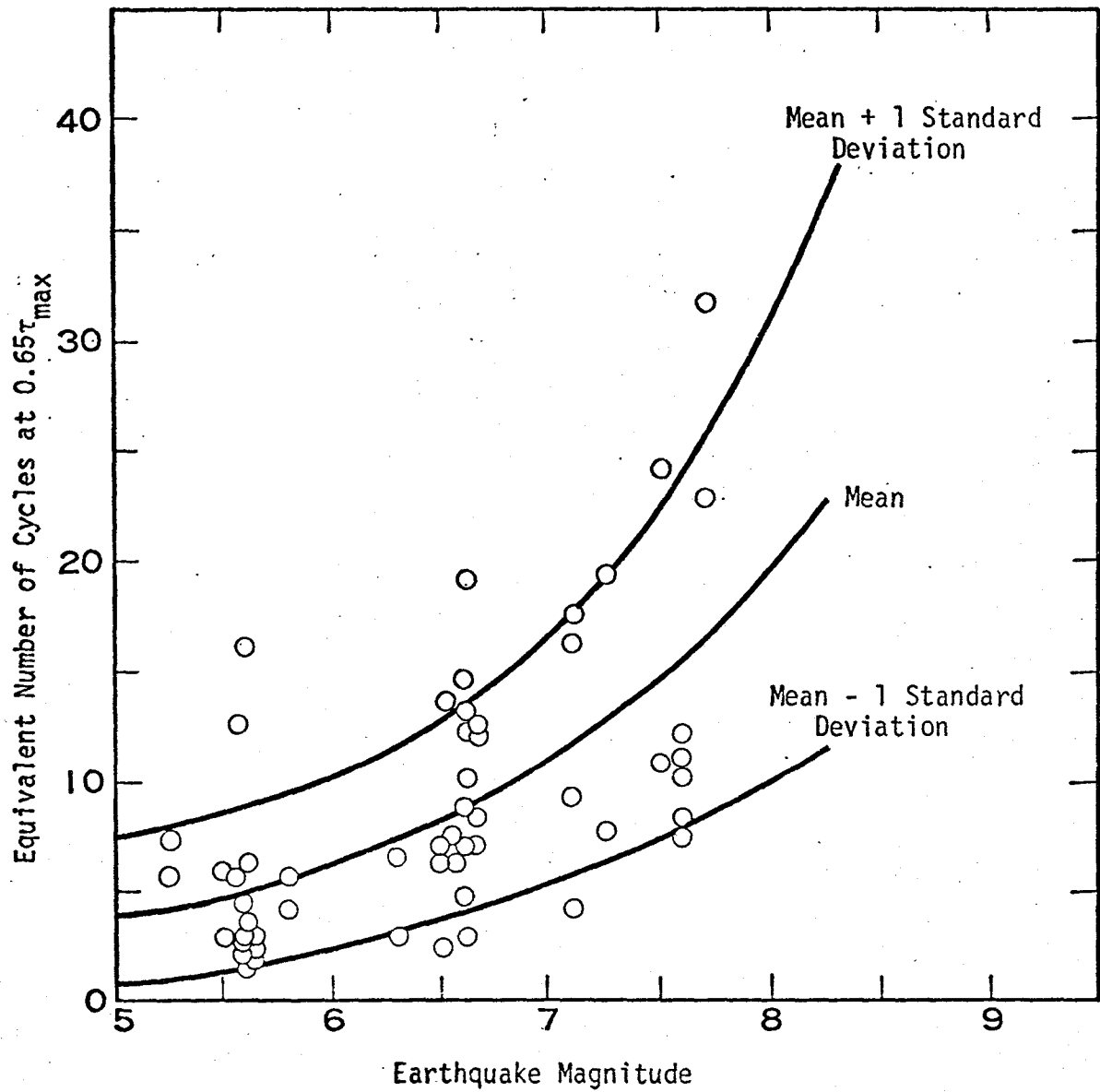


Fig. 2.5 Equivalent Numbers of Uniform Stress Cycles Based on All Components of Ground Motion ( After Seed et al, 1975 )

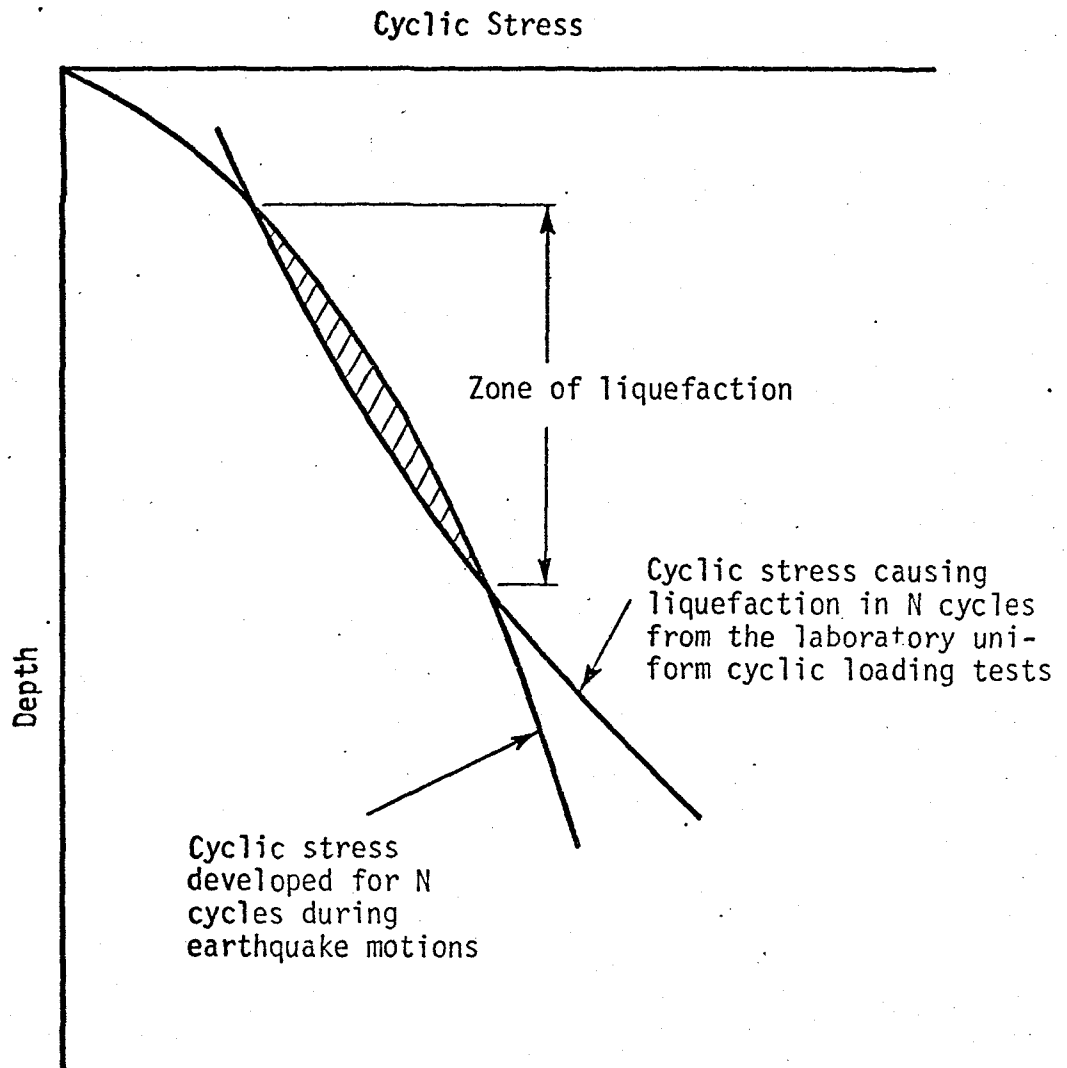


Fig. 2.6 Method of Evaluating Liquefaction Potential  
( After Seed et al, 1971 )

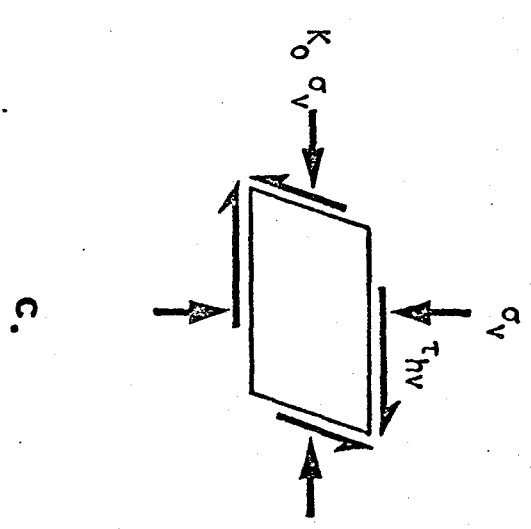
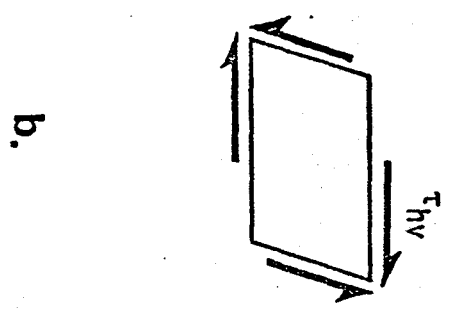
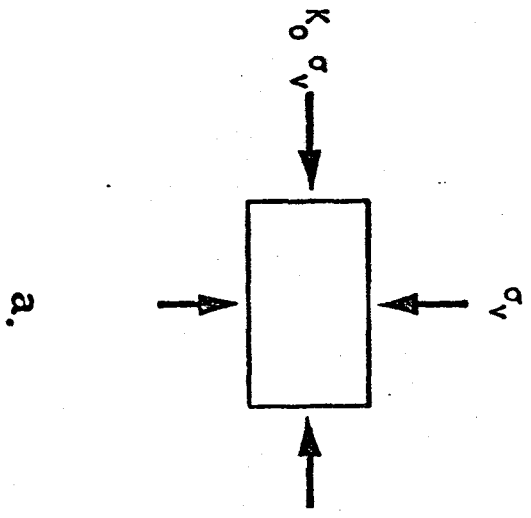


Fig. 2.7. Idealized Field Loading Conditions

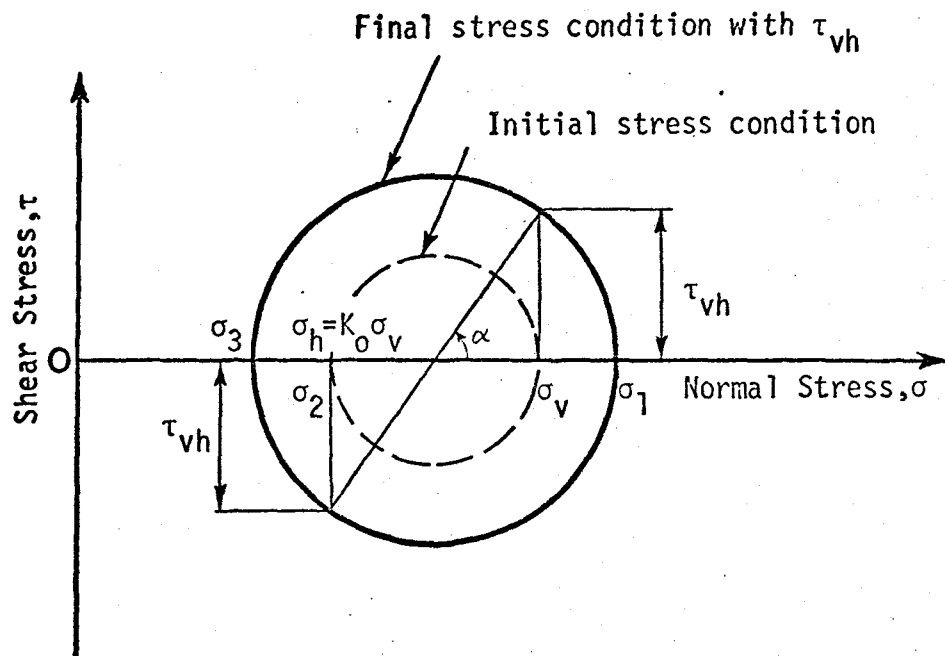


Fig. 2.8 Mohr's Diagram Representation of Stresses

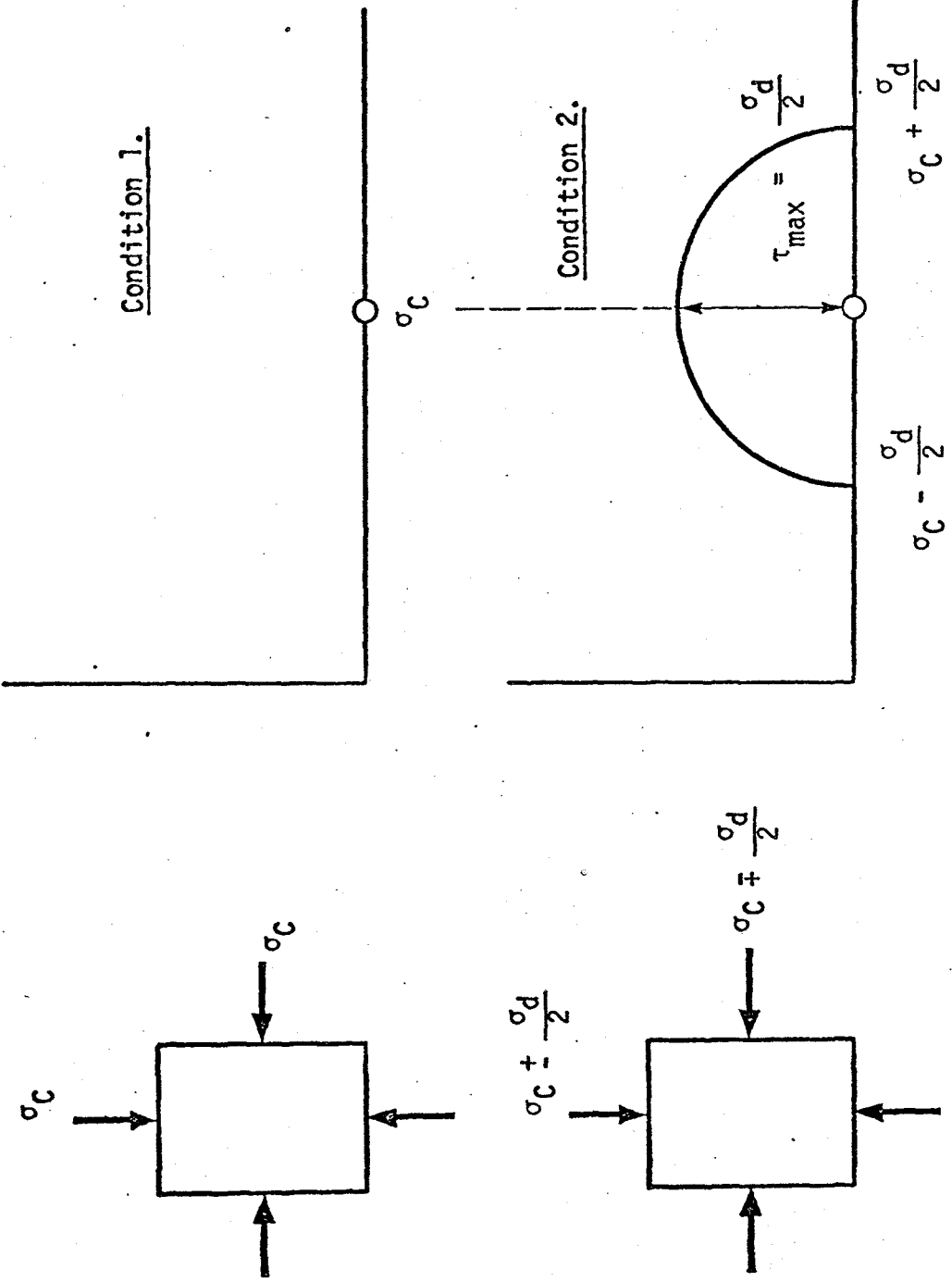


Fig. 2.9 Idealized Triaxial Test Conditions

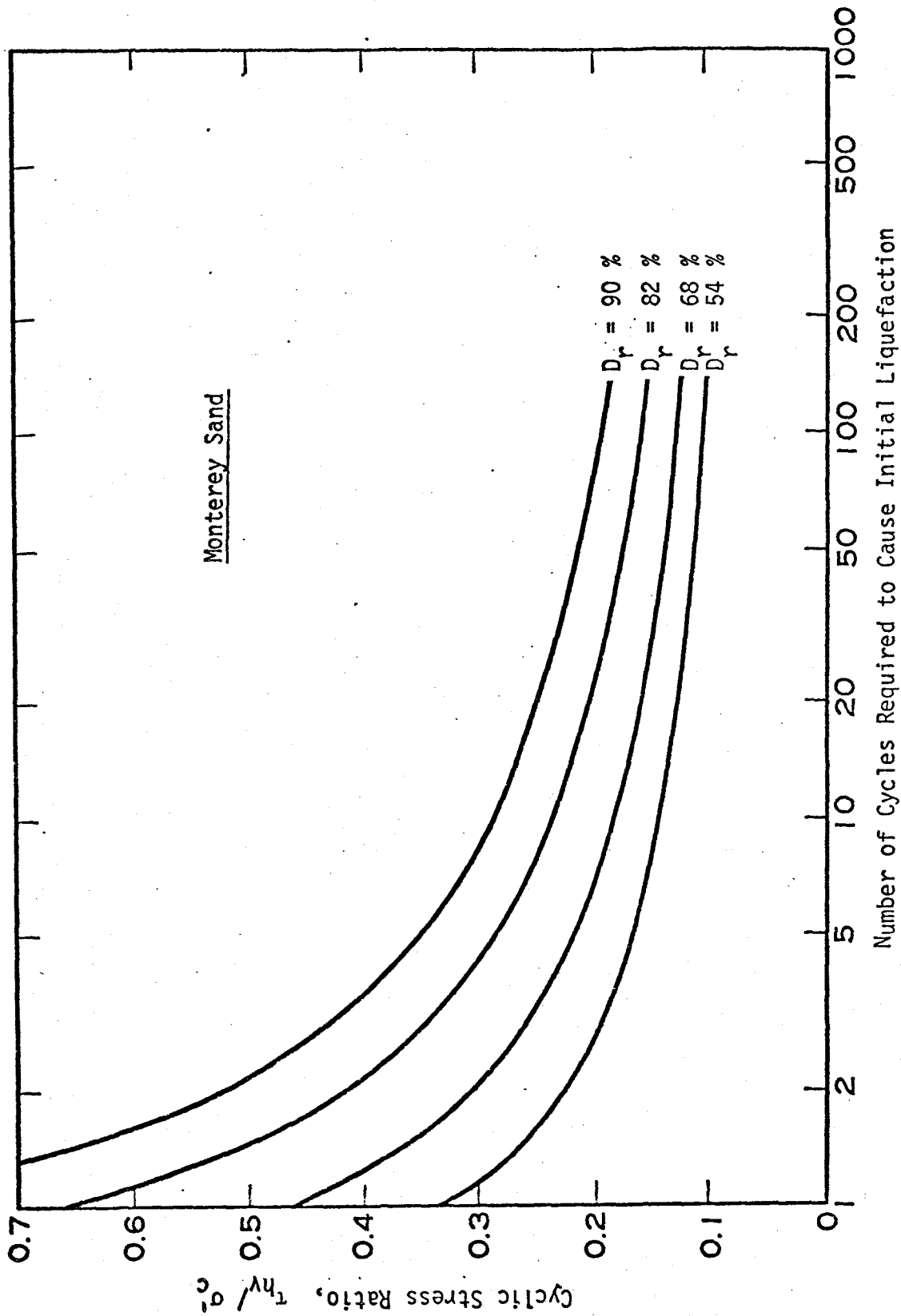


Fig. 2.10 Effect of Void Ratio on Liquefaction Potential ( After De Alba et al, 1975 )

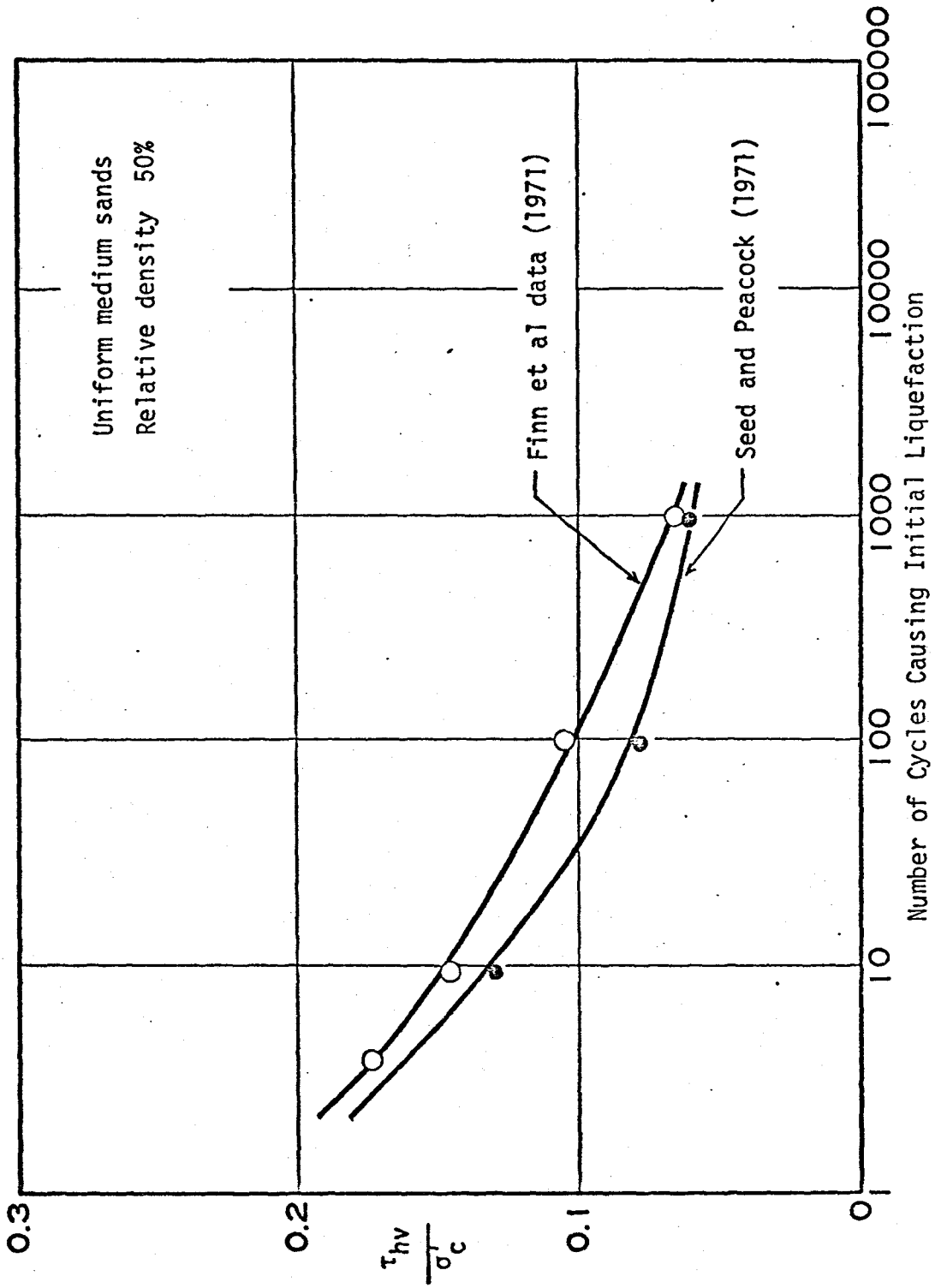


Fig. 2.11 Representation of Liquefaction Potential of Sand

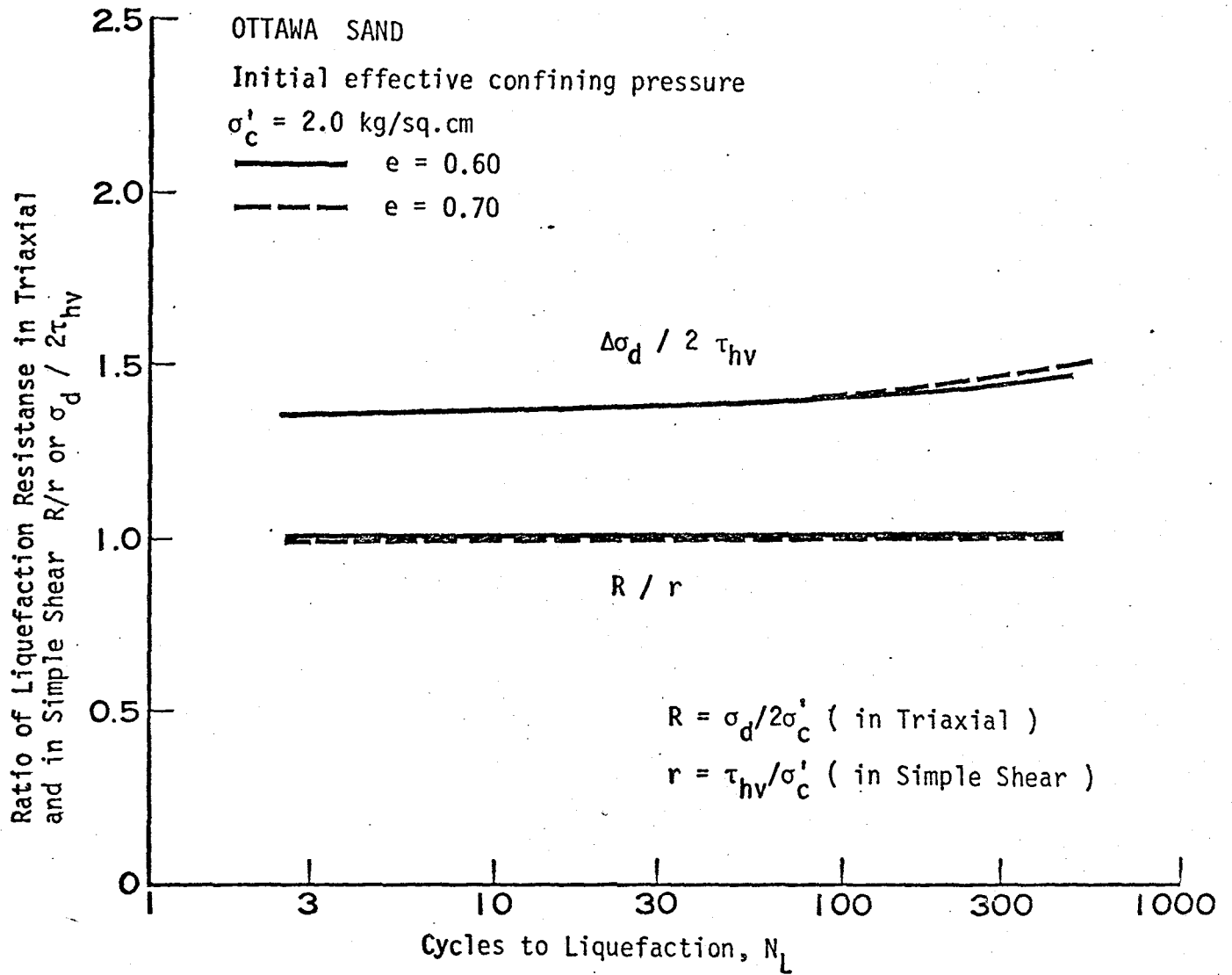


Fig. 2.12 Ratio of Liquefaction Resistance in Triaxial to that in Simple Shear, As Compared by Two Methods ( After Finn et al, 1971 )

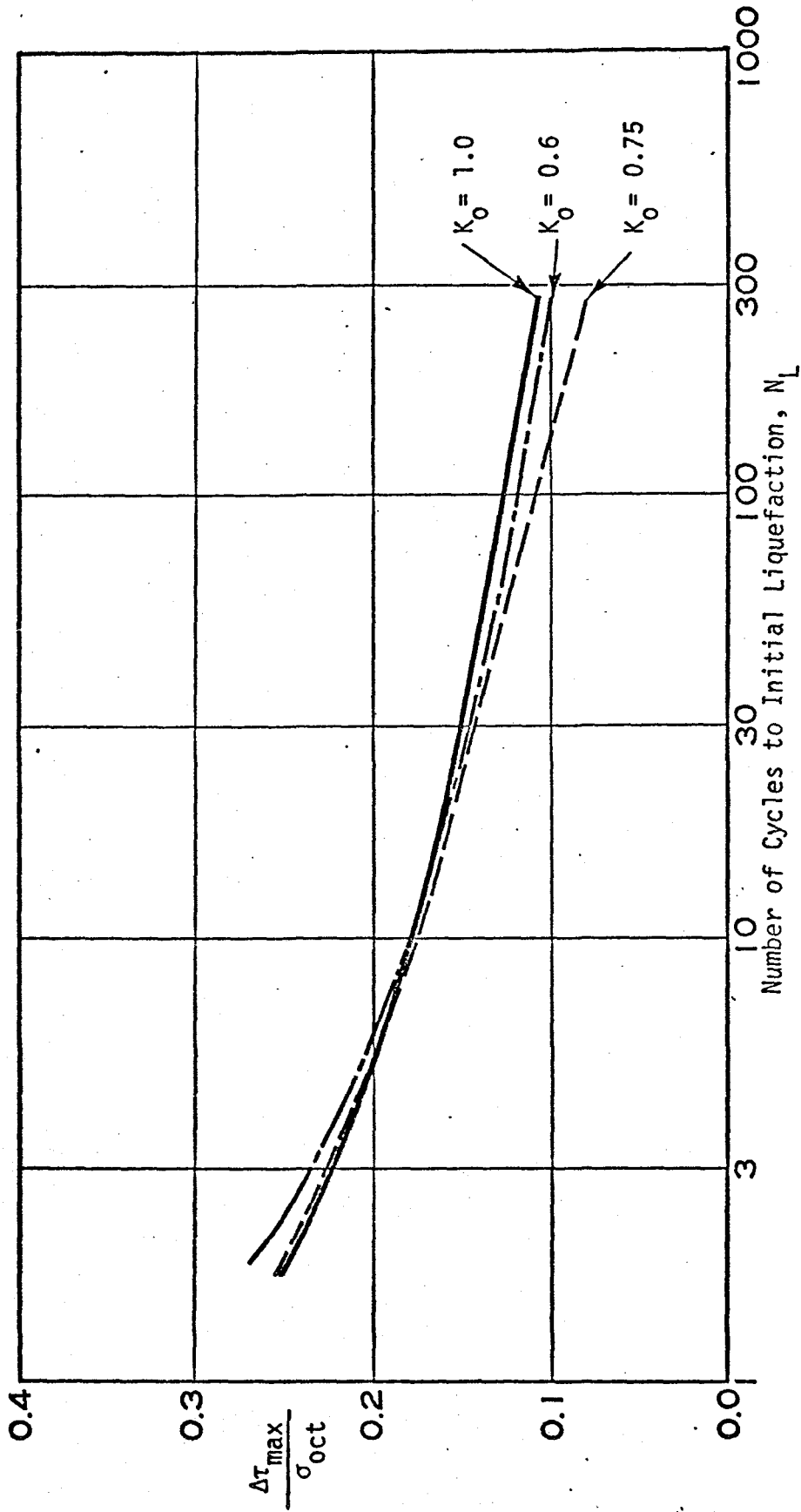


Fig. 2.13 Relationship between  $\frac{\Delta\tau_{\max}}{\sigma_{\text{oct}}}$  and The Number of Cycles to Liquefaction for Various  $K_0$  Values  
( After Ishibashi, 1974 )

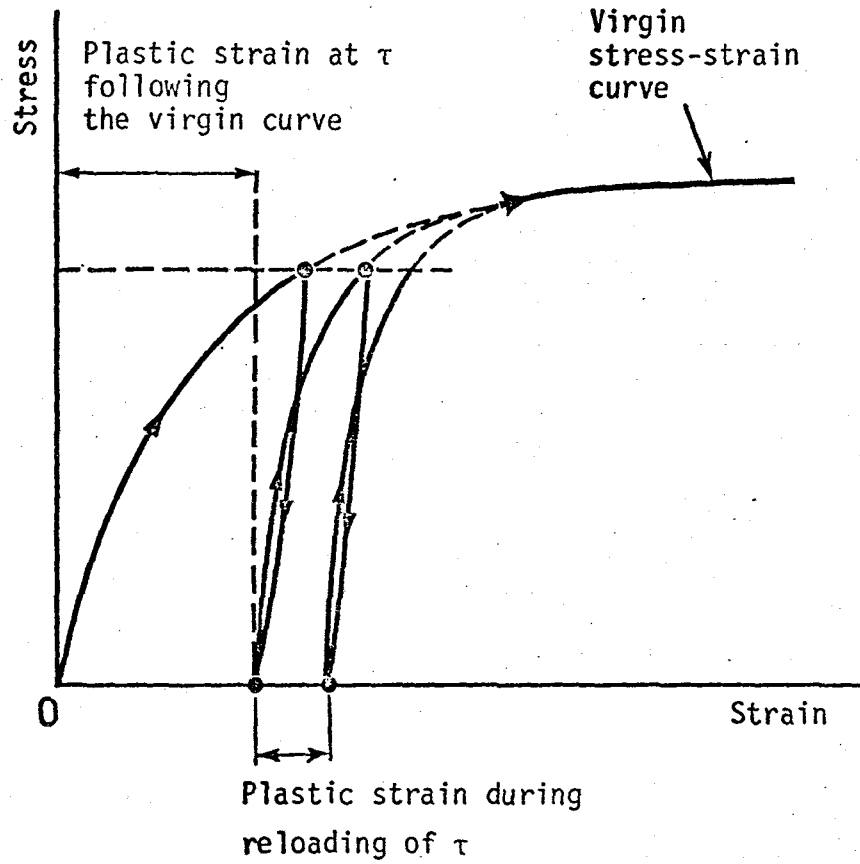


Fig. 2.14 Illustration of Stress-Strain Relationship in Loading and Reloading Process

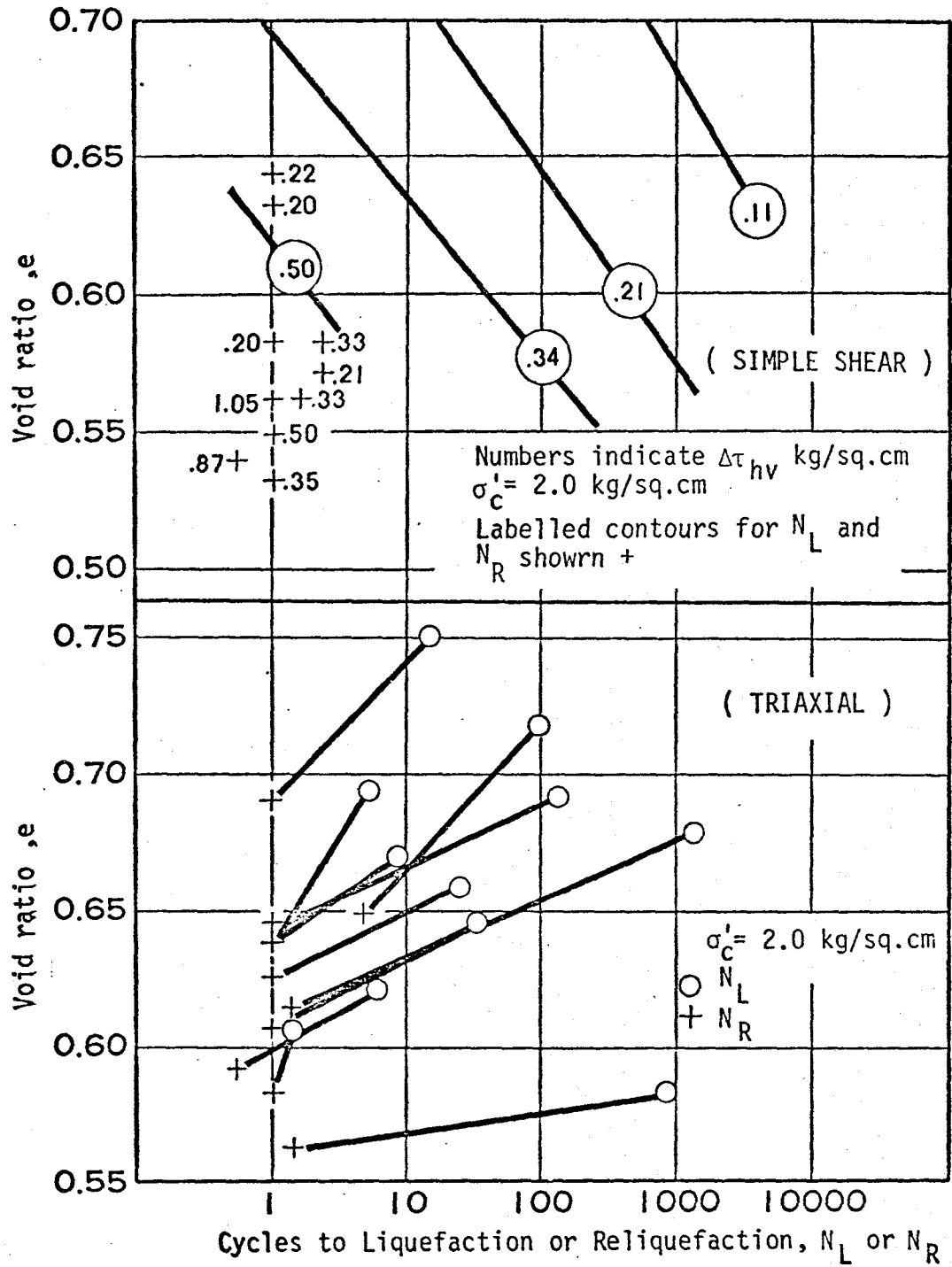


Fig. 2.15 Resistance to Reliquefaction Compared to Resistance to Liquefaction for Ottawa Sand ( After Finn, 1970 )

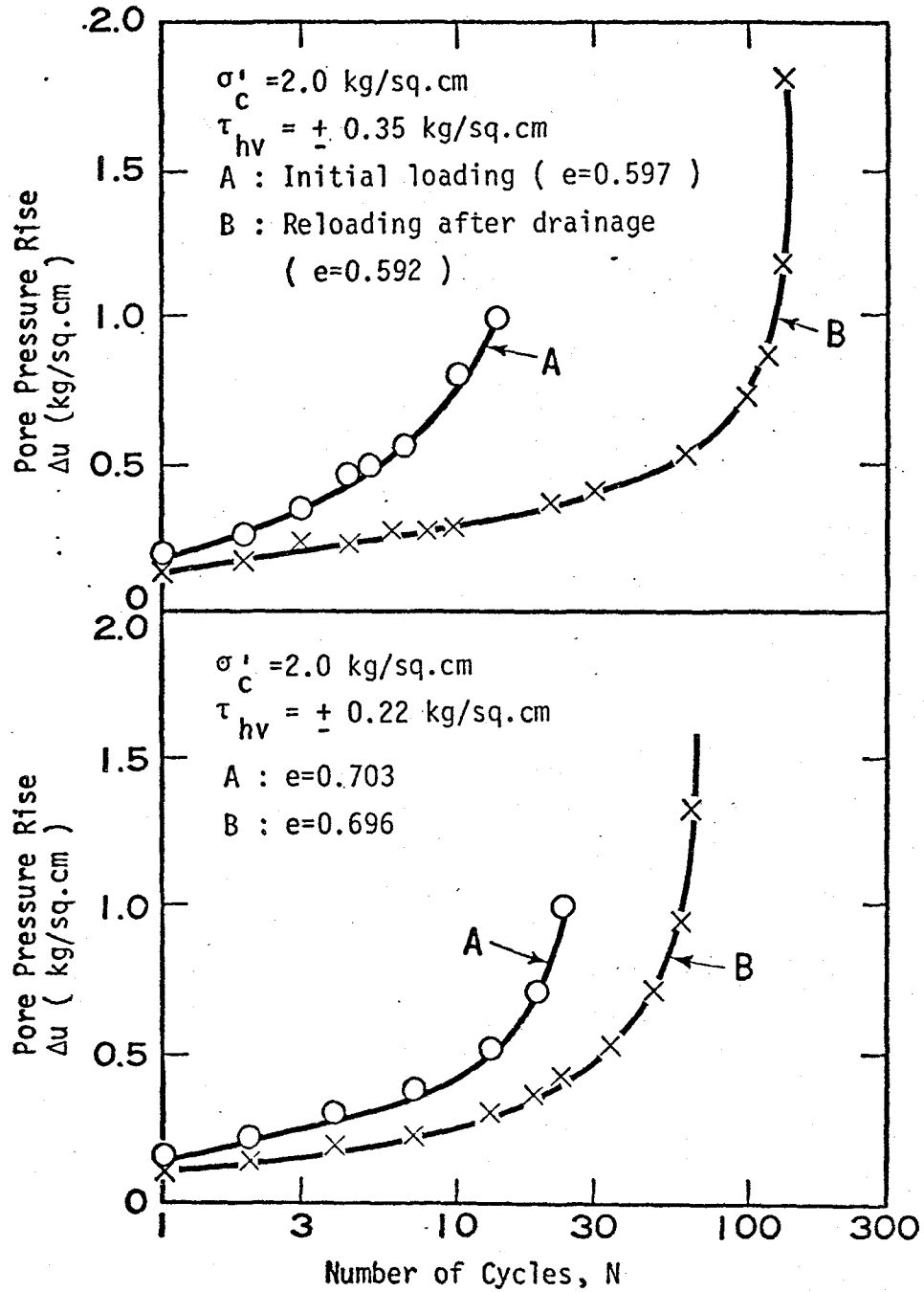


Fig. 2.16 Effect of the Previous Partial Liquefaction on the Pore Pressure Rise ( After Finn, 1970 )

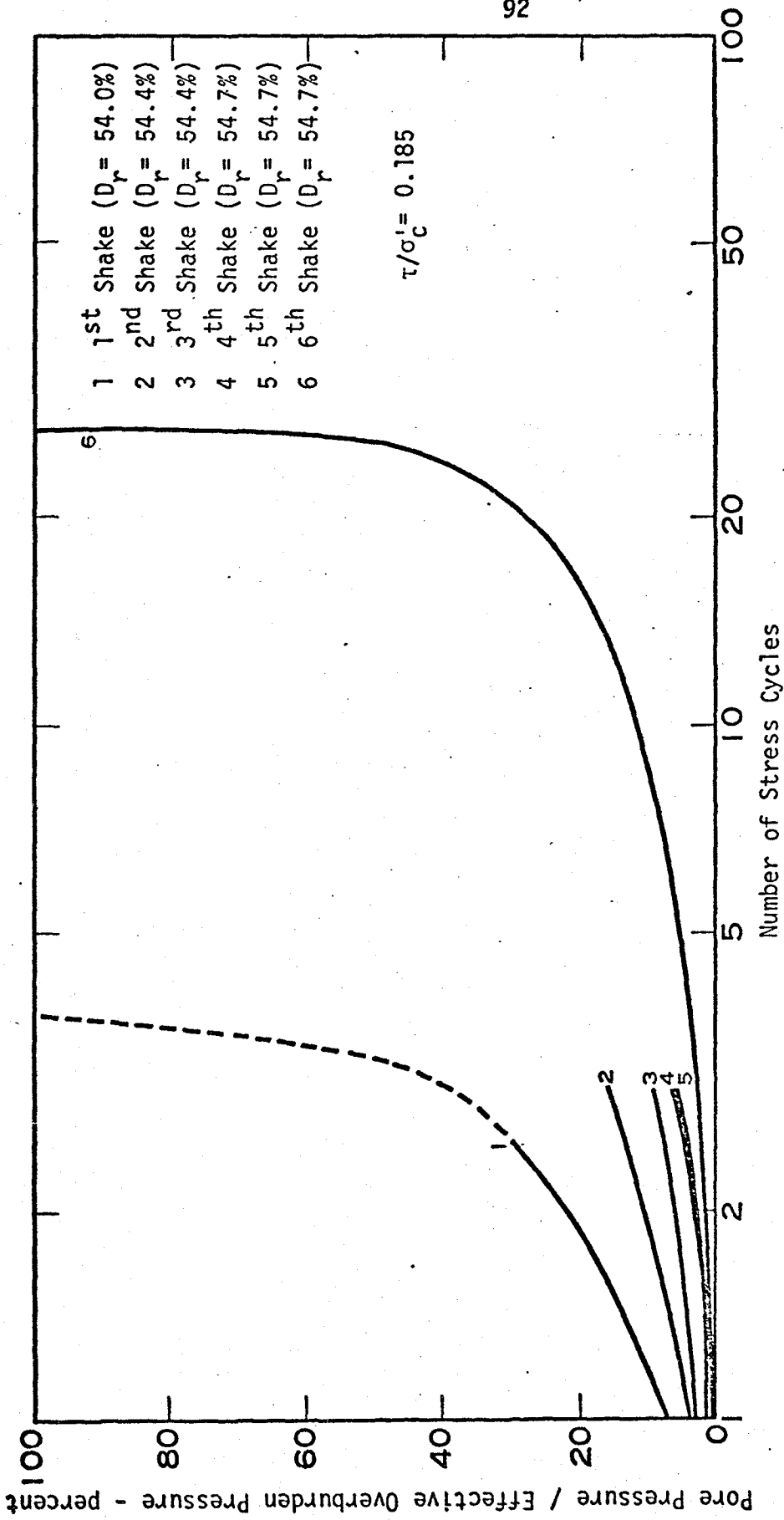


Fig. 2.17 Effect of Seismic Histories on Liquefaction Characteristics of Sand ( After Seed et al, 1975 )

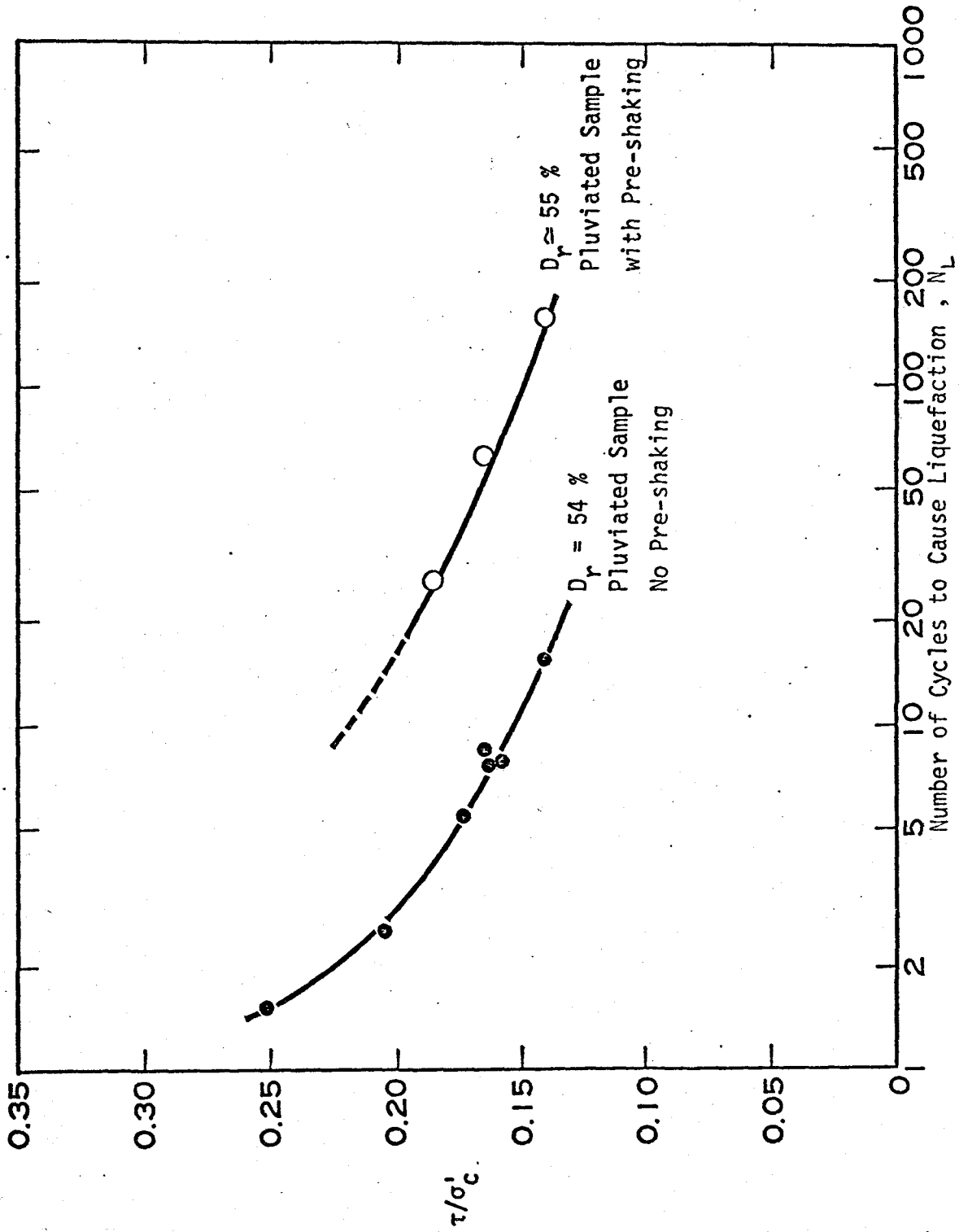


Fig. 2.18 Effect of Seismic Histories on Liquefaction Potential of Sand ( After Seed et al, 1975 )

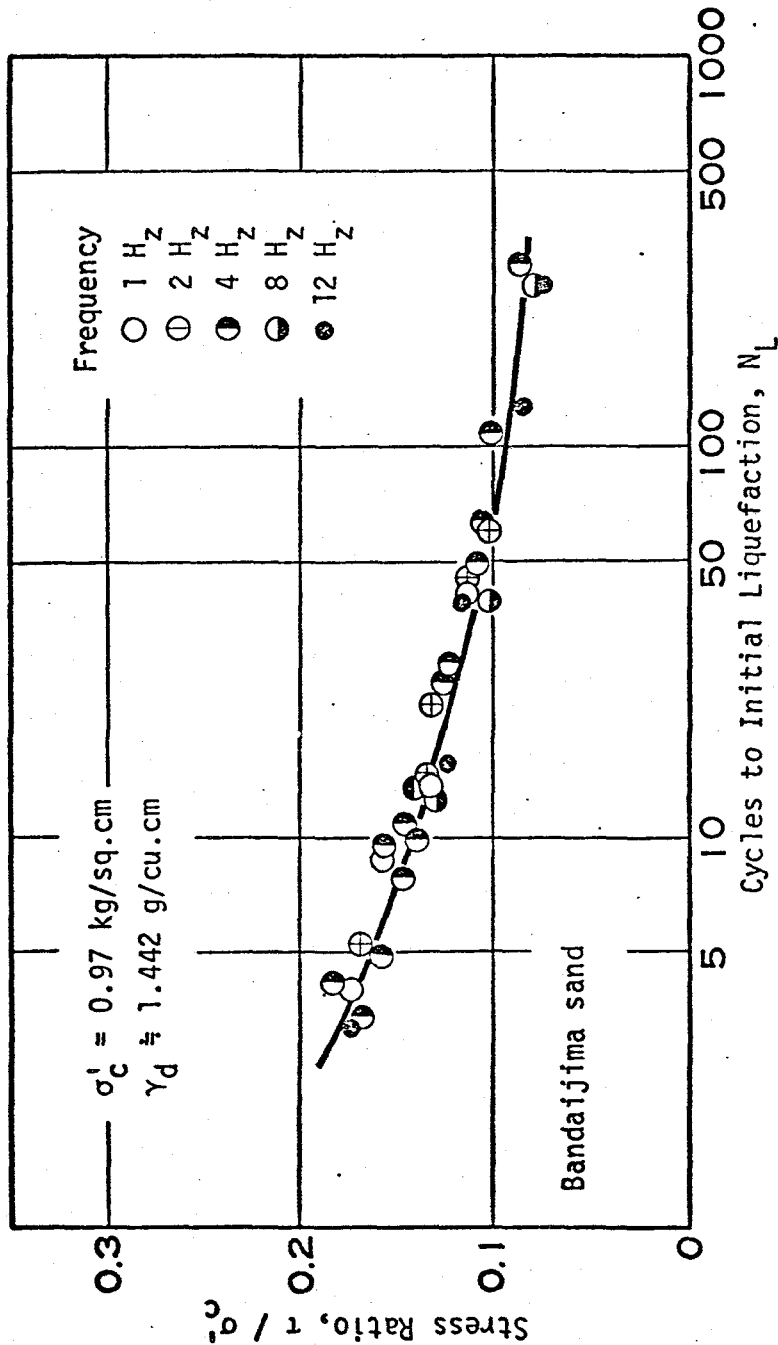


Fig. 2.19 Effect of Frequency on Liquefaction Potential ( After Yoshimi et al, 1975 )

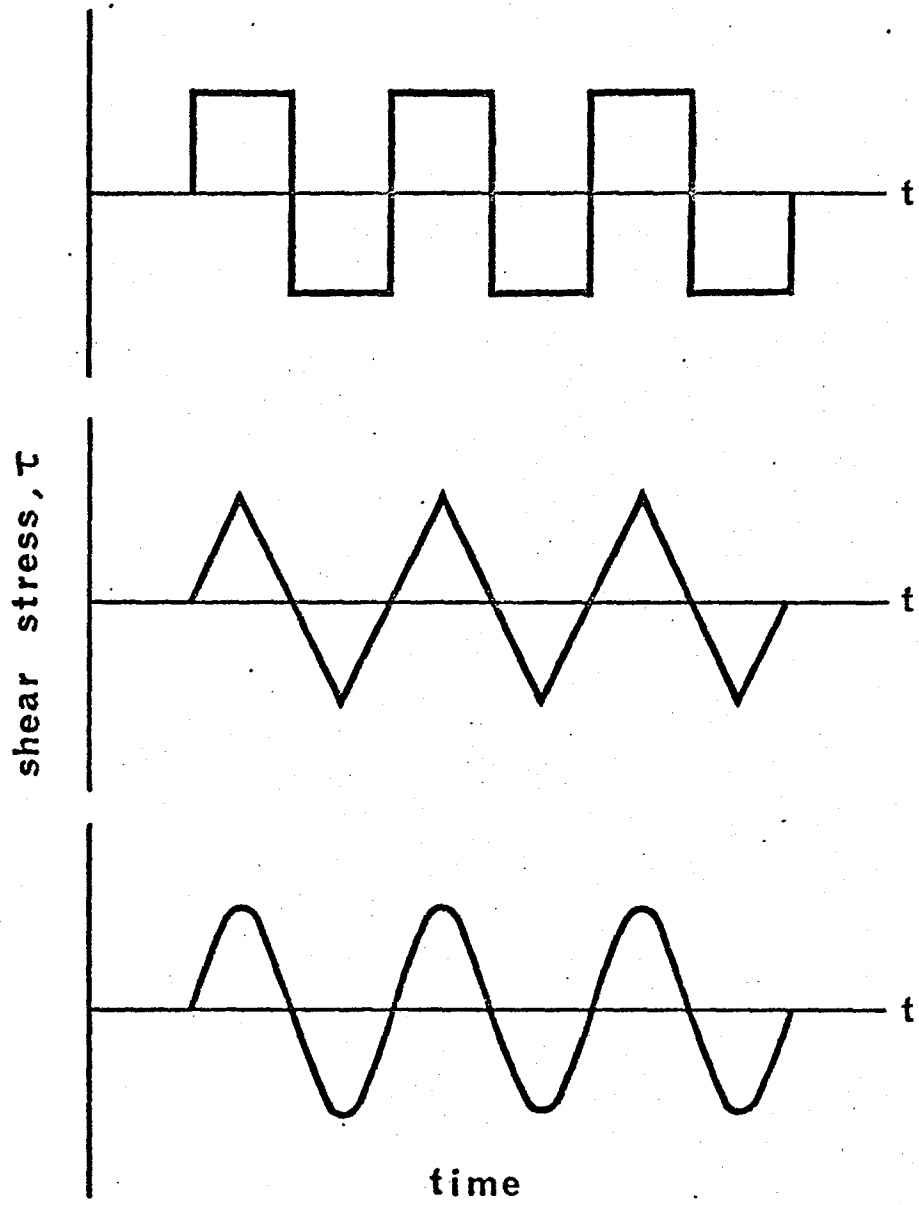


Fig. 2.20 Cyclic Shear Stress Wave Forms

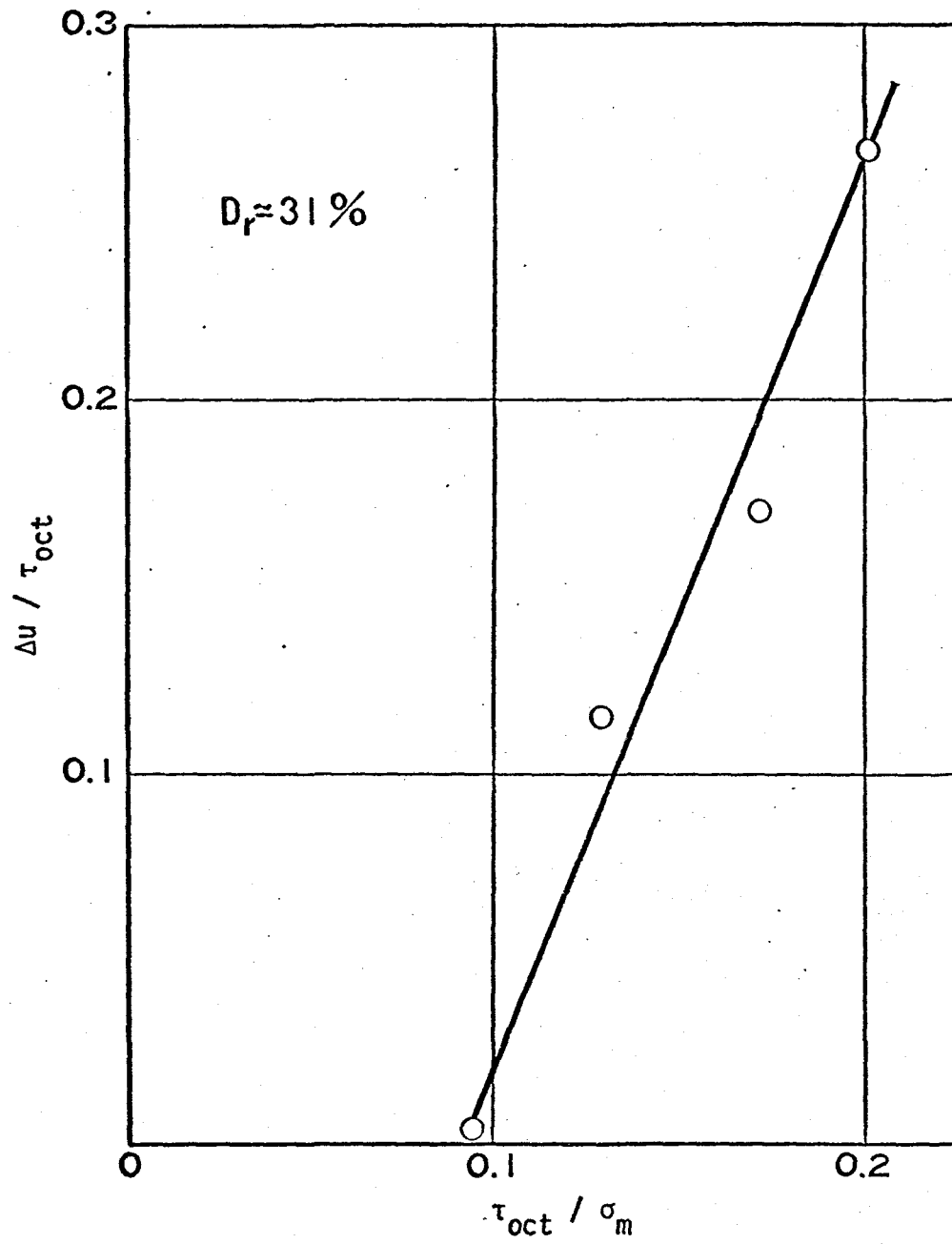


Fig. 2.21 Relationship between  $\Delta u / \tau_{oct}$  and  $\tau_{oct} / \sigma_m$   
( After Shibata et al, 1972 )

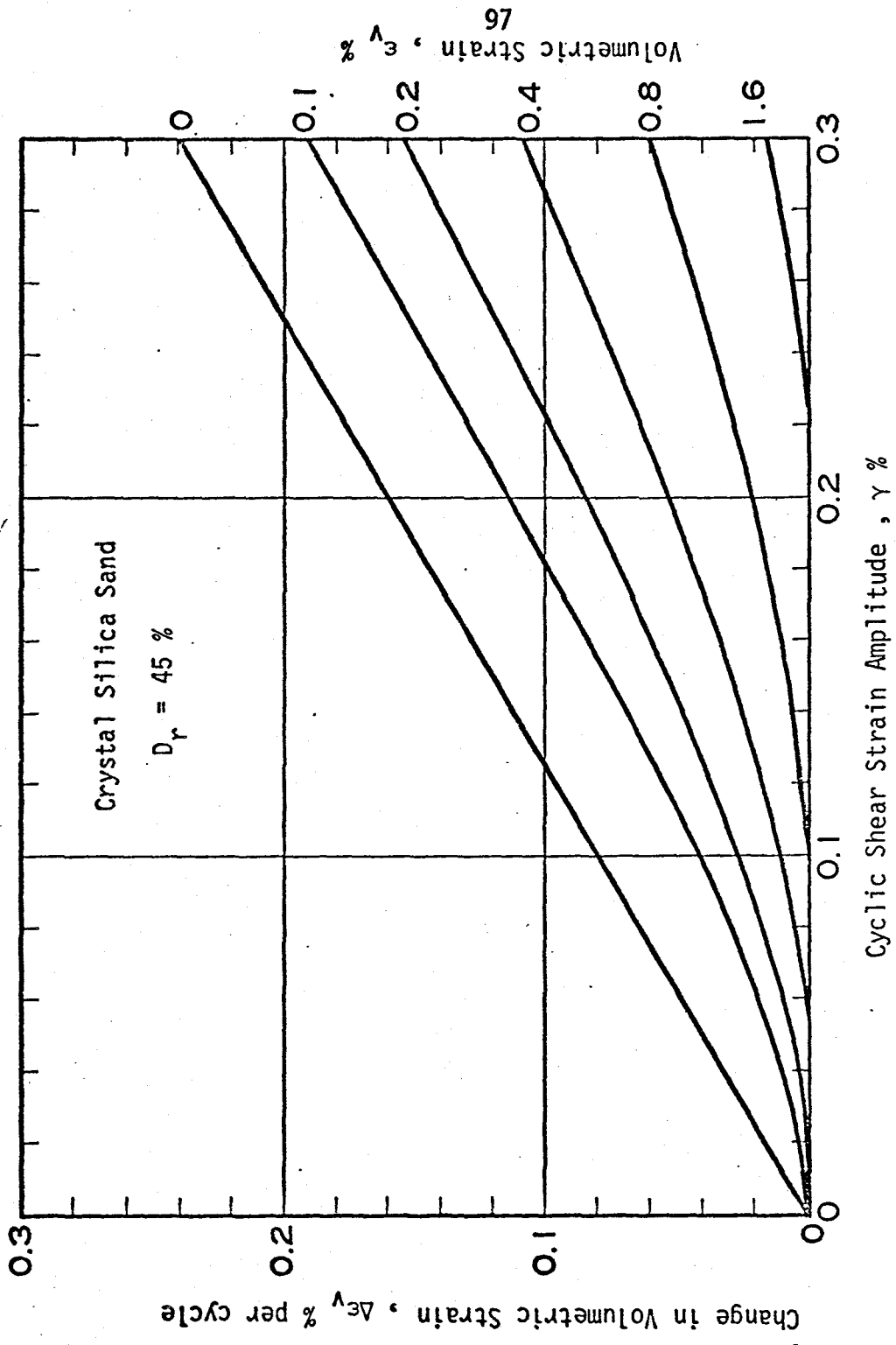


Fig. 2.22 Incremental Volumetric Strain Curves ( After Martin et al, 1975 )

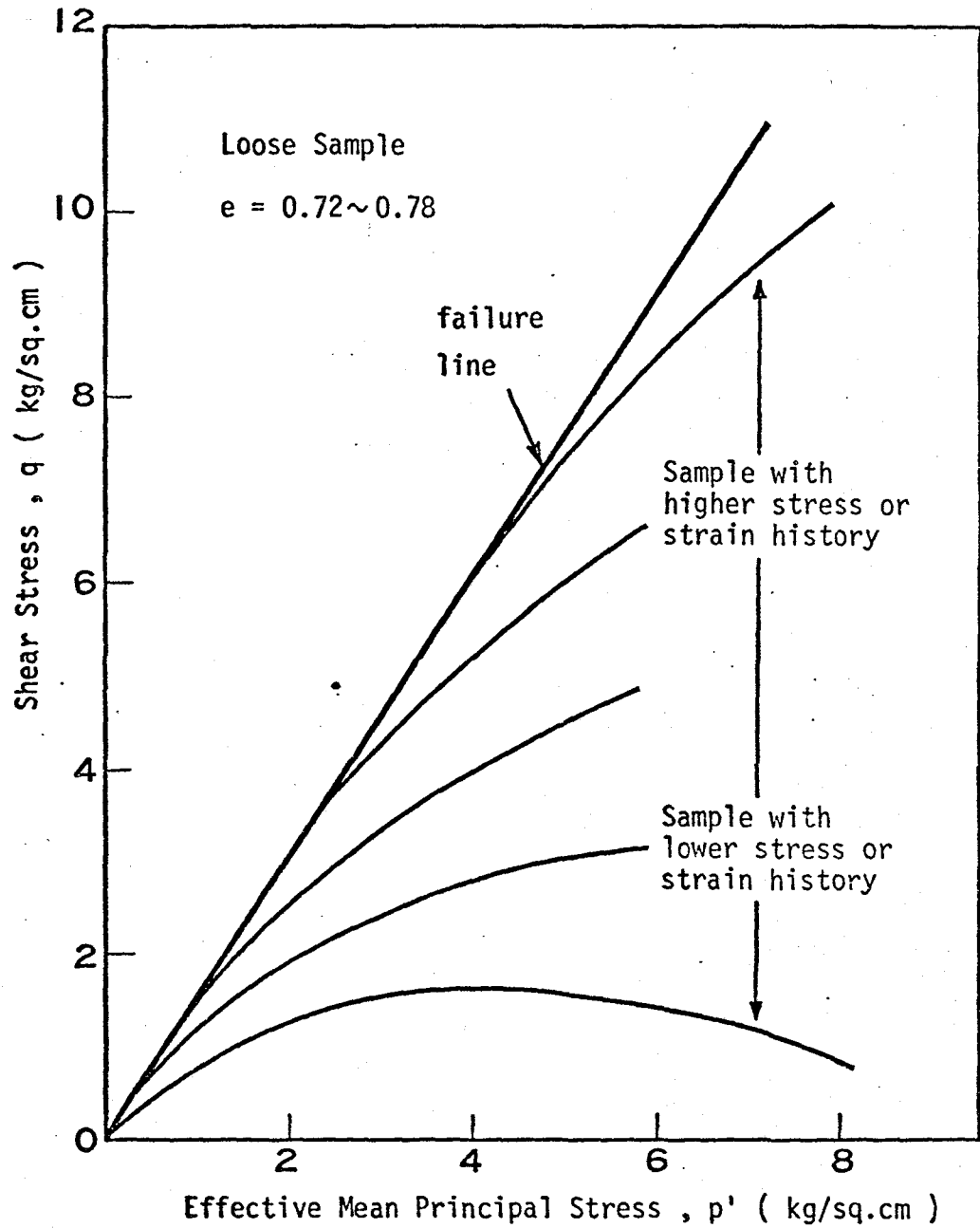


Fig. 2.23 Yield Loci for Loose Samples ( After Ishihara et al, 1976 )

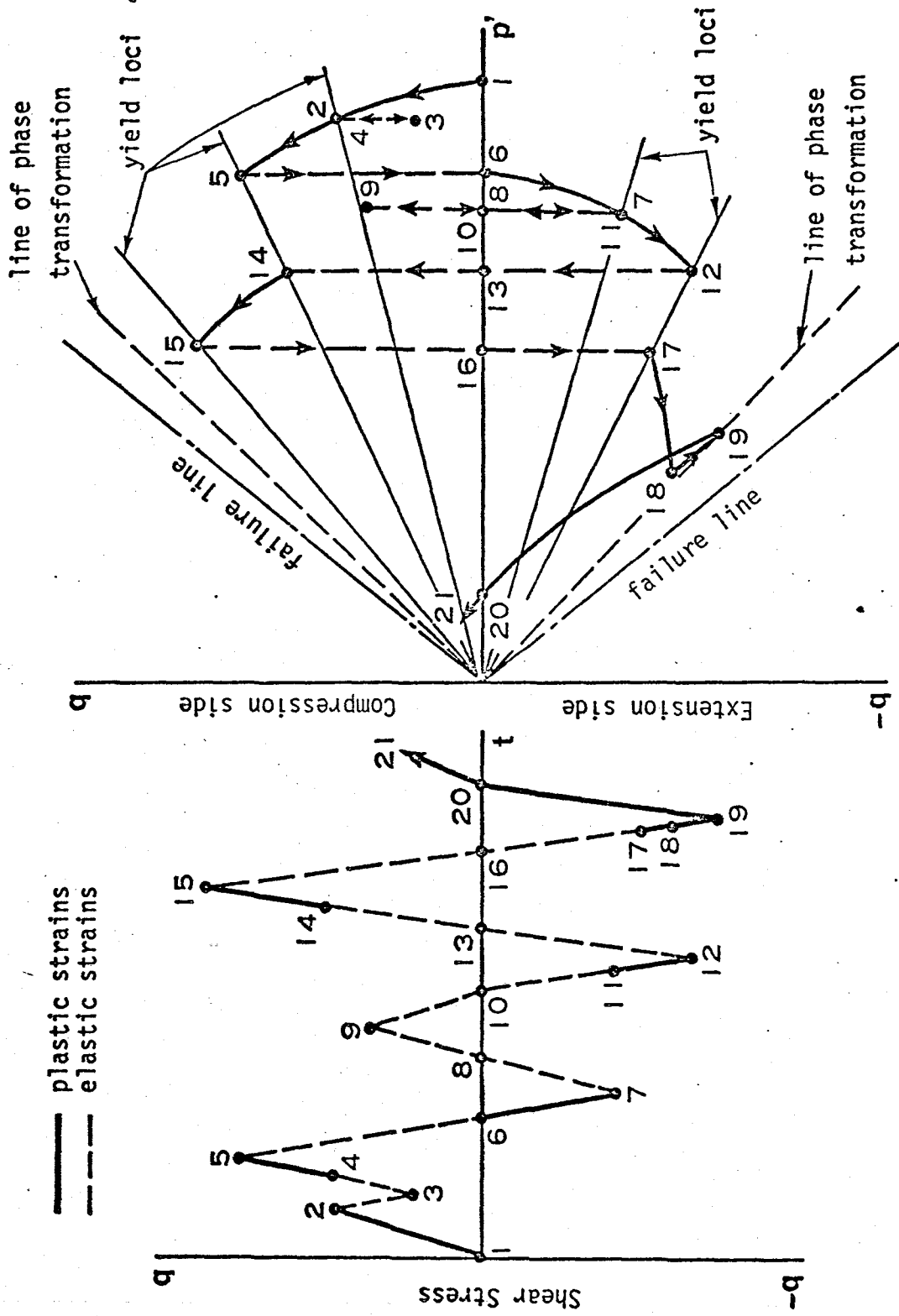


Fig. 2.24 Procedures for Establishing the Process of Pore Pressure Development  
 ( After Ishihara et al, 1976 )

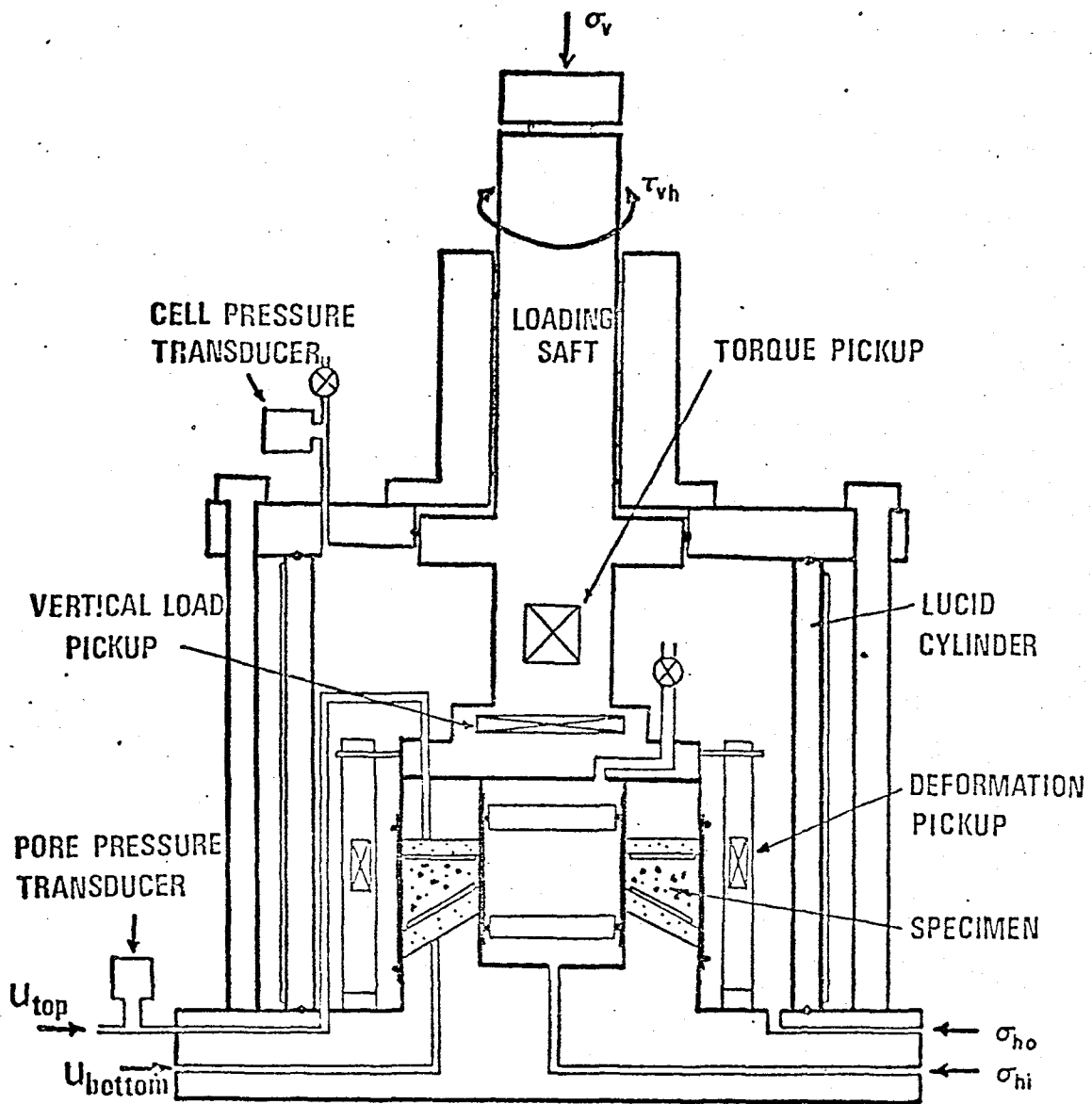
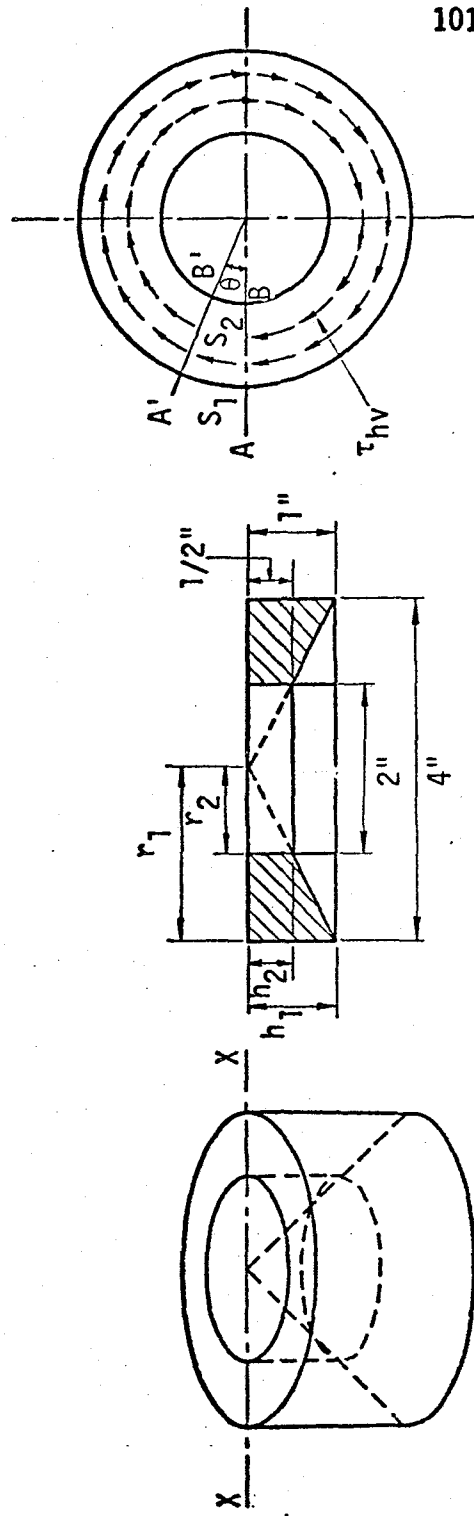


Fig. 3.1 Torsional Simple Shear Device ( TSSD )



(a) Donut-like Specimen

(b) Cross Section X-X

(c) Top View with  $\tau_{hv}$

Fig. 3.2 Sample Shape of the Torsional Simple Shear Device ( TSSD)

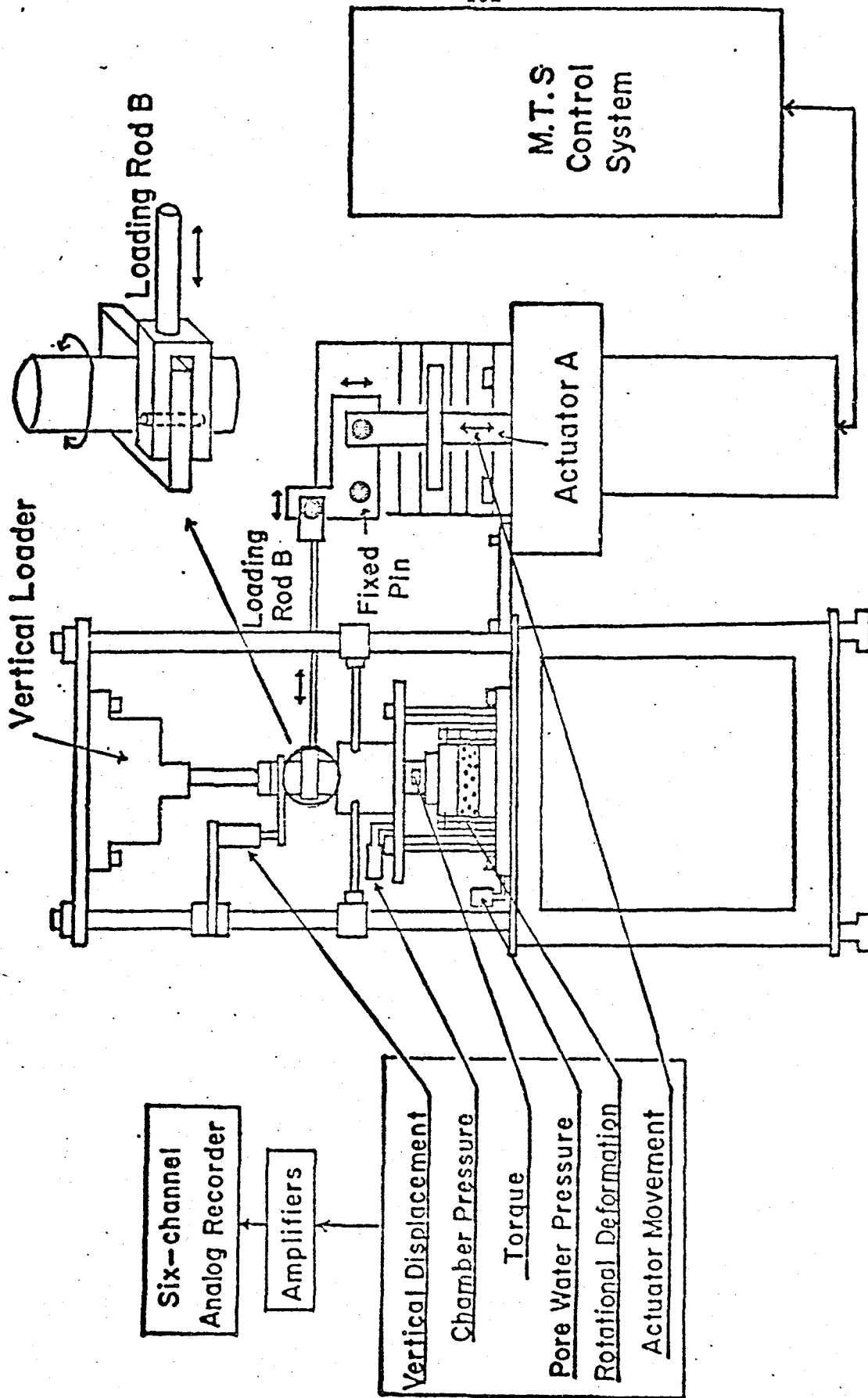


Fig. 3.3 Cyclic Loading and Reloading System

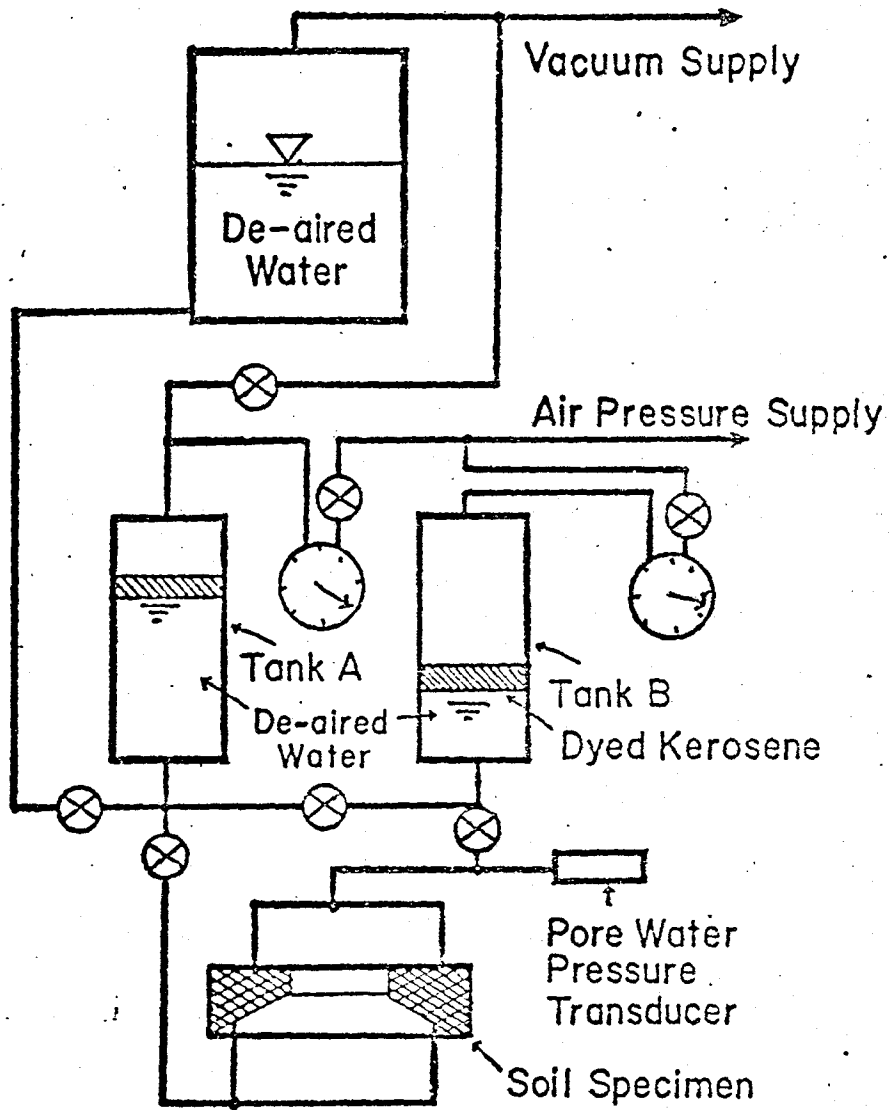


Fig. 3.4 Water Supply and Sample Saturation System

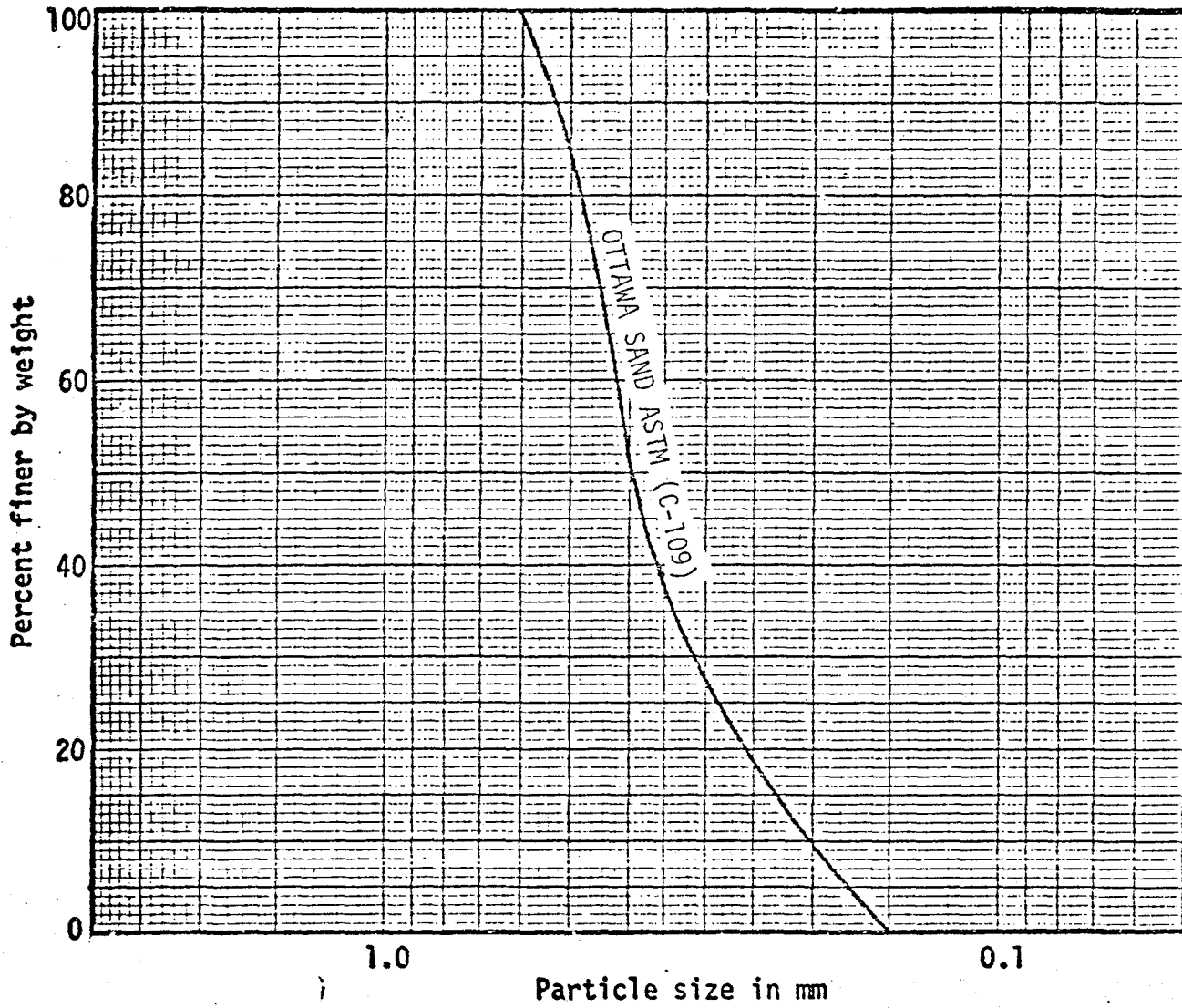


Fig. 3.5 Grain Distribution of Ottawa Sand

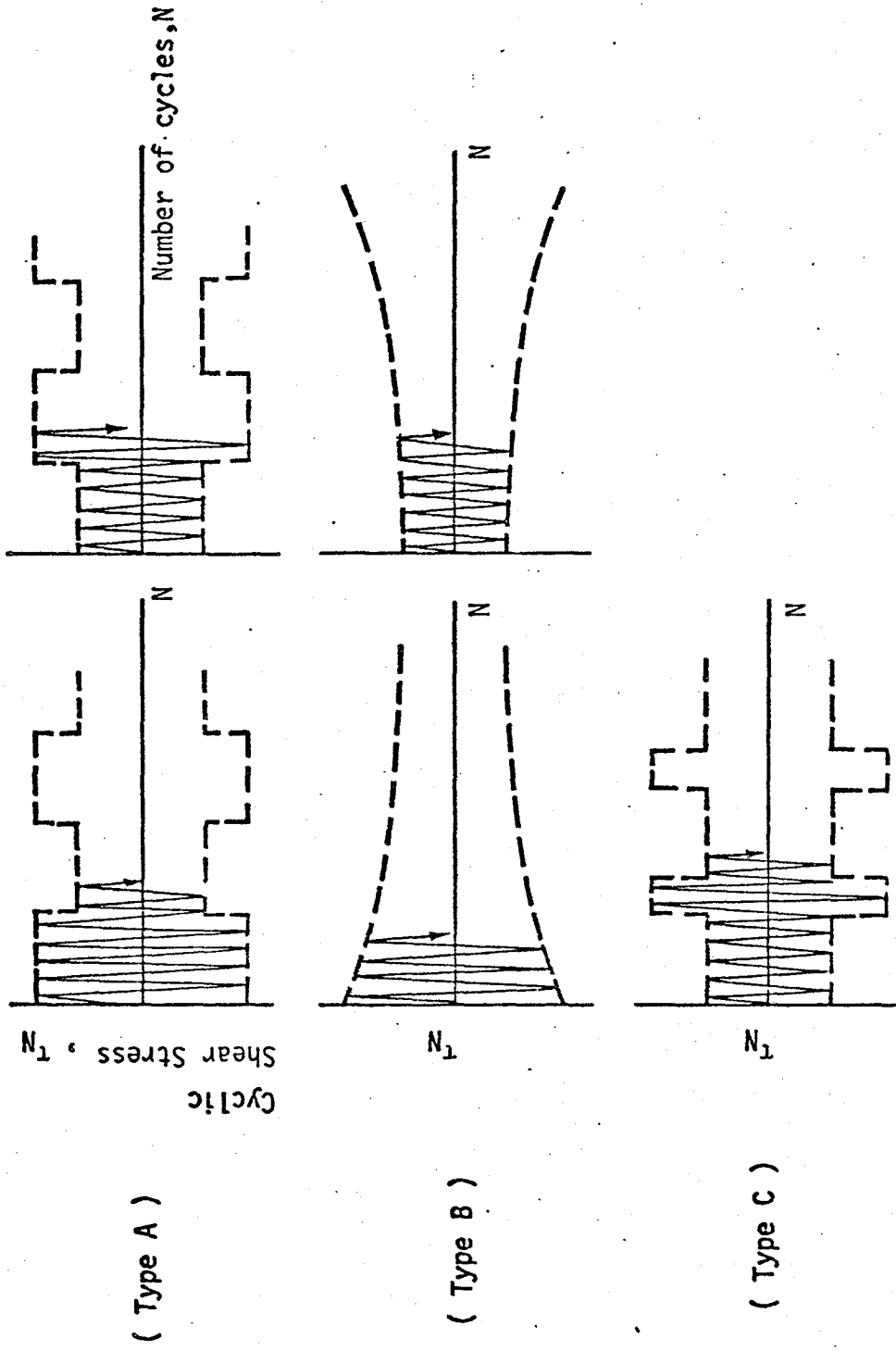


Fig. 3.6 Non-uniform Cyclic Loading Patterns

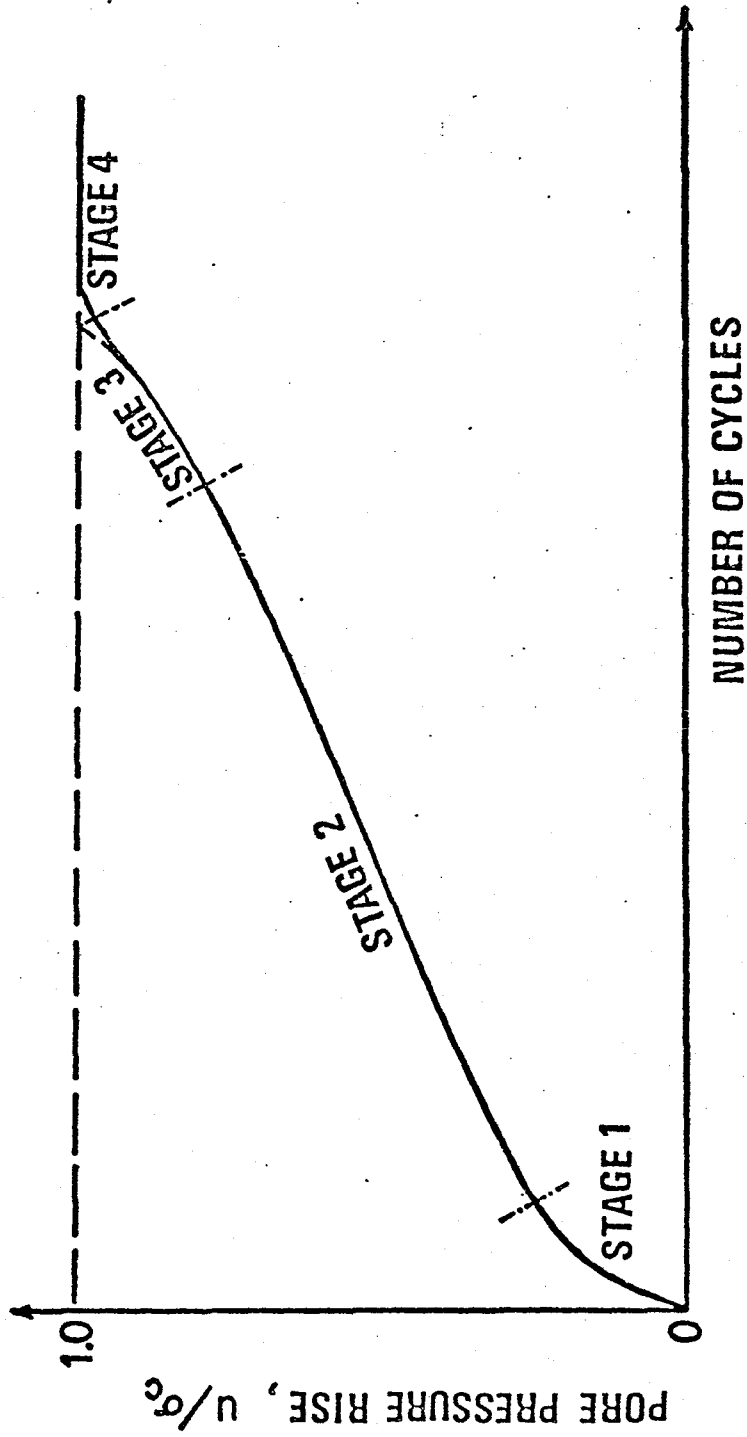
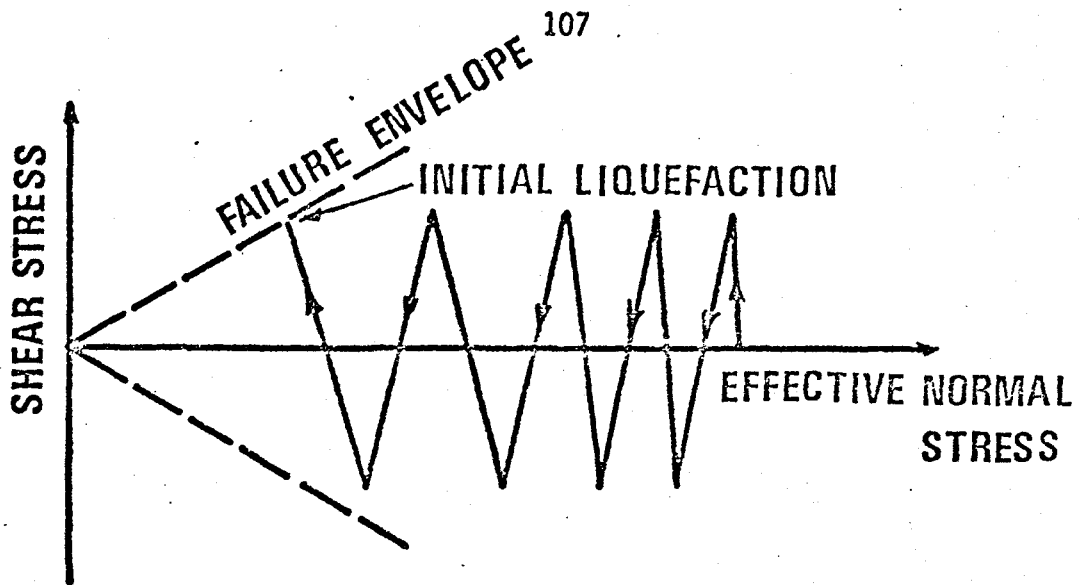
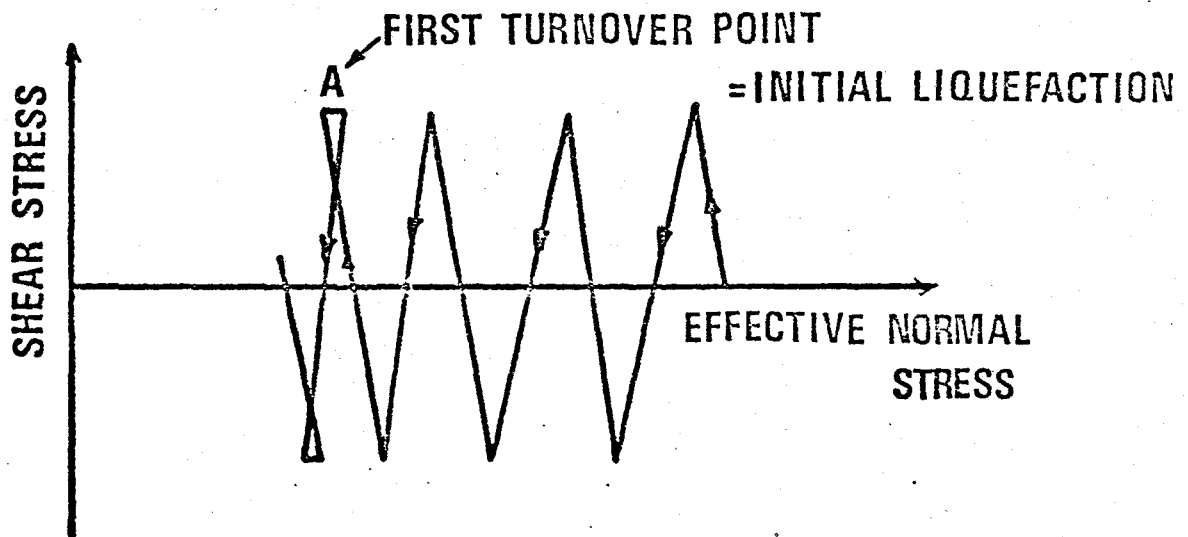


Fig. 4.1 Illustration of Pore Pressure Rise during Uniform Cyclic Loading



(a) STRESS RATIO CONCEPT



(b) FIRST TURNOVER POINT CONCEPT

Fig. 4.2 Definitions of Initial Liquefaction

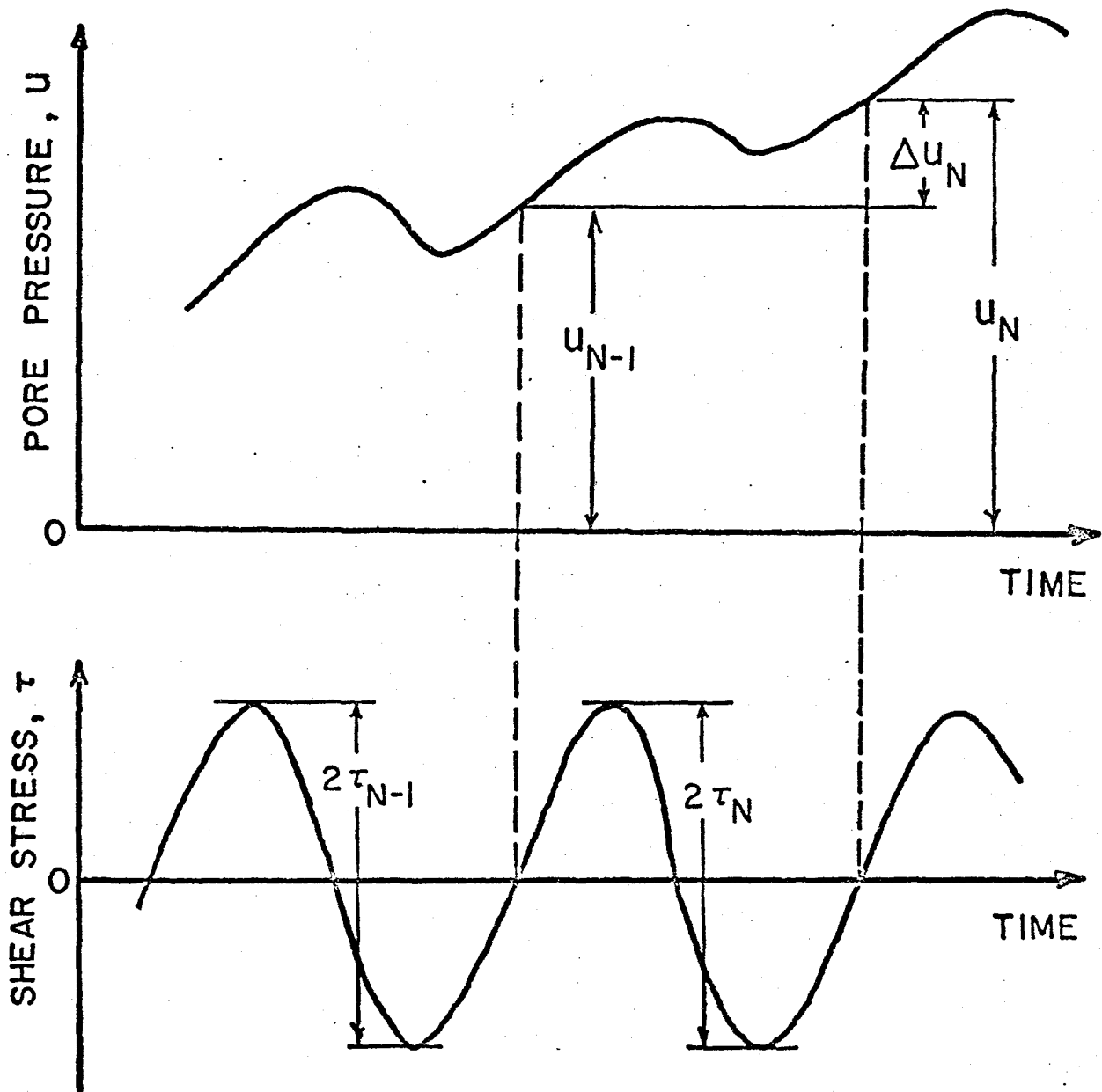


Fig. 4.3 Definition of Residual Pore Pressure

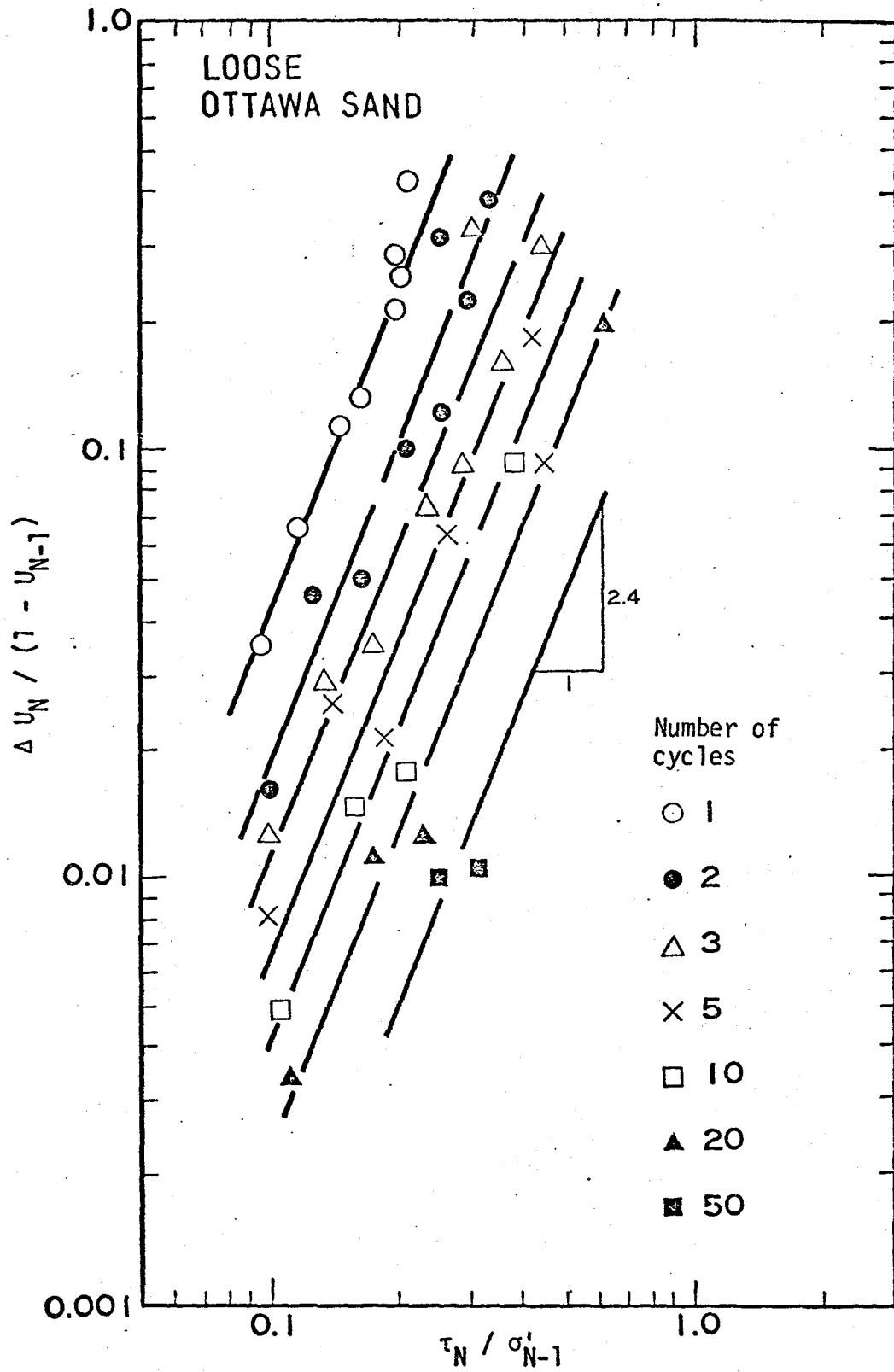


Fig. 4.4 Incremental Rise of Pore Pressure in Each Cycle  
( Loose Sand )

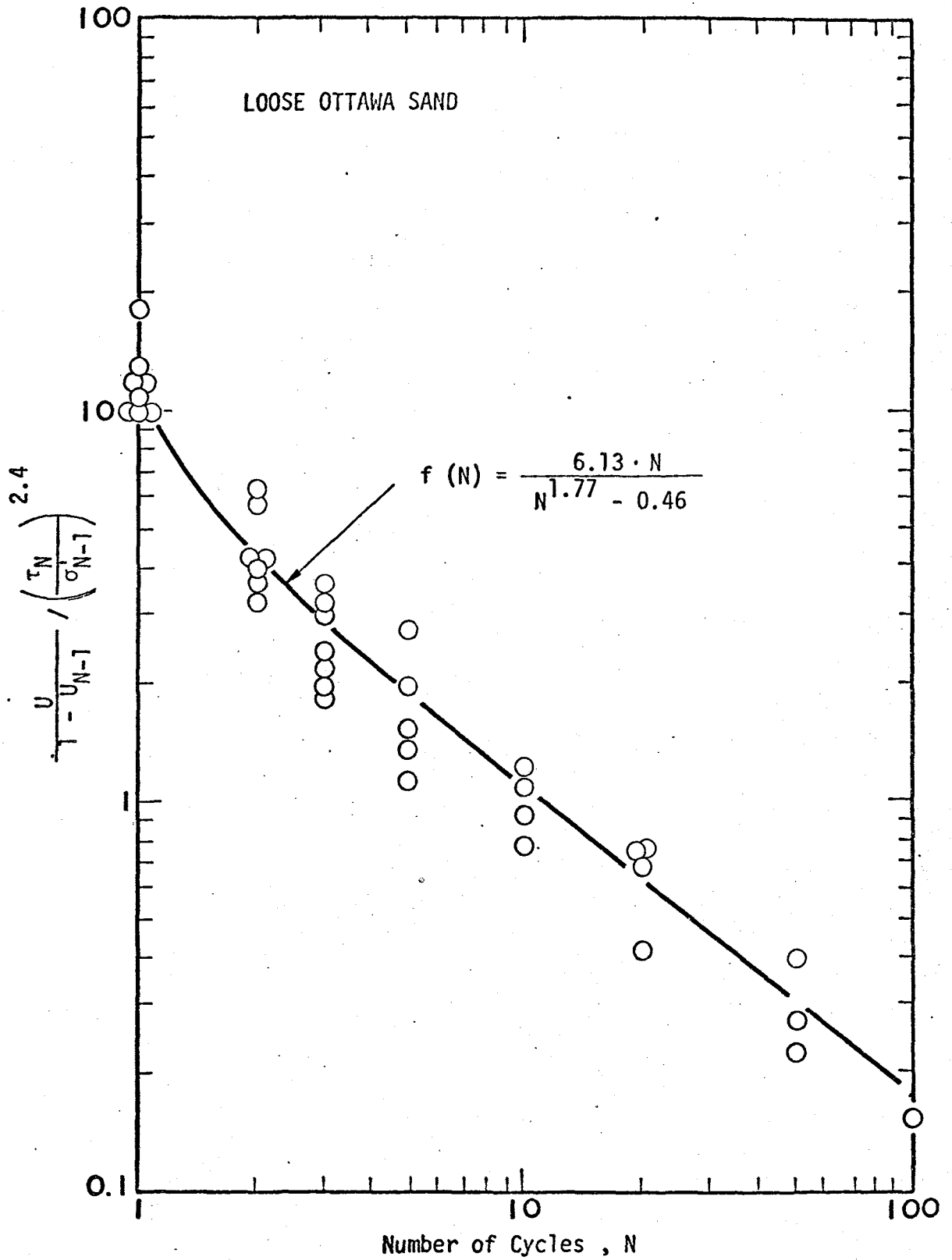


Fig. 4.5 Relationship between Incremental Rise of Pore Pressure and Number of Cycles

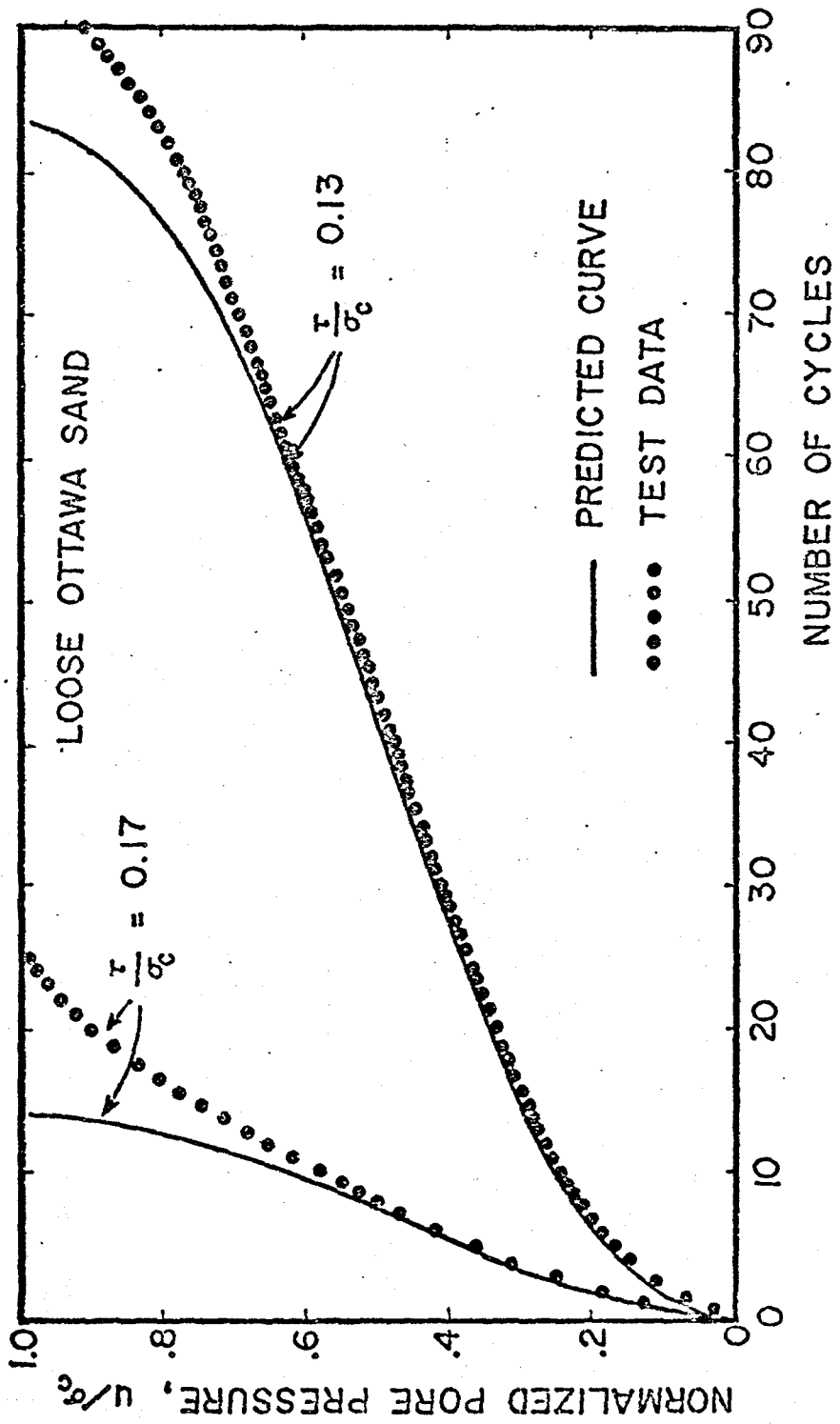


Fig. 4.6 Comparison between Predicted and Experimental Pore Pressure Rise during Uniform Cyclic Loading

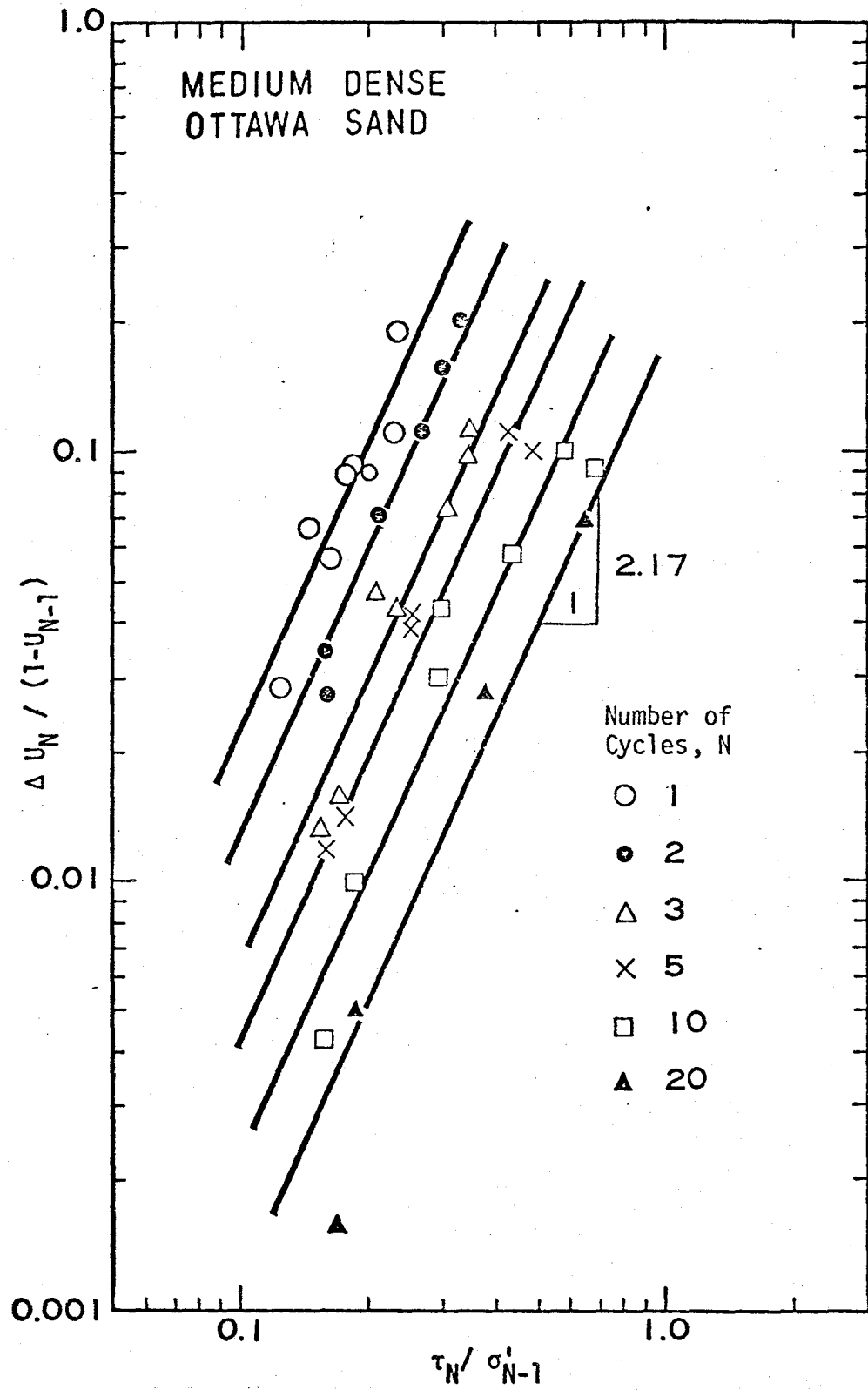


Fig. 4.7 Incremental Rise of Pore Pressure in Each Cycle

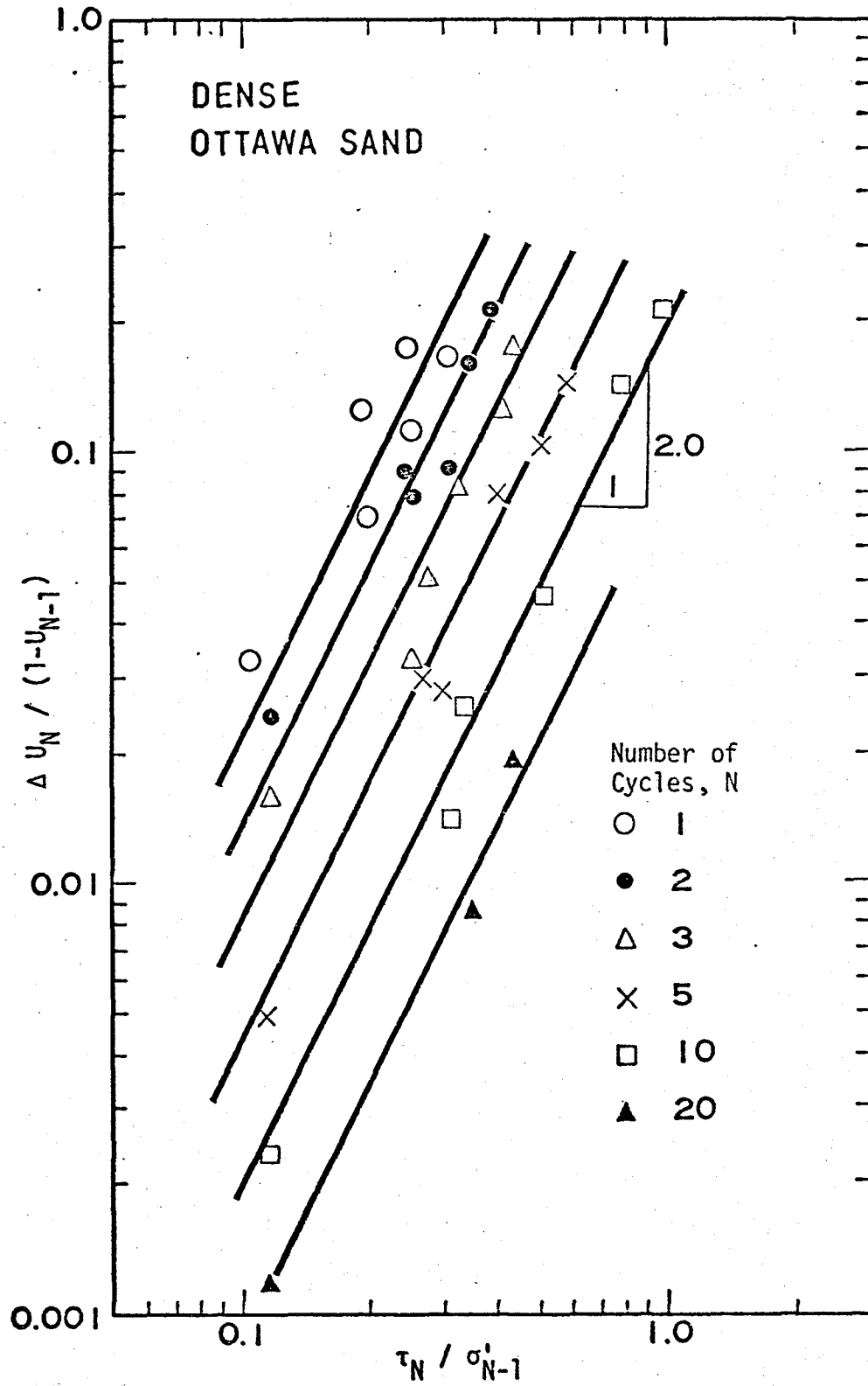


Fig. 4.8 Incremental Rise of Pore Pressure in Each Cycle

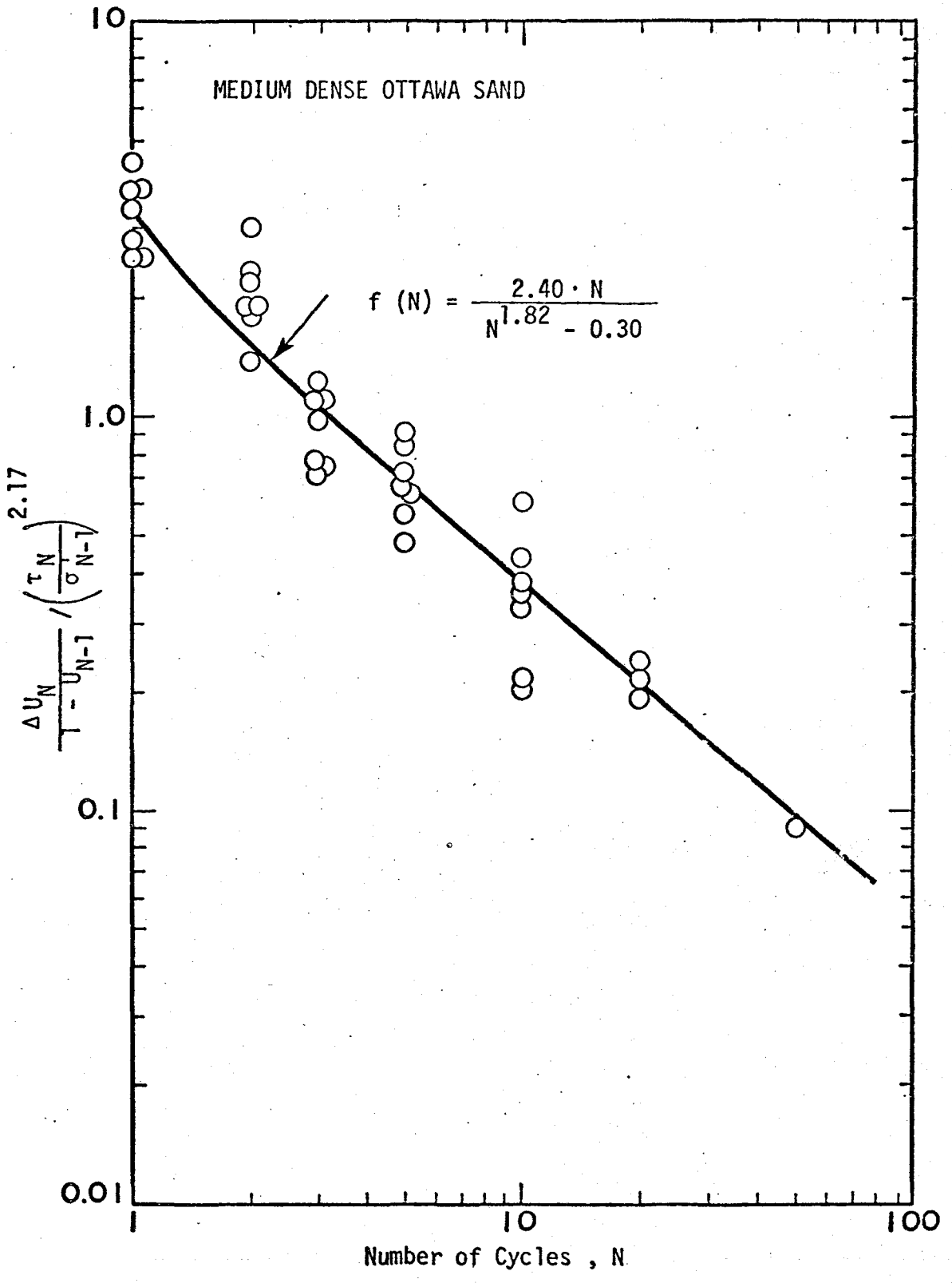


Fig. 4.9 Relationship between Incremental Rise of Pore Pressure and Number of Cycles

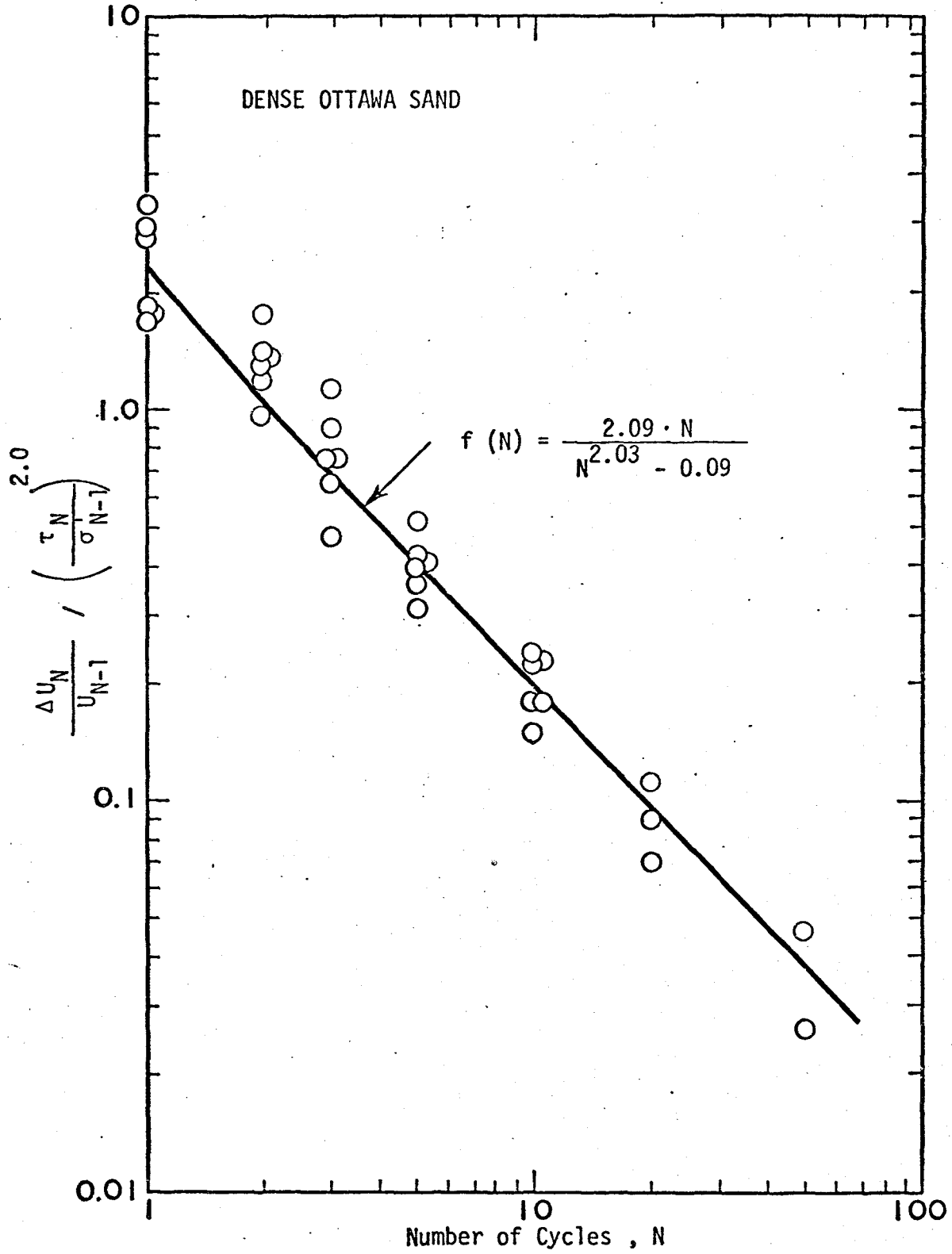


Fig. 4.10 Relationship between Incremental Rise of Pore Pressure and Number of Cycles

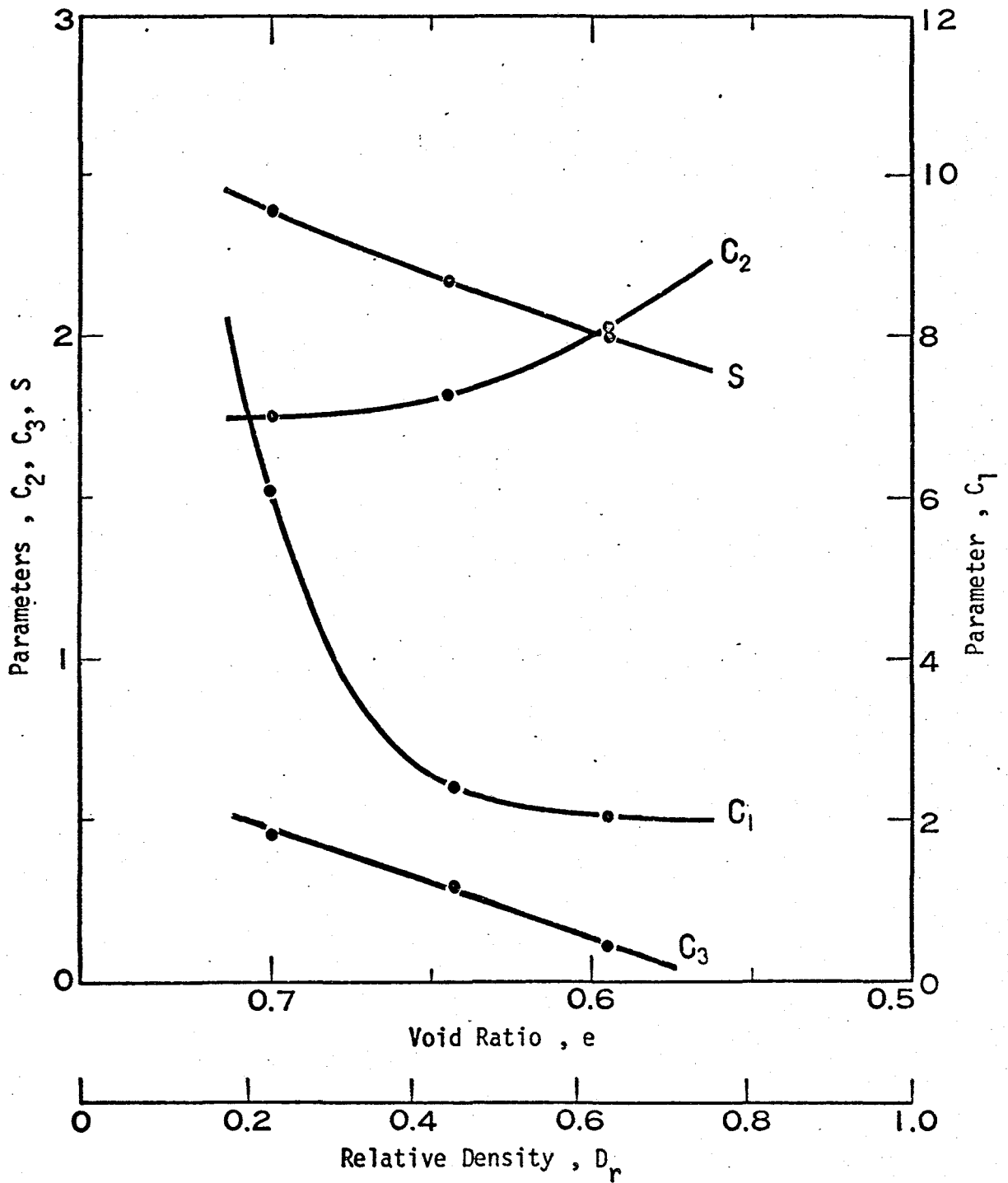
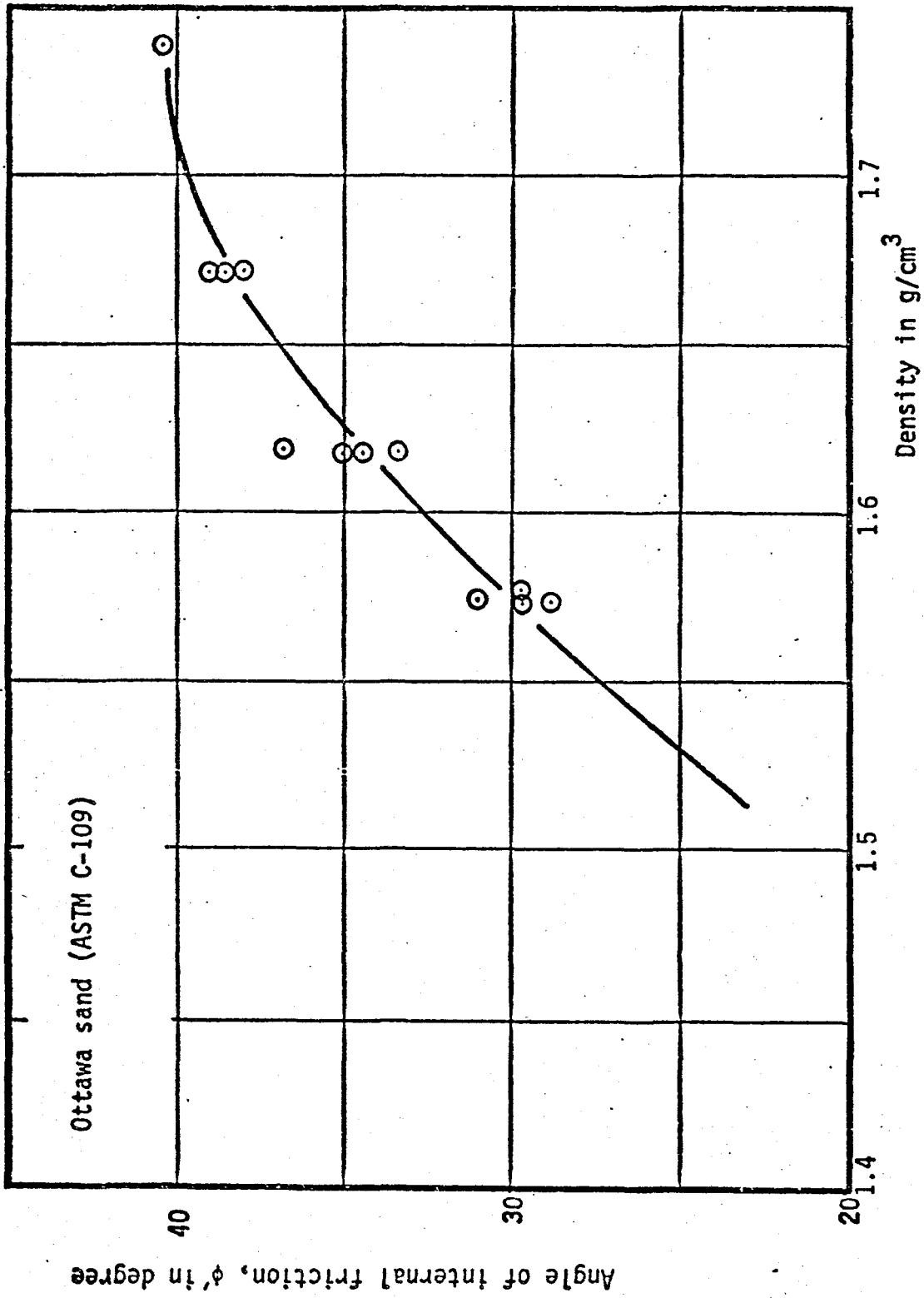


Fig. 4.11 Variation of Parameters  $C_1, C_2, C_3$  and  $S$  with Density

Fig. 4.12 Variation of  $\phi'$  with Density

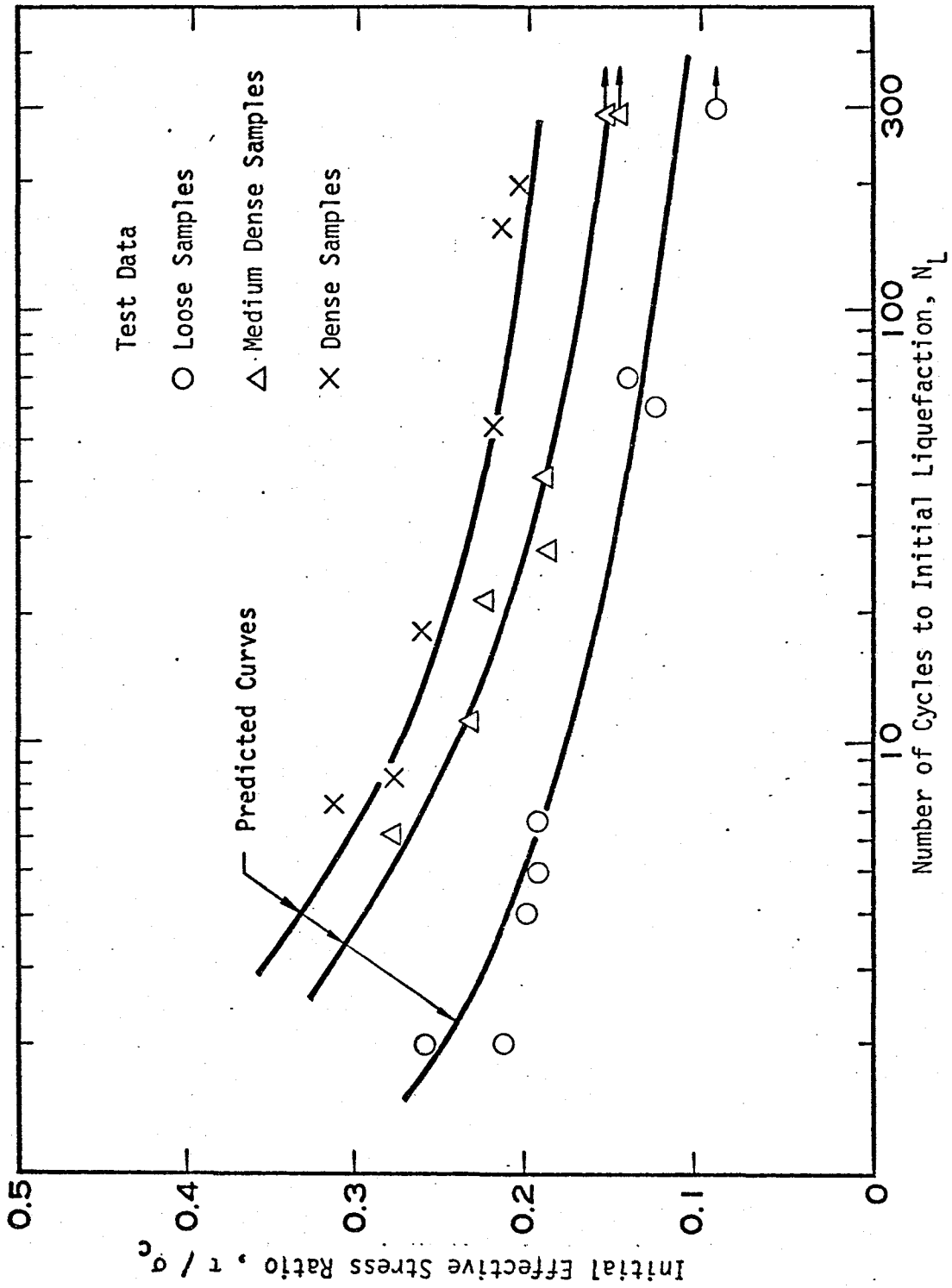


Fig. 4.13 Comparison between Predicted and Experimental Results of Initial Liquefaction

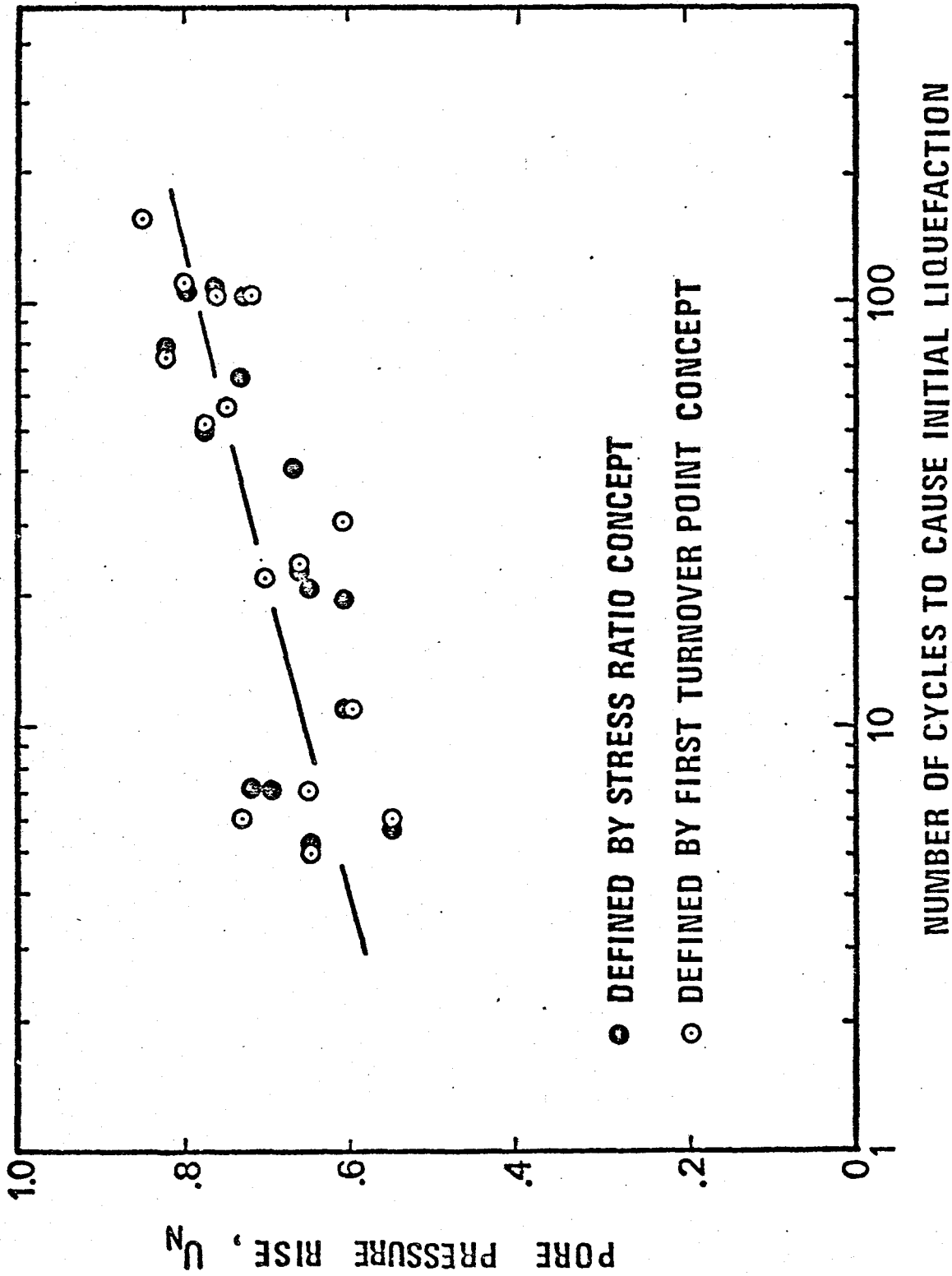


Fig. 4.14 Comparison of Pore Pressure Rises at Initial Liquefaction Determined by Two Different Definitions

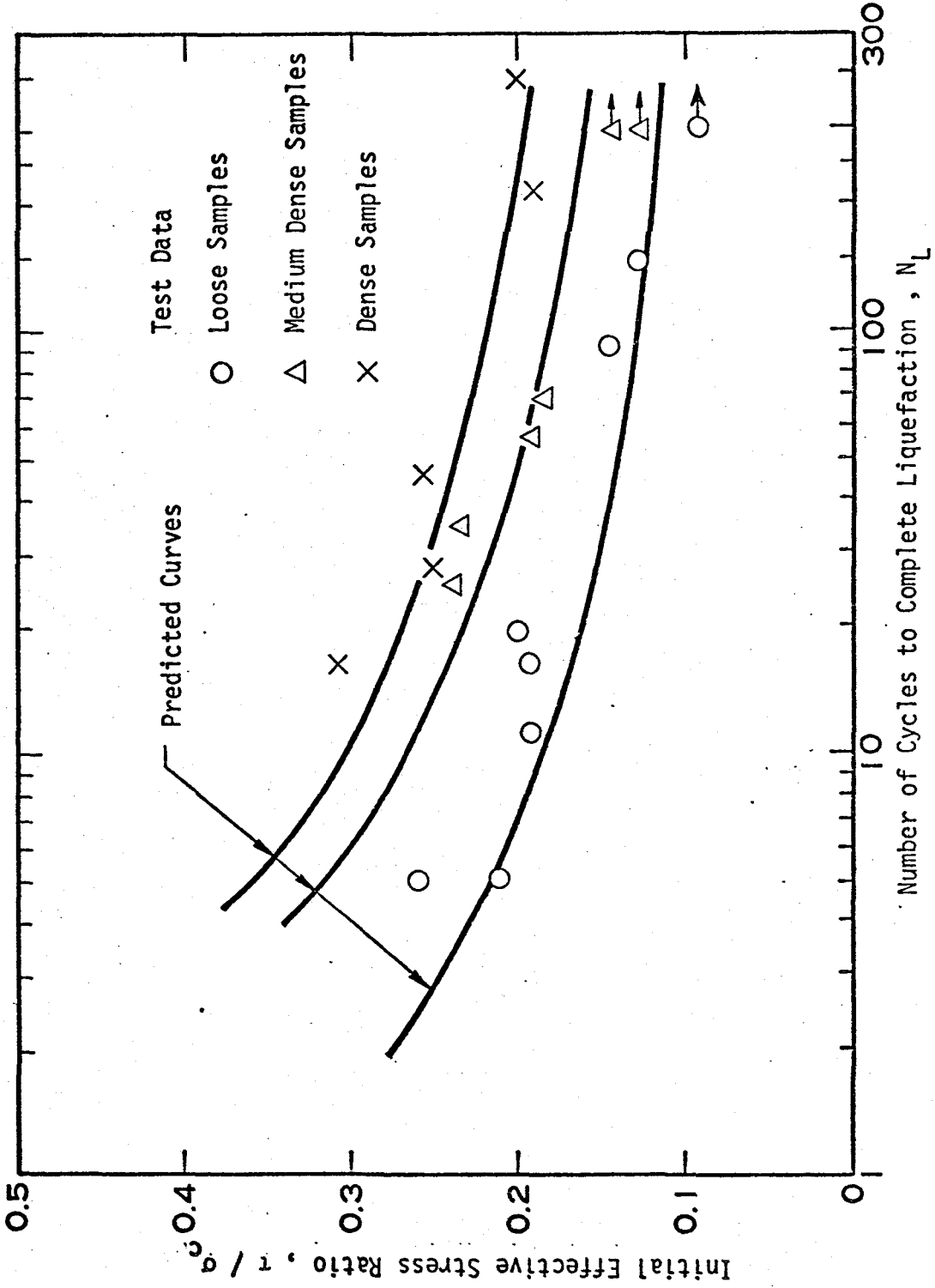


Fig. 4.15 Comparison between Predicted and Experimental Results of Complete Liquefaction

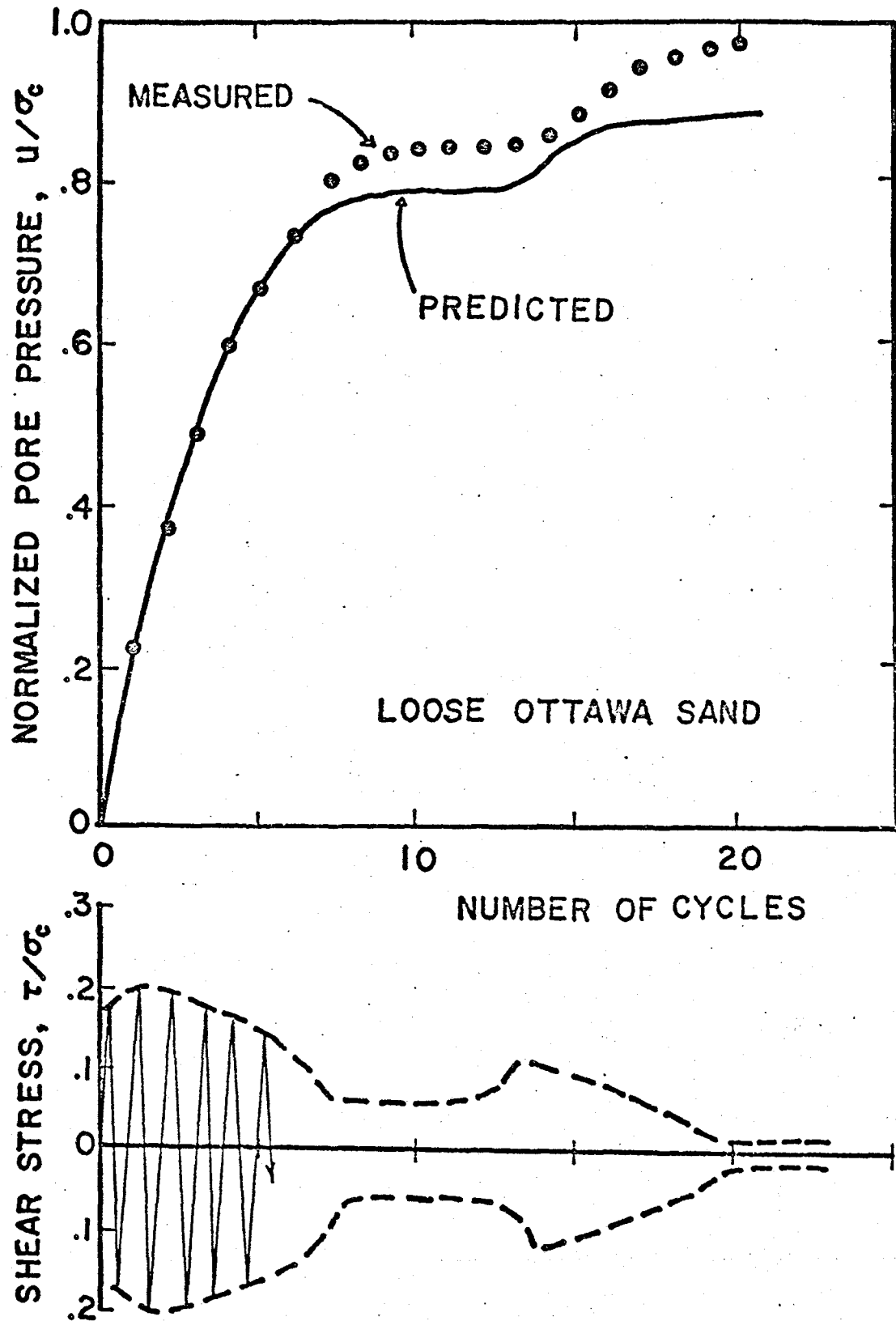


Fig. 4.16(a) Comparison between Predicted and Measured Pore Pressure Rise Under Non-uniform Cyclic Loading

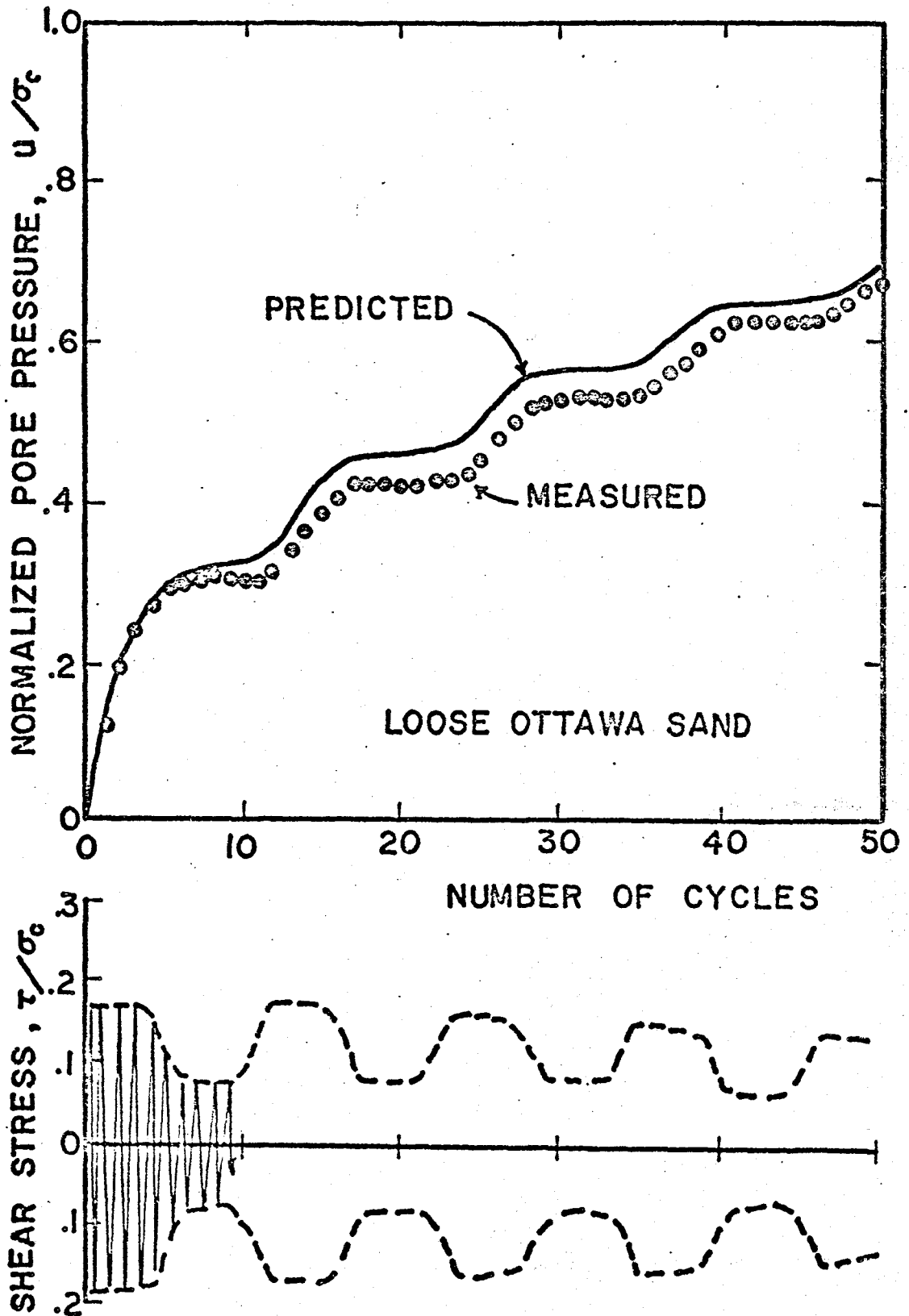


Fig. 4.16(b) Comparison between Predicted and Measured Pore Pressure Rise Under Non-uniform Cyclic Loading

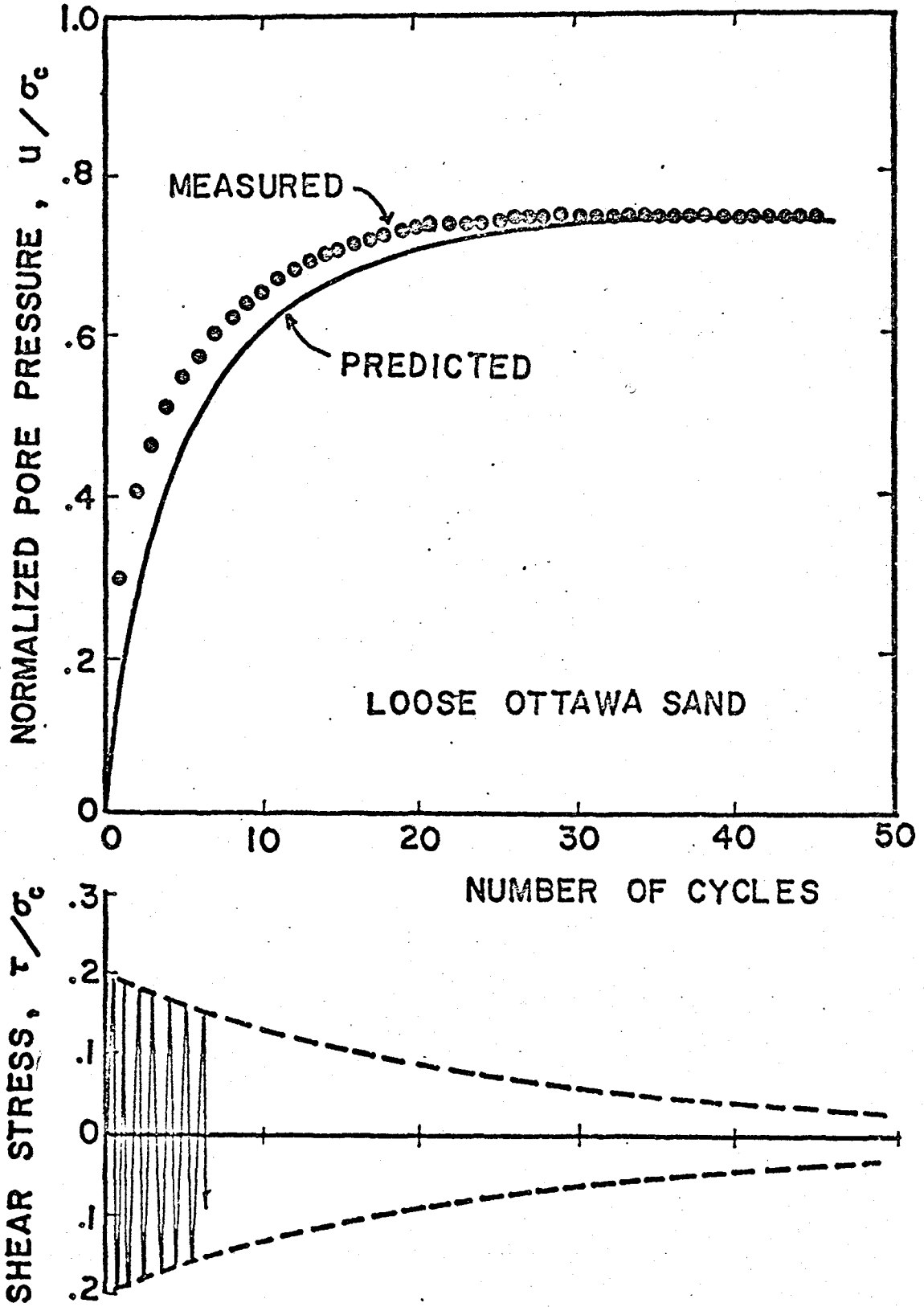


Fig. 4.16(c) Comparison between Predicted and Measured Pore Pressure Rise Under Non-uniform Cyclic Loading

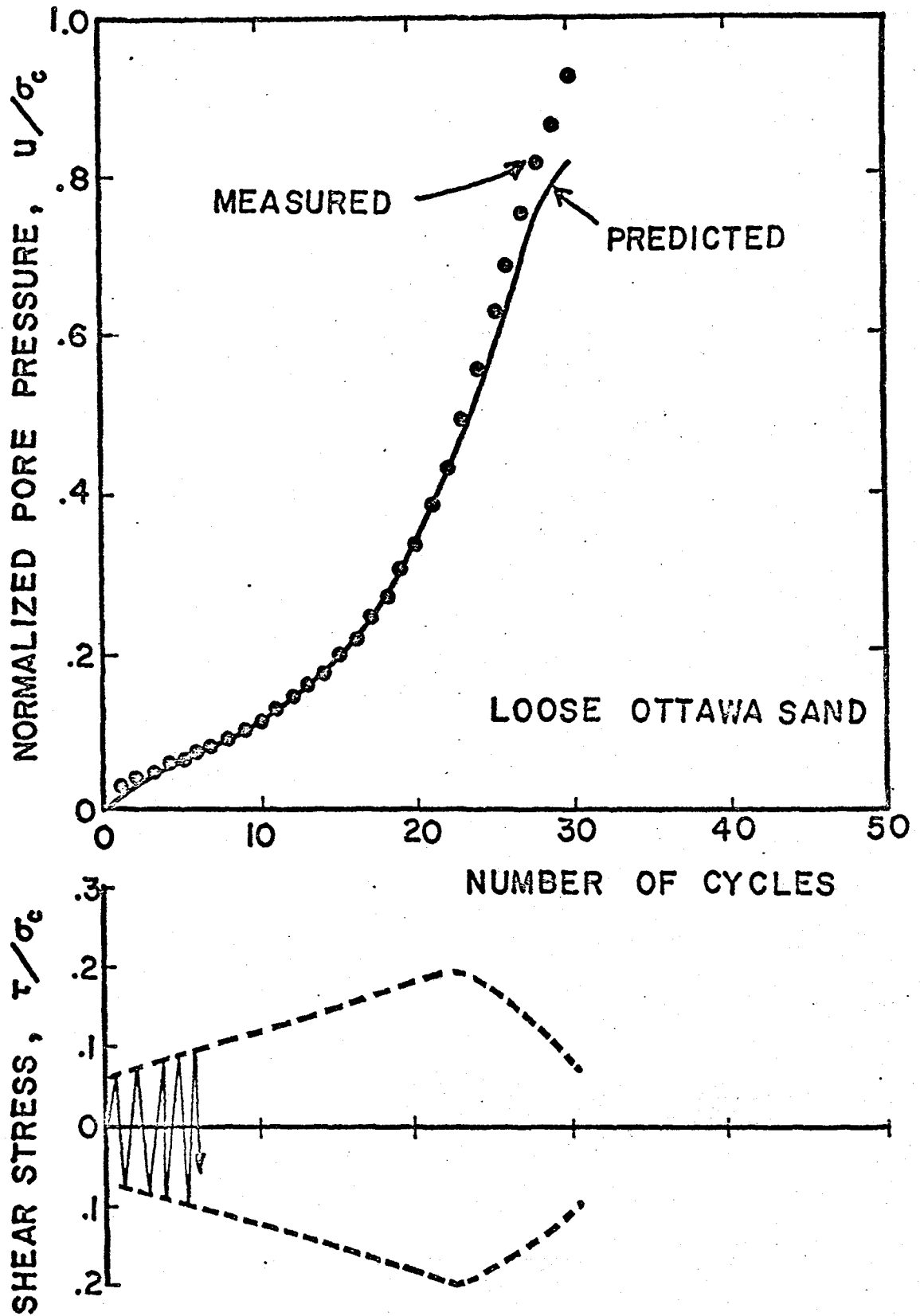


Fig. 4.16(d) Comparison between Predicted and Measured Pore Pressure Rise Under Non-uniform Cyclic Loading

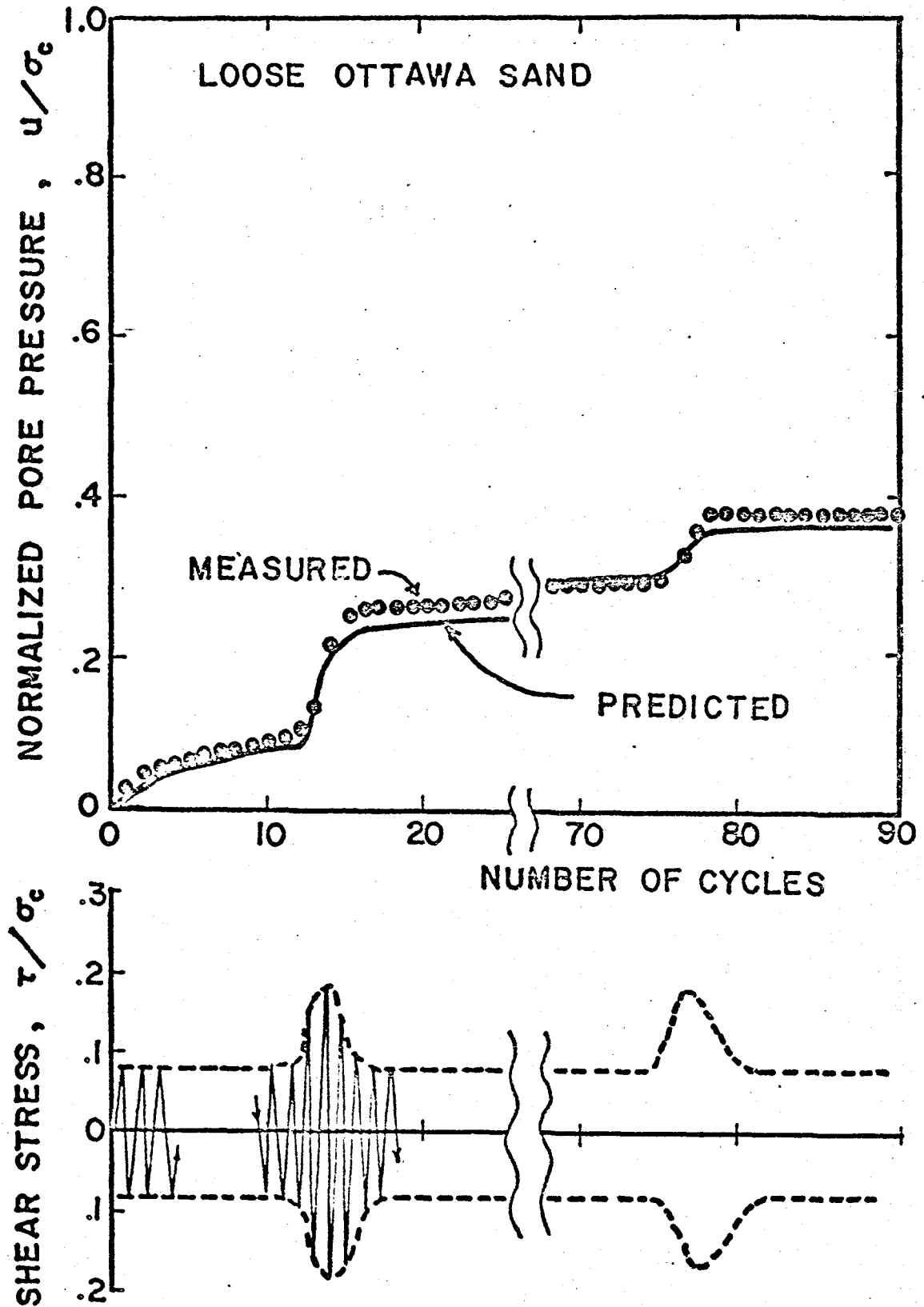


Fig. 4.16(e) Comparison between Predicted and Measured Pore Pressure Rise Under Non-uniform Cyclic Loading

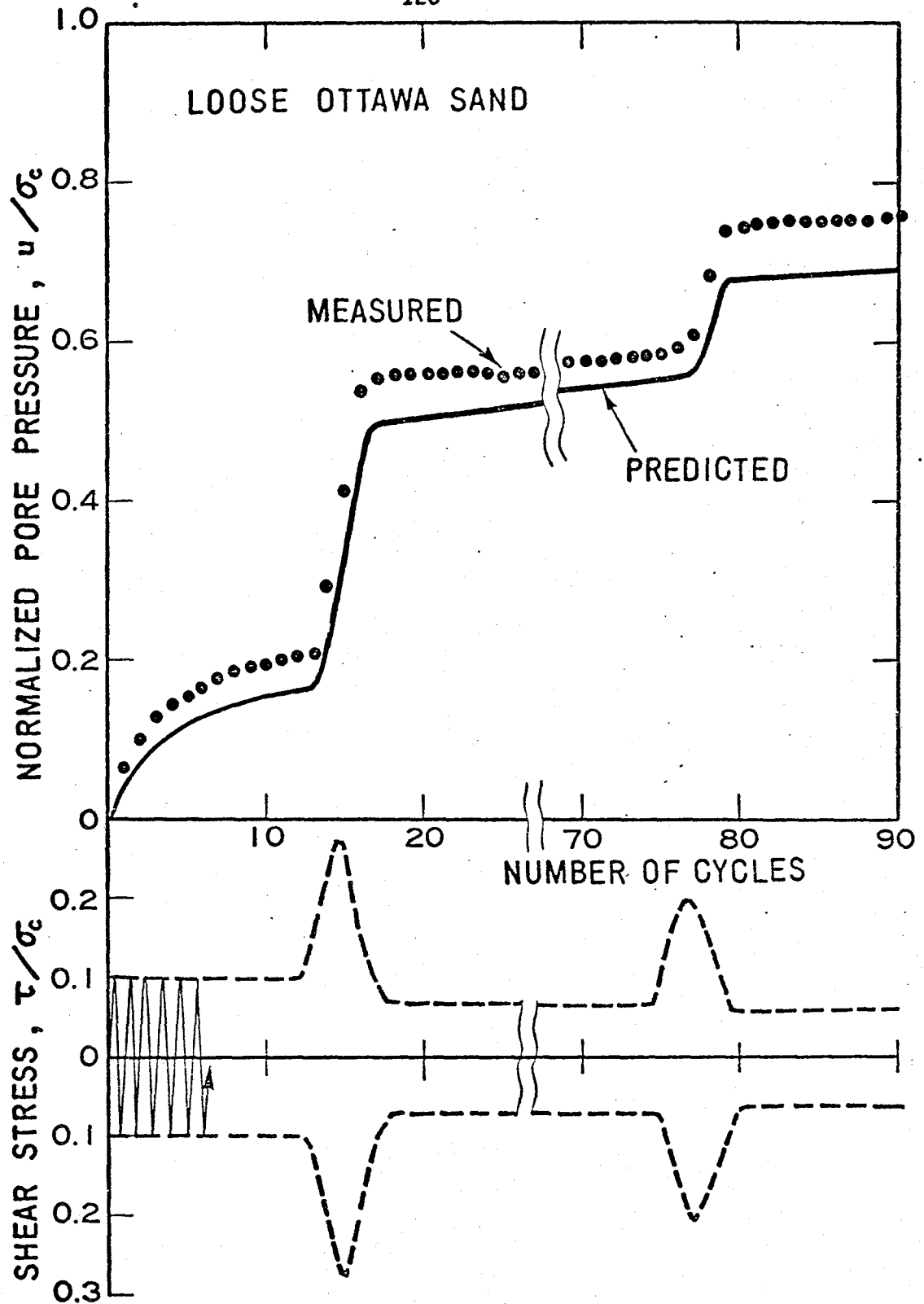


Fig. 4.16(f) Comparison between Predicted and Measured Pore Pressure Rise under Non-uniform Cyclic Loading

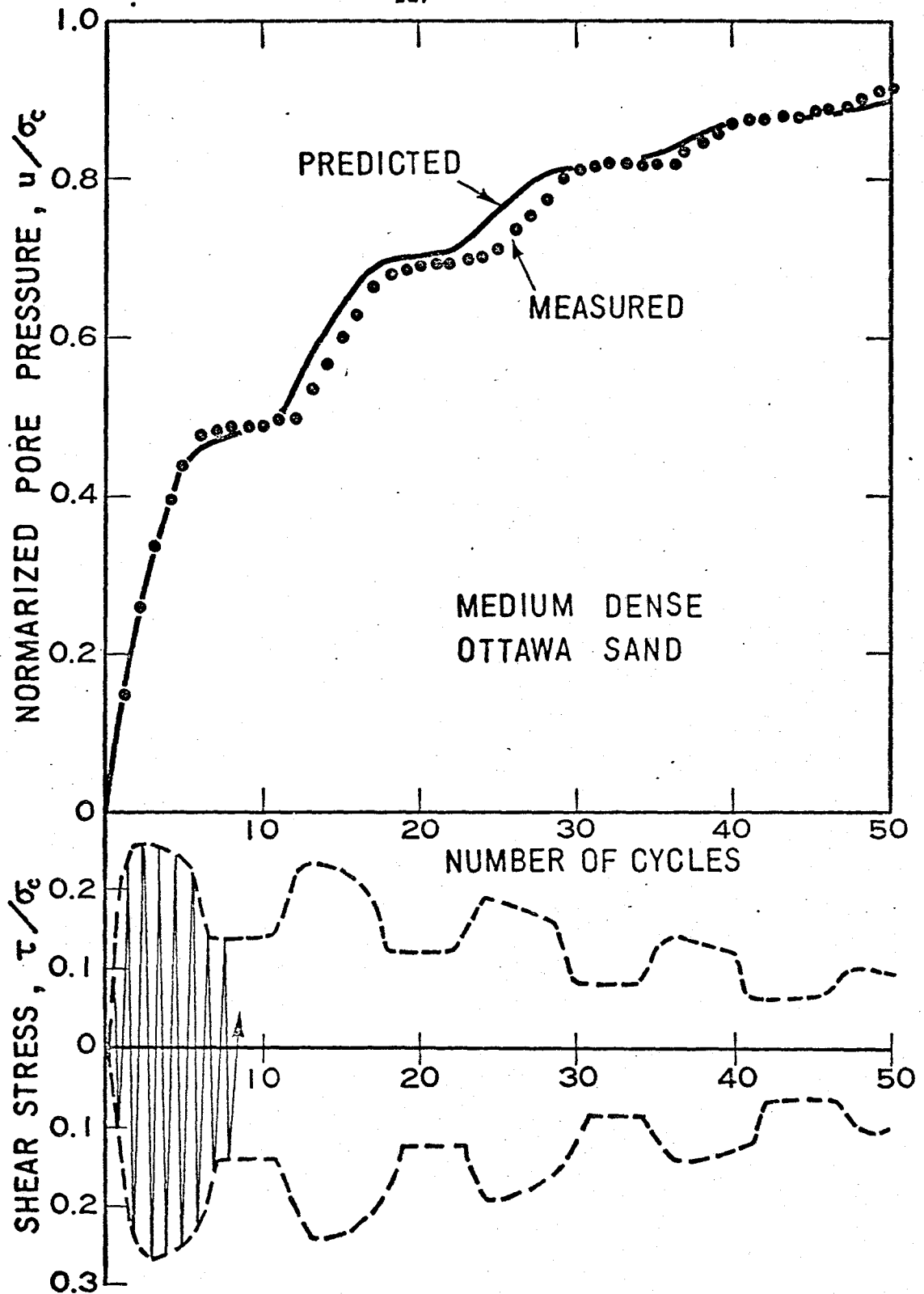


Fig. 4.16(g) Comparison between Predicted and Measured Pore Pressure Rise under Non-uniform Cyclic Loading

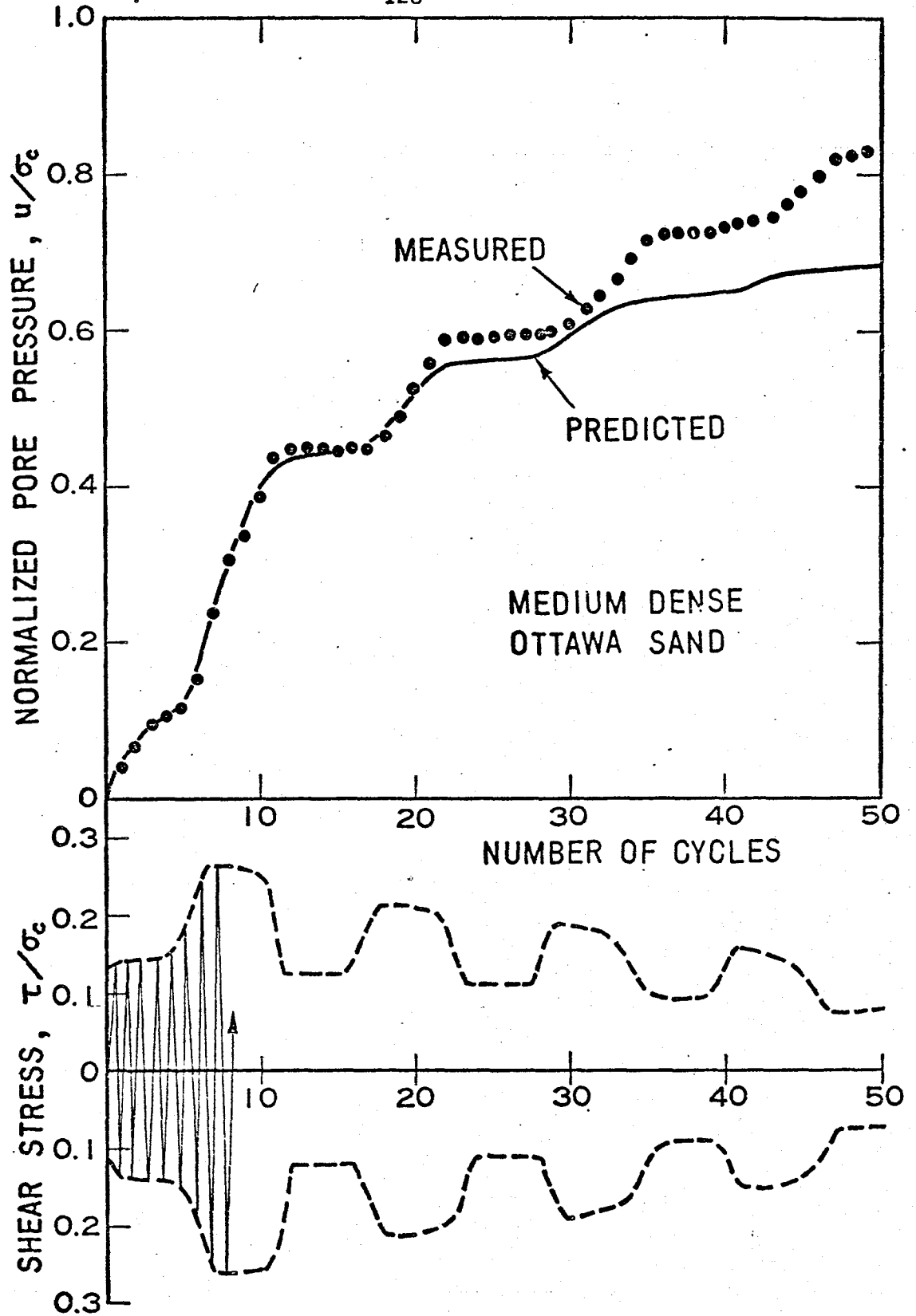


Fig. 4.16(h) Comparison between Predicted and Measured Pore Pressure Rise under Non-uniform Cyclic Loading

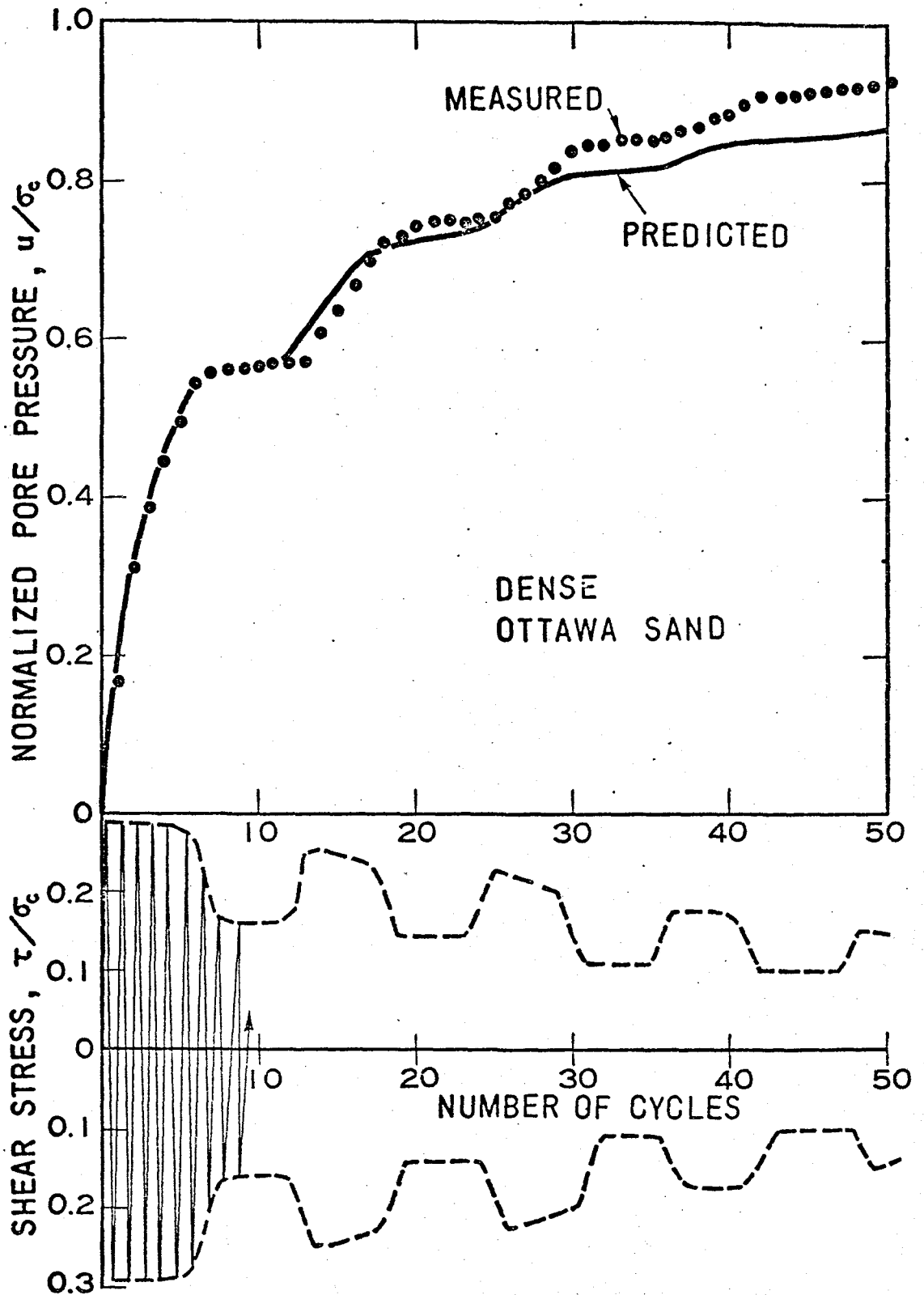


Fig. 4.16(i) Comparison between Predicted and Measured Pore Pressure Rise under Non-uniform Cyclic Loading

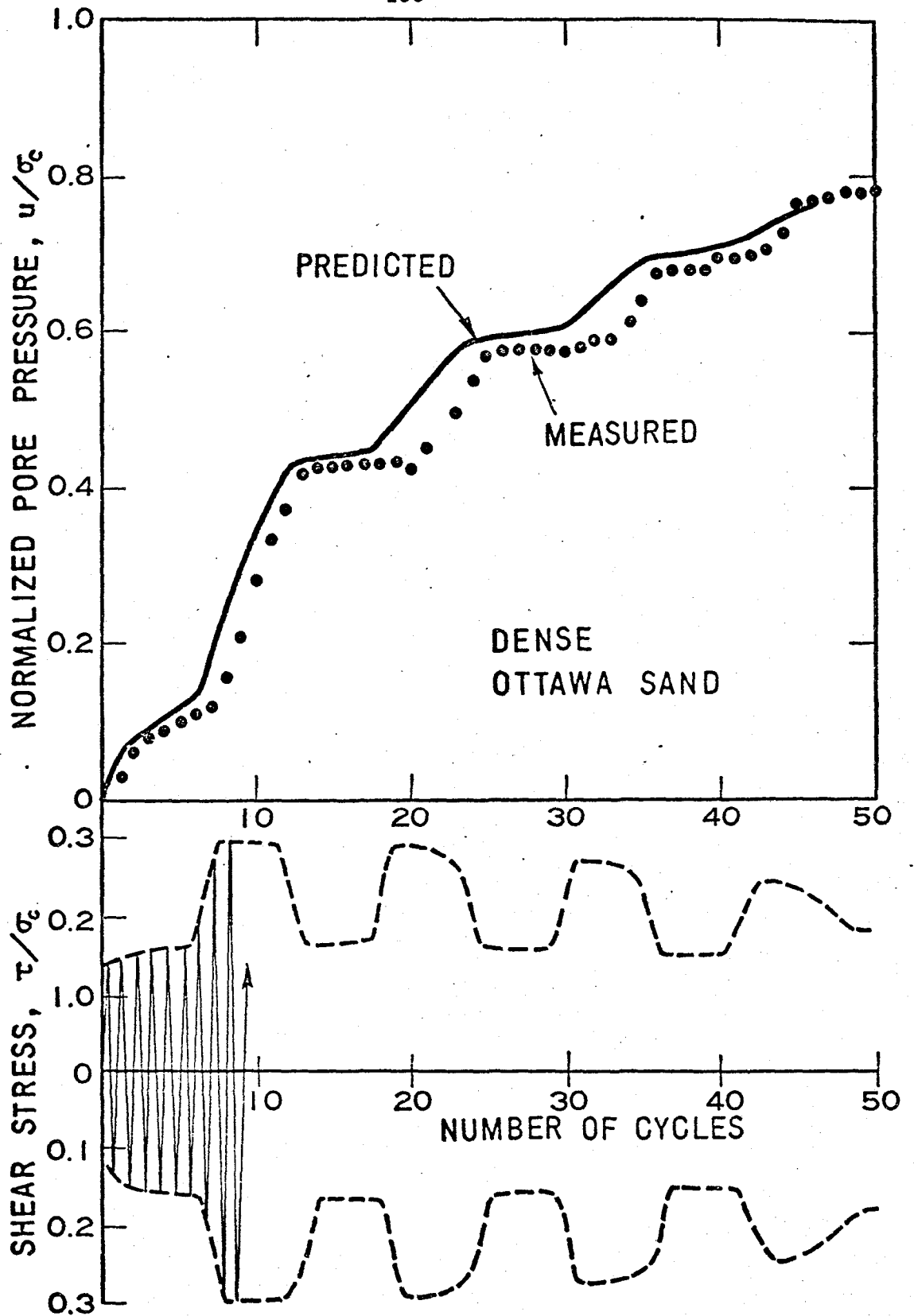


Fig.4.16(j) Comparison between Predicted and Measured Pore Pressure Rise under Non-uniform Cyclic Loading

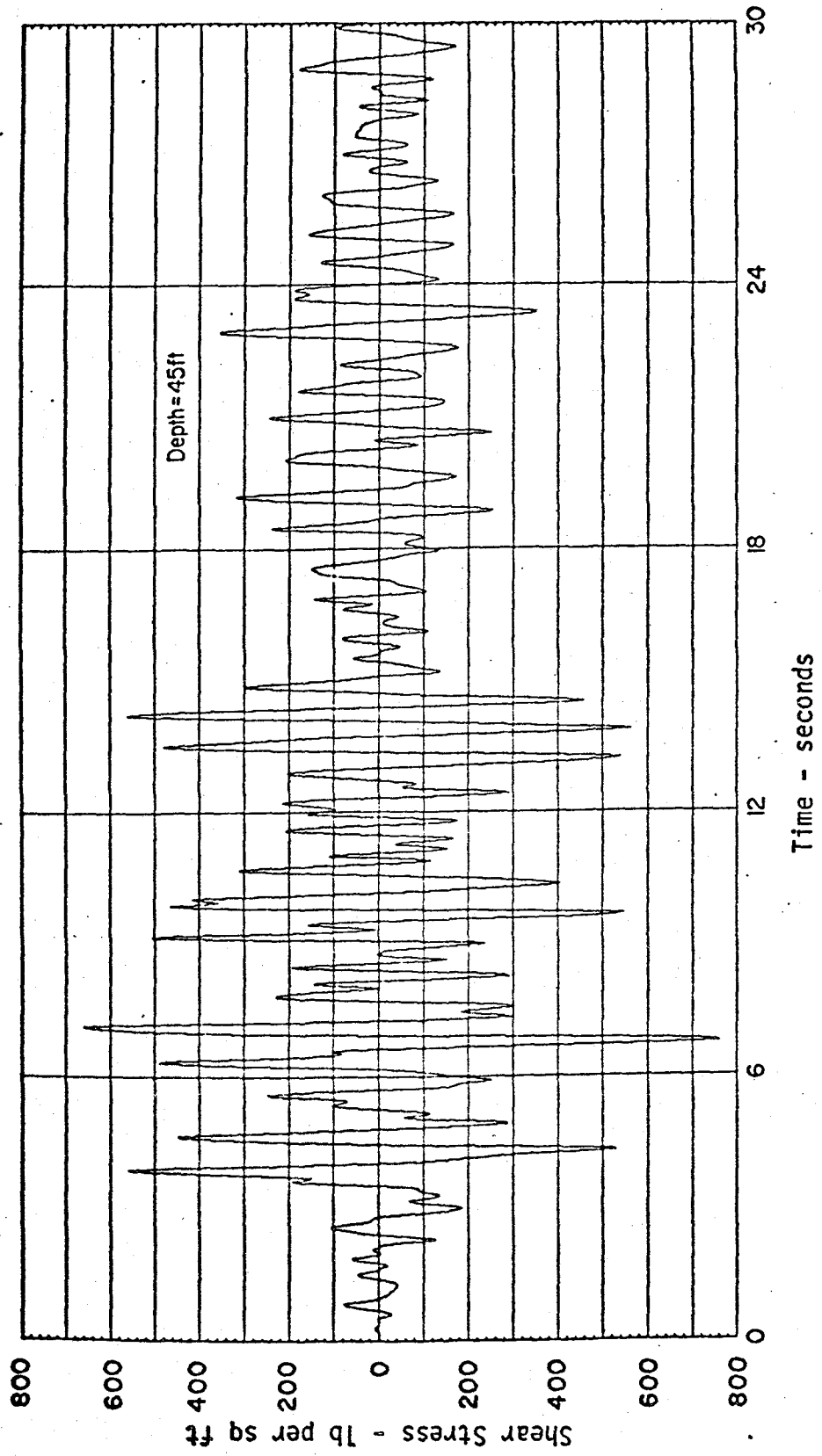


Fig 4.17 An Example of Time History of Actual Earthquake

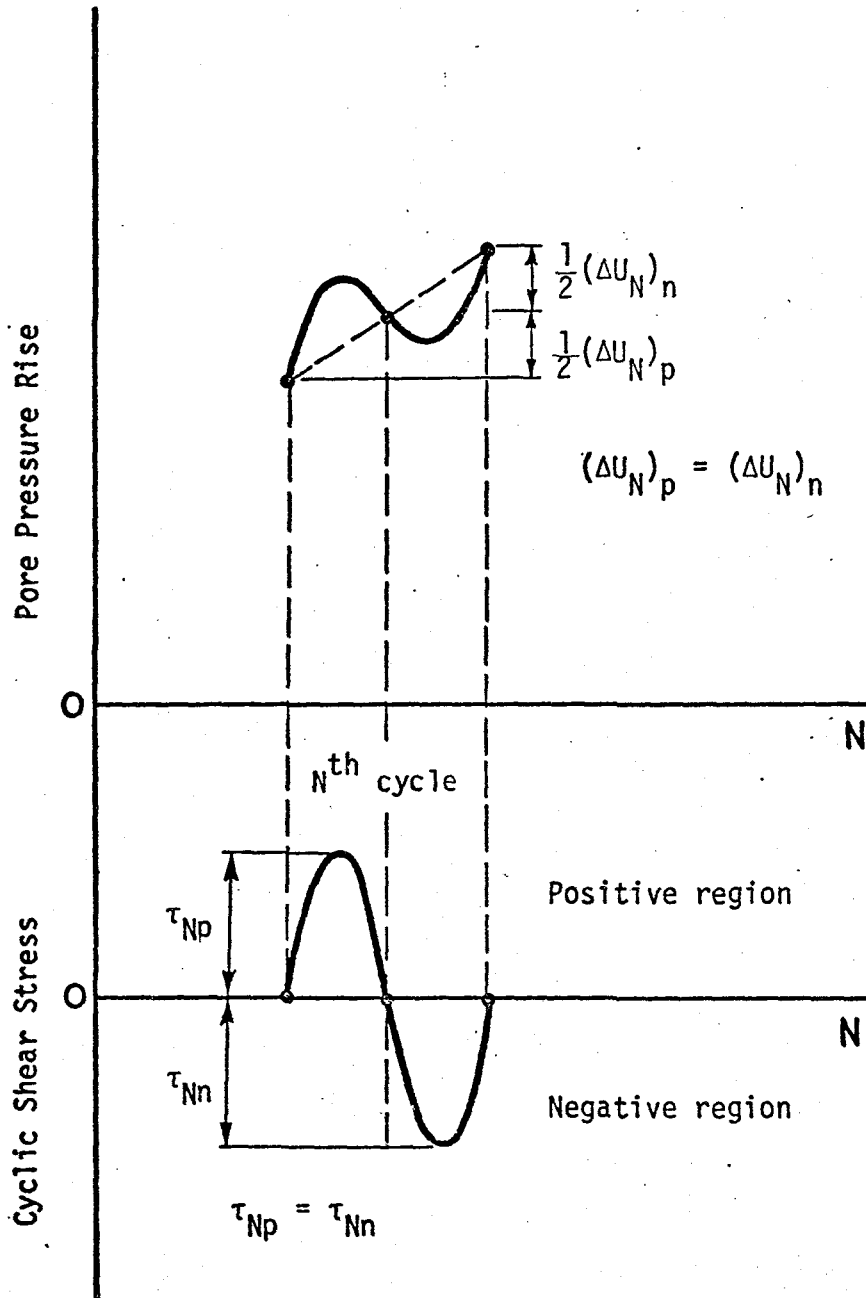


Fig. 4.18(a) Illustration of Pore Pressure Rise during Half-cycle of Loading ( Symmetrical case )

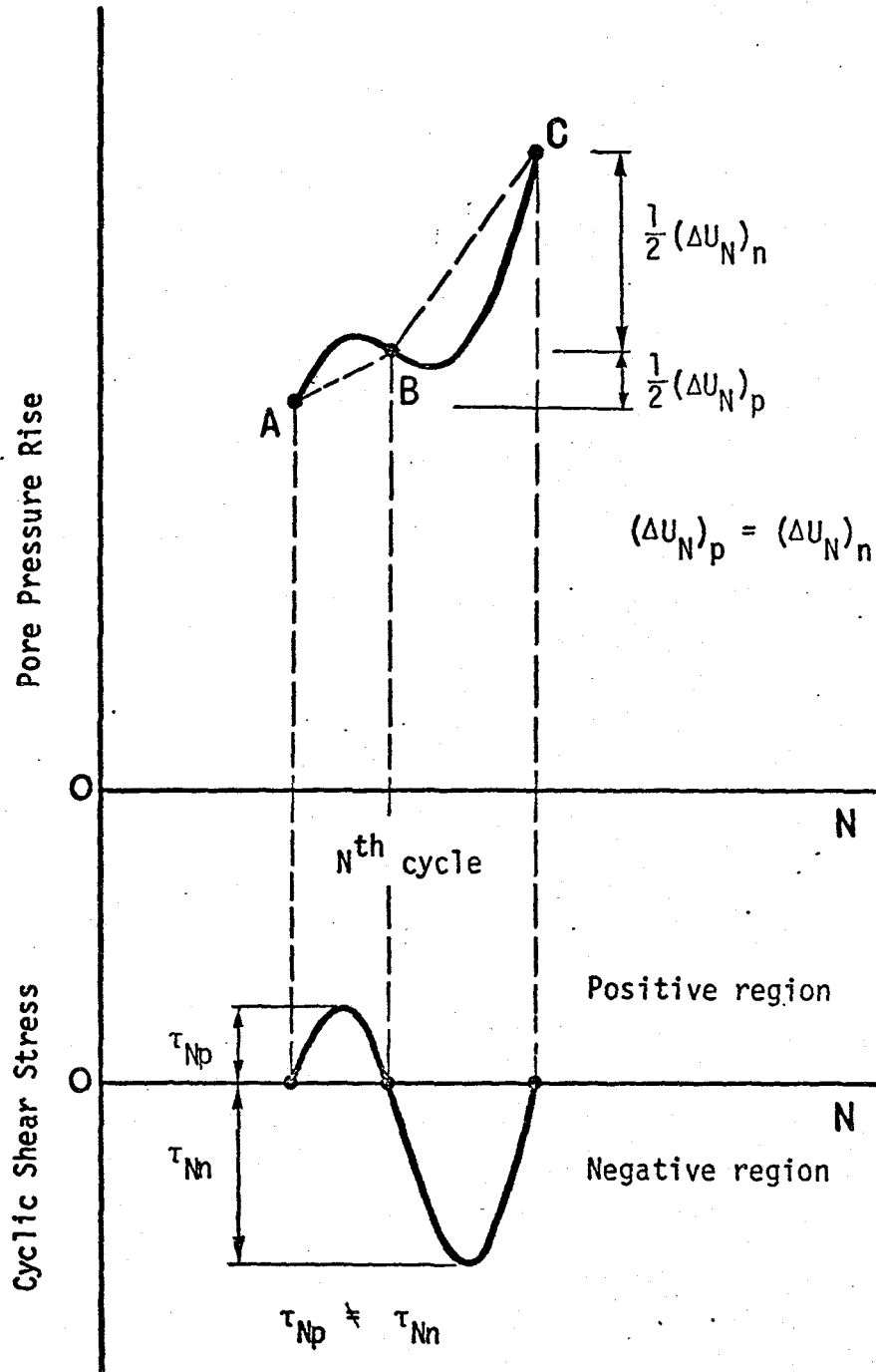


Fig. 4.18(b) Illustration of Pore Pressure Rise during Half-cycle of Loading ( Antisymmetrical case )

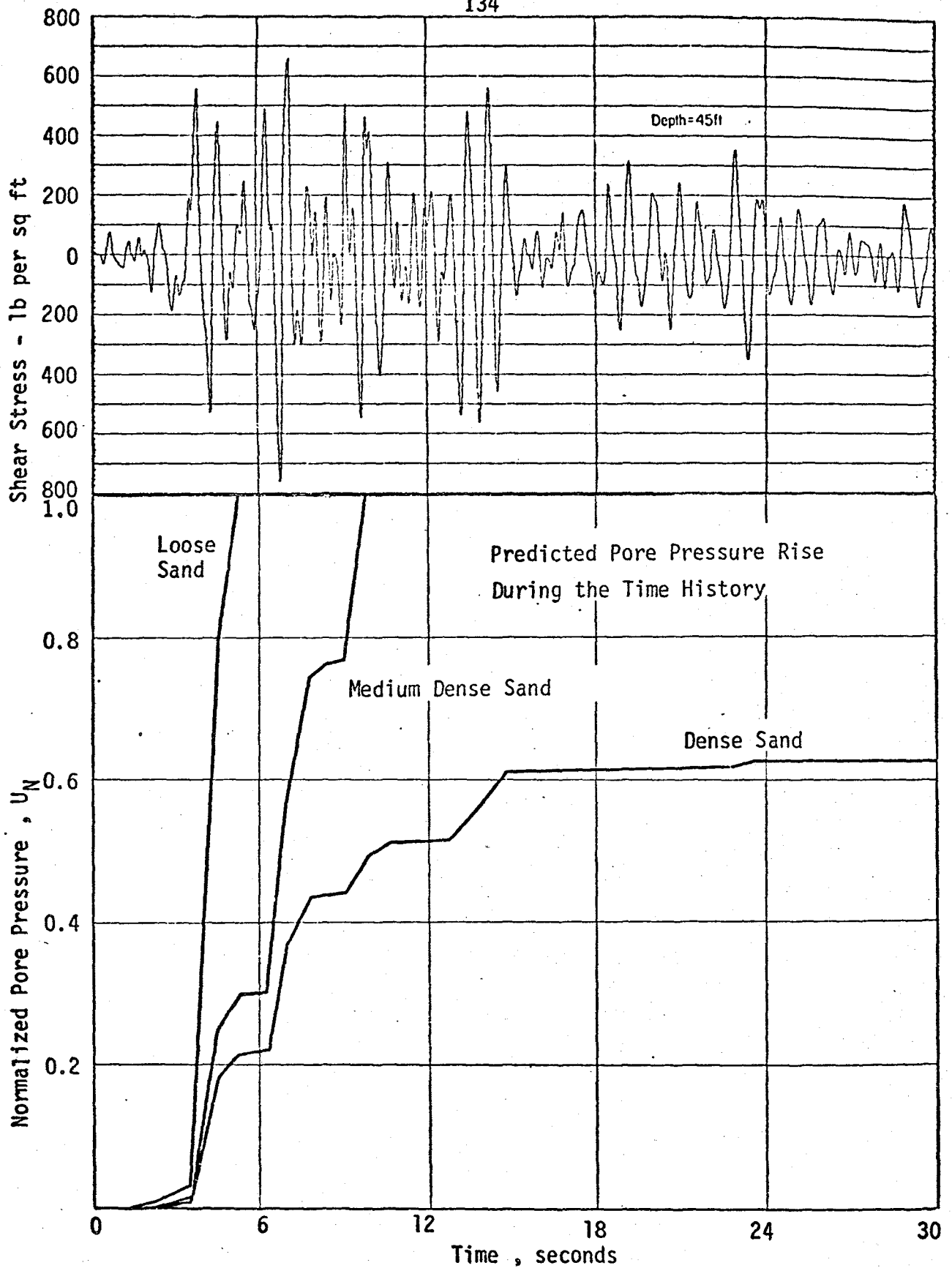


Fig. 4.19 Predicted Pore Pressure Rise during Actual Time History of an Earthquake

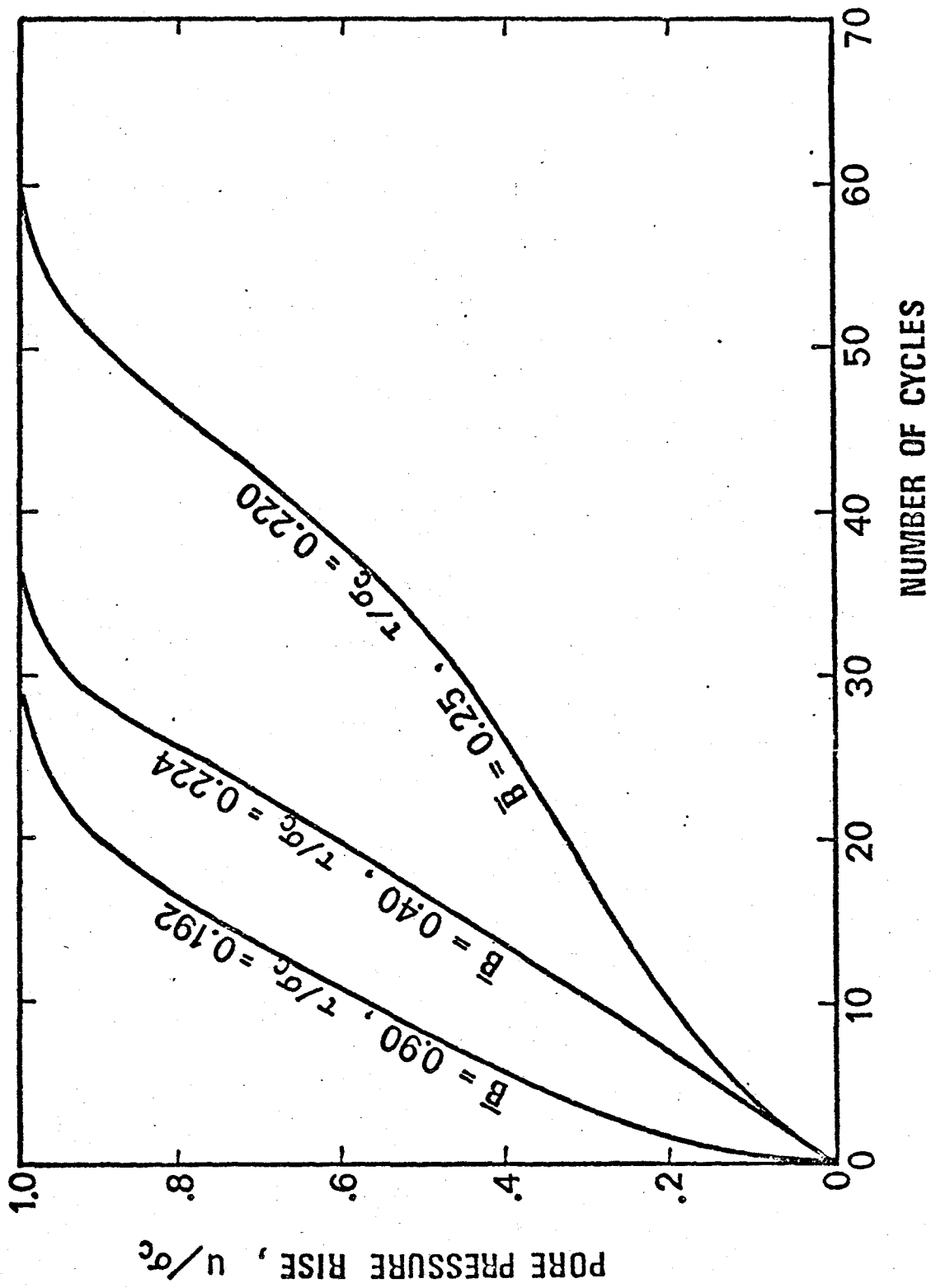


Fig. 4.20 Typical Liquefaction Data for a Low  $\bar{B}$  and a High  $\bar{B}$  Value

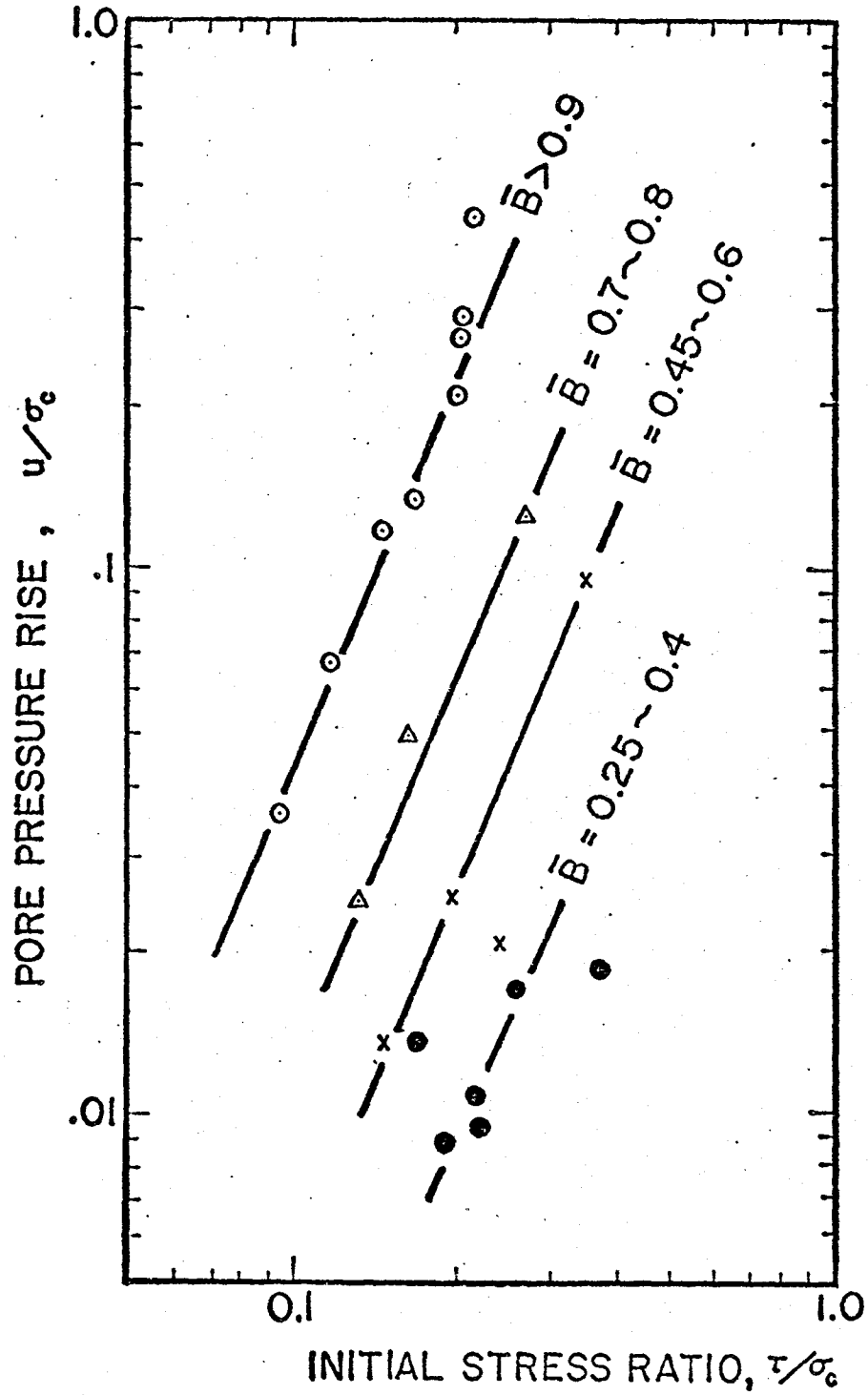


Fig. 4.21 Pore pressure Rise at the End of the First Cyclic Loading

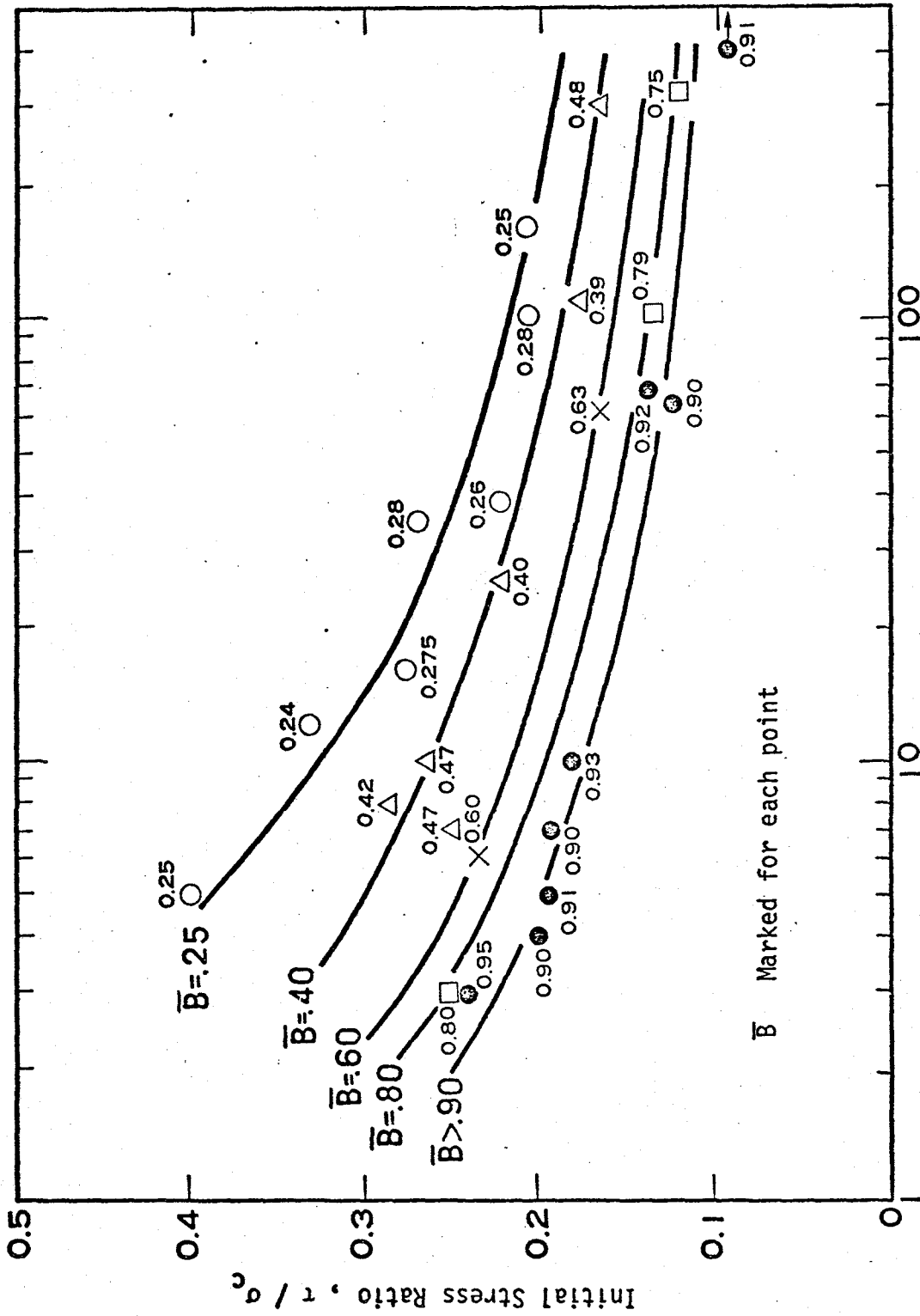


Fig. 4.22 Effect of  $\bar{B}$  values on Liquefaction Potential

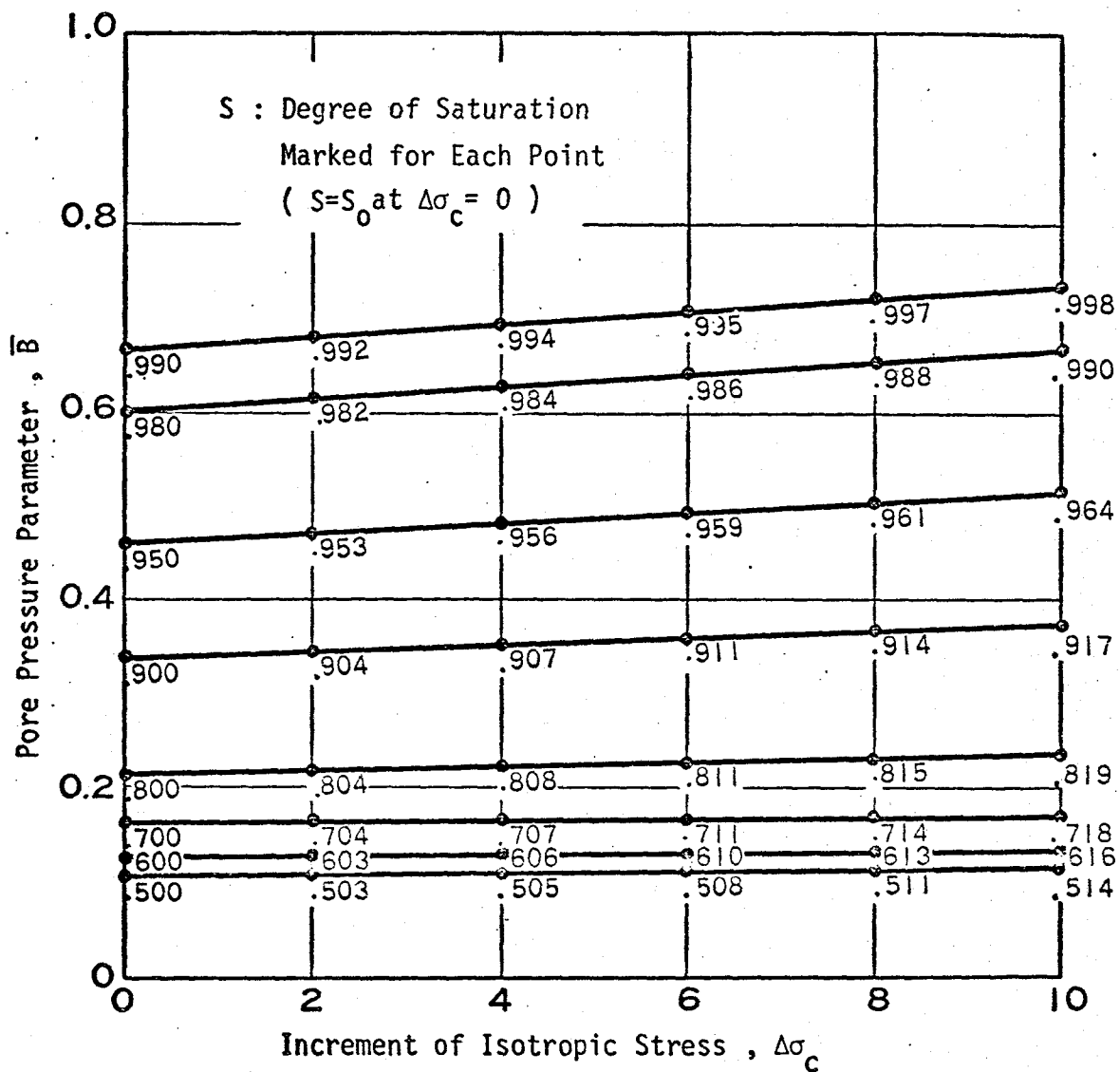


Fig. 4.23 Relationship between the  $\bar{B}$  values and the Initial Degree of Saturation ( back pressure  $u_b = 5$  psi )

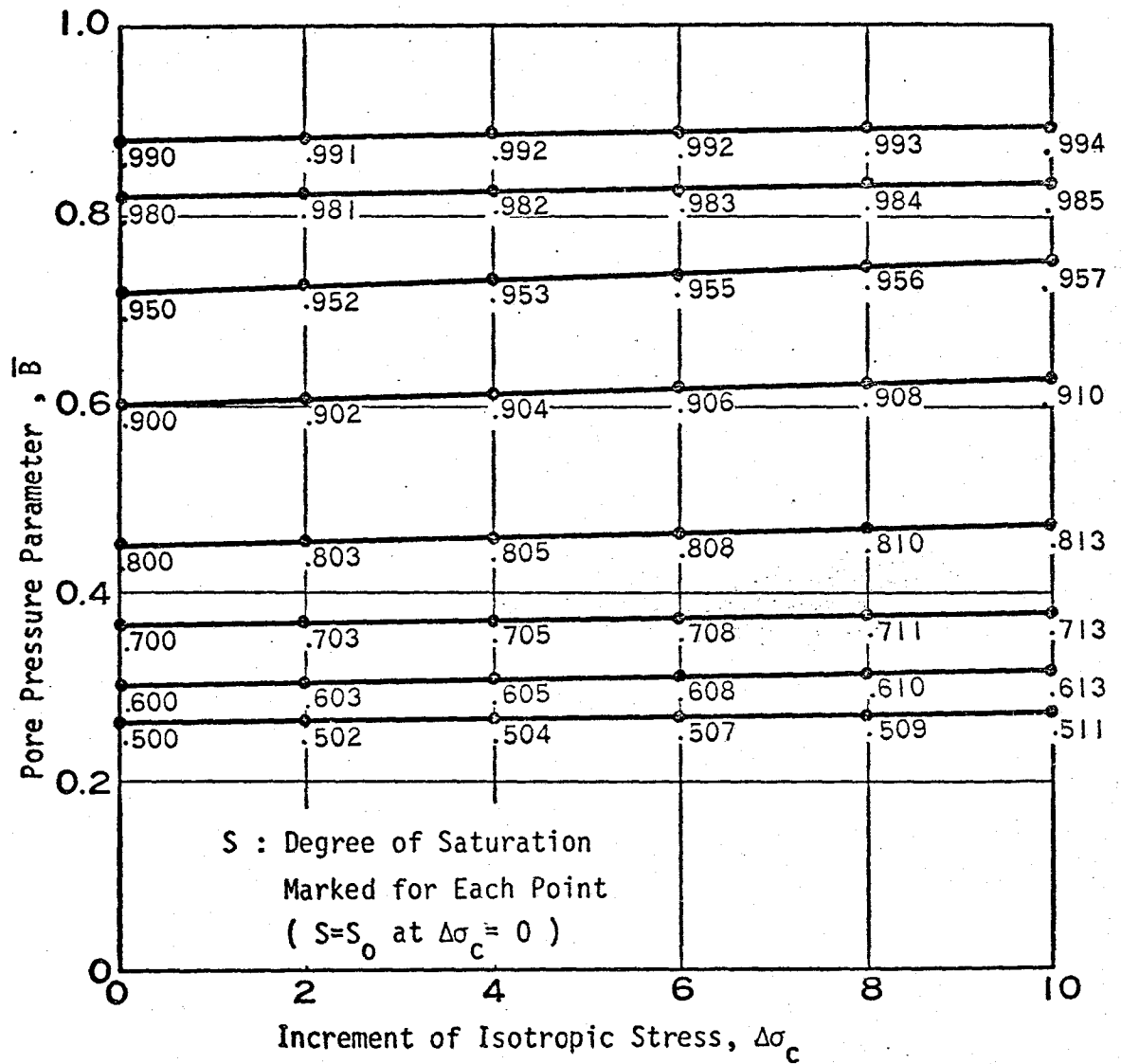


Fig. 4.24 Relationship between the  $\bar{B}$  values and the Initial Degree of Saturation ( back pressure  $u_b = 45$  psi )

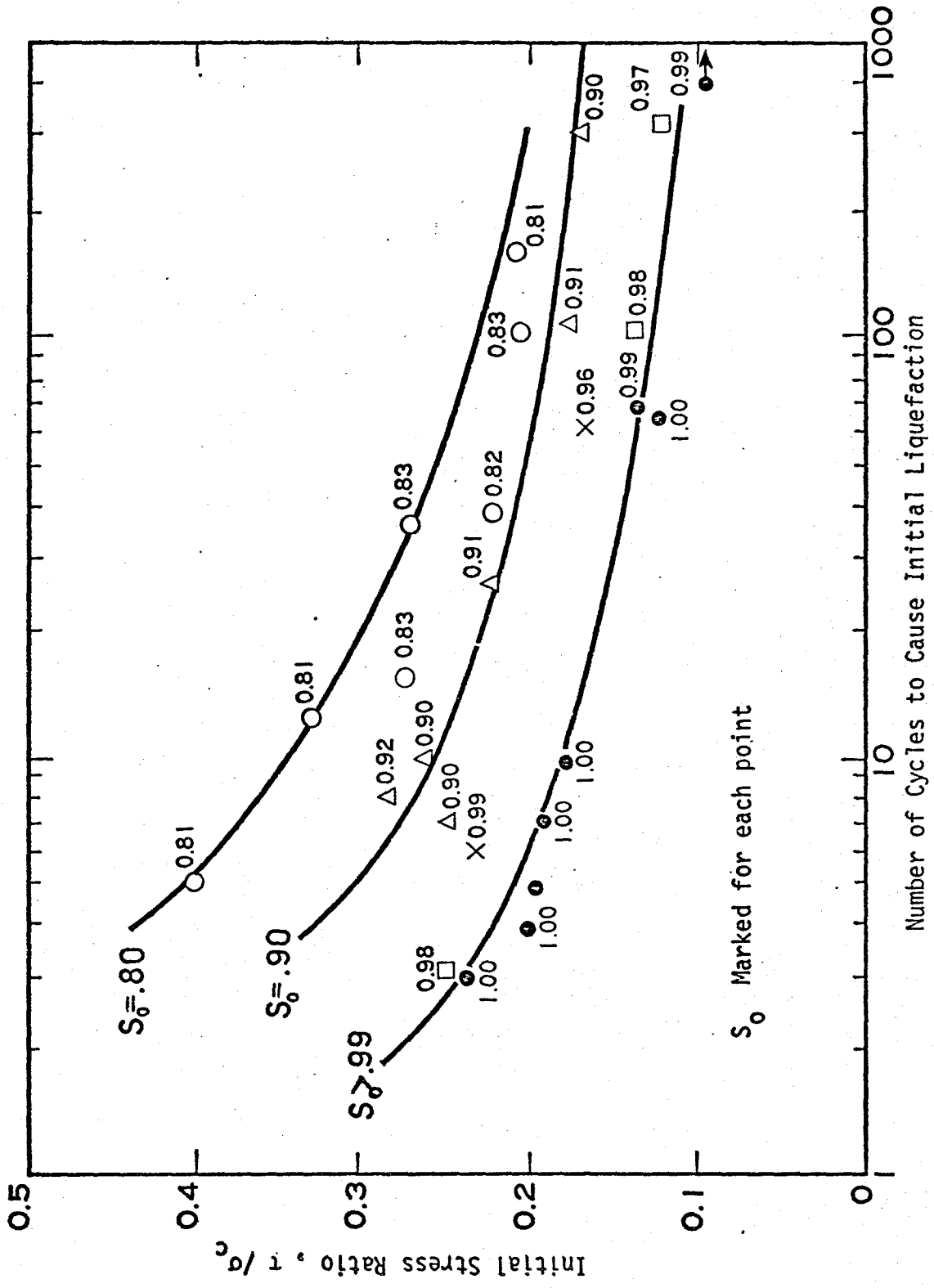


Fig. 4.25 Effect of the Initial Degree of Saturation on Liquefaction Potential

Reproduced from  
best available copy. 

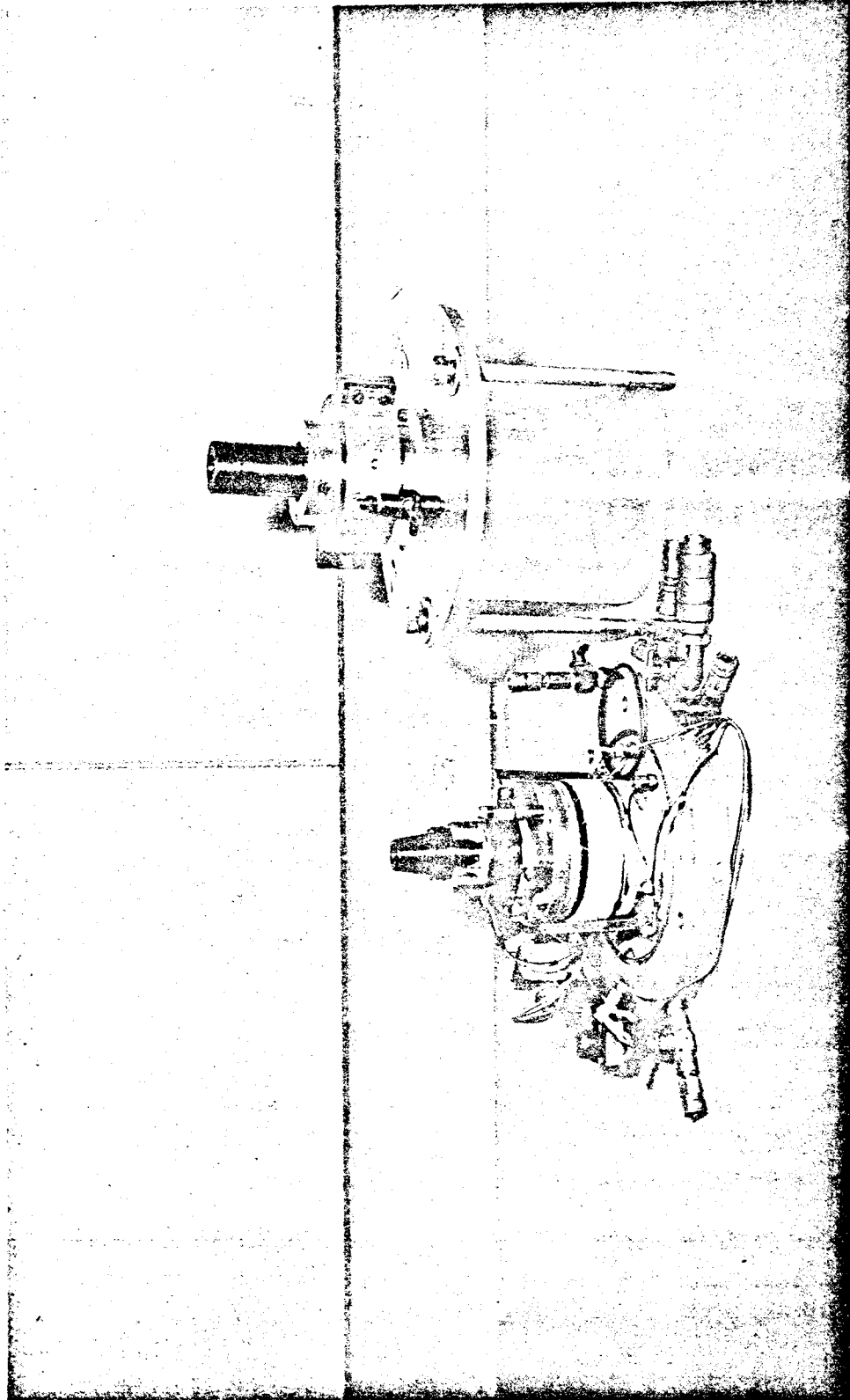


Plate II TSSD Base with Sample and Pickups

Plate II

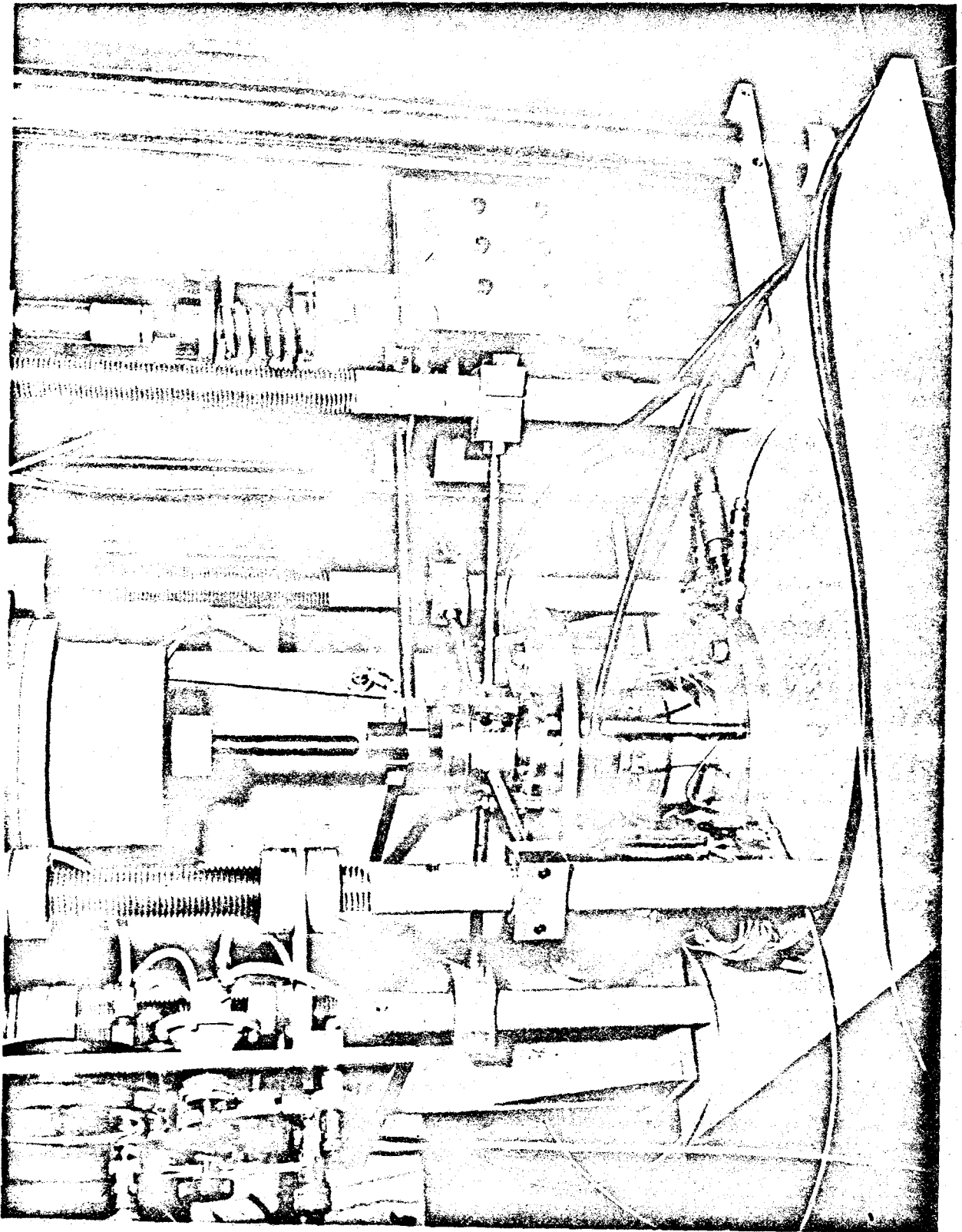


Plate I Torsional Simple Shear Device ( TSSD )